

Syracuse University

SURFACE

Dissertations - ALL

SURFACE

August 2018

Shock Tube and Mid-IR Laser Absorption Study of Combustion Kinetics

Shirin Jouzdani
Syracuse University

Follow this and additional works at: <https://surface.syr.edu/etd>



Part of the [Engineering Commons](#)

Recommended Citation

Jouzdani, Shirin, "Shock Tube and Mid-IR Laser Absorption Study of Combustion Kinetics" (2018).
Dissertations - ALL. 924.
<https://surface.syr.edu/etd/924>

This Dissertation is brought to you for free and open access by the SURFACE at SURFACE. It has been accepted for inclusion in Dissertations - ALL by an authorized administrator of SURFACE. For more information, please contact surface@syr.edu.

Abstract

This thesis focuses on the experimental characterization of the combustion properties of representative alternative fuels. Specifically, a shock tube and direct laser absorption systems are used to investigate the ignition and pyrolysis processes of target fuels. The research problem is motivated by concern about climate change and diminishing fossil fuels. There is a need to develop advanced combustion systems and use more alternative fuels. Innovative designs of combustion systems characterized by lower emissions and higher efficiencies can be facilitated by validated models of the chemical processes involved in combustion. The development of such validated models relies on extensive experimental measurements of various fundamental combustion properties.

The measured properties are global chemical times and species time-histories. For the global times, ignition is characterized by ignition delay time. A novel approach is developed to define pyrolysis time. The chemical reactions that control pyrolysis are generally also included in oxidation processes such as ignition. Pyrolysis is therefore a limiting case that can be used to isolate and test the model subset that is controlled by non-oxidative kinetics. Comparing ignition delay times and pyrolysis times at similar thermodynamic conditions brings out the competition between non-oxidative and oxidative kinetics. The species time-histories of fuel and CO are measured using direct absorption of mid-IR laser.

The target fuels are representative alternative fuels and some less characterized fossil fuel components. Among the alternative fuels studied are furans (2-methyl furan and 2-methyl tetrahydrofuran), alcohols (propanol isomers), and other relevant oxygenated fuels (methyl

tert-butyl ether, methyl propanoate). The fossil fuel components are 1,3-dimethylcyclohexane and methane. Methane and methyl propanoate blends are studied to establish the ability of biodiesel to enhance the ignition of methane. Global kinetic times are measured and used for model validation as well as establishing relative reactivity trends.

For the species time-histories, fuel time-histories of 2-methyl tetrahydrofuran and 1,3-dimethylcyclohexane are measured using mid-IR laser around $3.9\ \mu\text{m}$, associated with C–H bond stretching activities. CO time-histories during pyrolysis of propanol isomers, methyl tert-butyl ether, 2-methyl tetrahydrofuran, methyl propanoate and its blend with methane are obtained through mid-IR ro-vibrational absorption activities around $4.6\ \mu\text{m}$ using Quantum Cascade Laser (QCL).

These measurements of ignition times, pyrolysis times, fuel and CO time-histories provide useful kinetic datasets for validation, refinement, and development of chemical kinetic models of selected fuels. The datasets also establish insightful relative reactivity trends for which chemical explanations are advanced.

Shock Tube and Mid-IR Laser Absorption Study of Combustion Kinetics

by

Shirin Jouzdani

M.s., University of Dayton, 2013

B.s., Azad University, Iran, 2002

DISSERTATION

Submitted in partial fulfillment of the requirements for the degree of

Doctor of Philosophy in Mechanical and Aerospace Engineering

Syracuse University

August, 2018

Copyright © Shirin Jouzdani 2018

All Rights Reserved

Acknowledgements

First and foremost I want to thank my advisor, Dr. Ben Akih-Kumgeh for his guidance and support during my doctoral studies. I appreciate all his contributions of ideas and time. Words can not express my appreciation for his support, availability and constructive suggestions. He taught me to be a careful experimenter. Without his constant encouragement this thesis would not have been possible.

I am also thankful to Professor Ruth Chen and Jacques Lewalle, who have been always available to offer advice and guidance. They were always willing to guide and help me to overcome many obstacles in my work and life.

I would like to thank the members of my dissertation committee: Prof. Ashok Sangani, Prof. Melissa Green, Prof. Jacques Lewalle, Prof. Tara Kahan and Prof. Teng Zhang, for generously offering their time, guidance in preparation and review of this document.

I wish to thank the Department of Mechanical and Aerospace Engineering and the College of Engineering and Computer Sciences for the continued support of my studies and research. I am also grateful to the Syracuse Center of Excellence for the pleasant lab space in which I have had the pleasure of working and for all its support.

Throughout my time at Syracuse University and within the Thermodynamic and Combustion lab, I have worked with a great group of friends who have always been supportive. Thanks to Xuan Zheng, Apeng Zhou, Mazen Eldeeb, David Zheng, Nathan Peters, Lingshu Zhang, and Deshawn Coombs and all my other friends, who have helped me over the years.

More importantly, I would like to thank my family without which I would not be able to come this far. I am forever grateful to my parents for their unconditional love, support, powerful and endless prayers. Thanks to my sisters that have been a great source of encouragement and motivation. Most of all, I want to thank my dearest husband and my best friend, Ehsan. He has been a constant source of love, support and encouragement during life and the challenges of doctoral studies. I thank God for enlightening my life with his presence.

Finally, I am grateful to God for the inspiration and guidance that have been provided to me throughout my life.

Syracuse, New York

August, 2018

Contents

Abstract	i
Acknowledgements	v
List of Figures	ix
1 Introduction and literature review	1
1.1 Background and motivation	1
1.2 Literature review	3
1.2.1 Previous work on the targeted fuels	4
1.2.2 Combustion chemistry modeling	19
1.2.3 Fuel and species concentration using shock tube	20
1.3 Objectives and organization of thesis	22
2 Experimental Methods	25
2.1 Introduction	25
2.2 Shock tube reactor	25
2.2.1 Experimental setup and procedure	26
2.2.2 Determination of reactor conditions	28
2.2.3 Uncertainties in ignition delay times	31
2.2.4 Simulation of the shock tube reactor	34
2.3 Laser absorption diagnostic	35
2.3.1 Uncertainties in direct laser absorption measurements	40

2.4	Data processing	41
2.4.1	Ignition delay time measurements	41
2.4.2	Species time-history measurements	43
2.4.3	Characteristic chemical kinetic time scale of pyrolysis	47
3	Measurement of global chemical times	53
3.1	Ignition delay times of 2-methyl tetrahydrofuran and 2-methyl furan	53
3.2	Ignition delay times of 1,3-Dimethylcyclohexane	61
3.3	Global kinetic times of propanol isomers	65
3.3.1	Ignition delay times	65
3.3.2	Pyrolysis times of propanol isomers	70
3.3.3	Chemical kinetic model analysis	76
3.4	Global kinetic times of methyl tert butyl ether and 2-methyl tetrahydrofuran	80
3.4.1	Ignition delay times	80
3.4.2	Pyrolysis times	83
3.5	Global kinetic times of methyl propanoate and methane blends	88
3.5.1	Ignition delay times	88
3.5.2	Pyrolysis times	96
4	Fuel and CO time-history measurements	100
4.1	Fuel time-history measurement	100
4.1.1	2-Methyl tetrahydrofuran time-history measurements	100
4.1.2	1,3-Dimethylcyclohexane time-histories during ignition and pyrolysis .	107
4.2	CO time-history measurements	112
4.2.1	CO time-histories during pyrolysis of propanol isomers	112
4.2.2	CO time-histories during pyrolysis of 2-methyl tetrahydrofuran and methyl tert butyl ether	116

4.2.3	CO time-histories during pyrolysis of methyl propanoate and its blend with methane	121
5	Conclusion and outlook	124
	Bibliography	128
	Vita	155

List of Figures

1.1	Annual world energy consumption by energy source [2].	2
1.2	Chemical structure of the investigated fuels.	4
2.1	Conditions in a shock tube before the diaphragm ruptures.	26
2.2	Wave processes in the various regions of shock tube after the diaphragm ruptures.	28
2.3	Representative shock wave arrival time determination. Shown is the pressure signal near the endwall with corresponding arrival time for a MTHF/O ₂ /Ar mixture with $\phi = 0.5$, argon/oxygen ratio, $D = 3.76$, $p = 4.7$ atm and $T = 1243$ K.	32
2.4	Representative shock velocity profile. Shown are shock velocities at midway locations between pressure transducers with a linear fit, for a MTHF/O ₂ /Ar mixture with $\phi = 0.5$, argon/oxygen ratio, $D = 3.76$, $p = 4.7$ atm and $T = 1243$ K.	32
2.5	Strong absorption bands of various molecules in the IR wavelength range. . .	36
2.6	Representative ignition delay time measurement. Shown are the sidewall pres- sure and CH emission signals, for a 2-MTHF/O ₂ /Ar mixture with $\phi = 1.0$, $p = 3.35$ atm, $T = 1179$ K and ratio of argon to oxygen, D , is 3.76.	42
2.7	a) Laser absorption experimental setup. b) Representative photo detector signals for a 2-MTHF ignition experiment at pressure 3 atm and T=1179 K.	43
2.8	Reaction pathway for CO production during <i>n</i> -propanol pyrolysis (1% fuel, 3 atm and 1450 K) from models by Johnson et al. [110] and Sarathy et al. [119]. Instant at which 20% fuel is consumed.	48

2.9	Pyrolysis time definition on the basis of product species time-histories during pyrolysis. Shown are results from simulations of 1% <i>iso</i> -propanol in argon at 1450 K and 12 atm using the model by Johnson et al. [110]. In 2.9a, the time is based on maximum of $X_{fuel}X_{CO}$, whereas in 2.9b, it is based on product of X_{CO} and its rate of production.	49
2.10	Determining a pyrolysis time scale from an experimental realization of <i>iso</i> -propanol pyrolysis in the case of 1% <i>iso</i> -propanol in Ar at 1395 K and 3.6 atm. a) Absorbance time-histories of CO (A_{CO}) with its polynomial fit b) Time-histories of $\frac{dA_{CO}}{dt}$ and $A_{CO}\frac{dA_{CO}}{dt}$, indicating respective pyrolysis times. .	50
2.11	Simulated pyrolysis times of <i>iso</i> -propanol based on correlation of fuel and CO compared with times based on correlations of CO and its rate of production for 1% fuel in argon at 3.5 atm. Models: Johnson et al. [110] and Sarathy et al. [119].	51
2.12	Simulated pyrolysis times of <i>n</i> -propanol based on correlation of fuel and CO compared with times based on correlations of CO and its rate of production for 1% fuel in argon at 3.5 atm. Models: Johnson et al. [110] and Sarathy et al. [119].	51
3.1	Ignition delay times of 2-MF and 2-MTHF for stoichiometric mixtures at a nominal pressure of 3 atm.	54
3.2	Ignition delay times of 2-MF and 2-MTHF at a nominal pressure of 12 atm under lean and rich conditions.	55
3.3	Effect of equivalence ratio on 2-MTHF ignition delay times at a nominal pressure of 12 atm.	56
3.4	Ignition delay times of 2-MF and 2-MTHF at a nominal pressure of 3 atm. Model predictions: solid line is 2-MTHF model by Moshhammer et al. [219] and dash line is 2-MF model by Somers et al. [18].	56

3.5	Ignition delay time of 2-MTHF at a nominal pressure of 12 atm, $\phi = 0.5$. Model predictions: solid line is 2-MTHF model by Moshhammer et al. [219] and dash line is 2-MF model by Somers et al. [18].	57
3.6	Ignition delay time of 2-MTHF at a nominal pressure of 12 atm, $\phi = 2$. Model predictions: solid line is 2-MTHF model by Moshhammer et al. [219] and dash line is 2-MF model by Somers et al. [18].	58
3.7	Comparison of bond dissociation energies calculated by direct atomization (CBS QB3 method) using the Gaussian 09 software package.	59
3.8	Most important reactions from the sensitivity analysis of the 2-MTHF mechanism by Moshhammer et al. [219].	59
3.9	Most important species from the sensitivity analysis of the 2-MTHF mechanism by Moshhammer et al. [219]. The fuel, O ₂ , CO ₂ , and H ₂ O are considered indispensable for oxidation and are therefore not part of the analysis.	60
3.10	Ignition delay times of stoichiometric mixtures of fuel, oxygen, argon for 1,3-DMCH and ECH with an argon/oxygen ratio of 3.76 at a pressure of 5.0 atm. Solid lines represent Arrhenius fits.	62
3.11	Ignition delay times of 1,3-DMCH at a pressure of 5.0 atm, an Ar/O ₂ ratio of 10.0, and equivalence ratios of 0.5, 1.0, and 2.0. Dashed lines: model predictions.	63
3.12	Ignition delay times of 1,3-DMCH at a pressure of 12 atm, an Ar/O ₂ ratio of 10.0, and equivalence ratios of 0.5 and 1.0. Dashed lines: model predictions.	64
3.13	Effect of pressure on ignition delay times of 1,3-DMCH for $\phi = 1.0$, Ar/O ₂ ratio of 3.76, and pressures of 3.0, 5.0, and 12 atm. Dashed lines: model predictions.	64
3.14	Comparison with <i>n</i> -propanol experiment correlations [84, 112] at 3.5 atm.	66
3.15	Comparison with <i>iso</i> -propanol experiment correlation [112] at 3.5 atm.	66
3.16	Isomer effect on propanol ignition (3.5 atm).	67
3.17	Isomer effect on propanol ignition (5 atm).	67

3.18 Comparison of measured <i>n</i> -propanol ignition delay times at 3.5 atm with model predictions.	68
3.19 Comparison of measured <i>iso</i> -propanol ignition delay times at 3.5 atm with model predictions.	68
3.20 Comparison of measured <i>n</i> -propanol ignition delay times at three equivalence ratios with predictions of model by Sarathy et al. [119].	69
3.21 Comparison of measured <i>iso</i> -propanol ignition delay times at three equivalence ratios with predictions of model by Sarathy et al. [119].	69
3.22 Isomer effect on ignition of stoichiometric mixtures at a higher average pressure of 12 atm and less dilute condition ($D = 3.76$). Model simulations: Sarathy et al. [119].	69
3.23 Pyrolysis time scales of <i>n</i> - and <i>iso</i> -propanol for 1% in argon at 3.5 atm. . .	71
3.24 Effect of fuel concentration on pyrolysis time scales of <i>n</i> -propanol. No distinct influence is observed.	71
3.25 Pyrolysis times of 1% of <i>n</i> -propanol at 3.5 atm and 11 atm.	72
3.26 Pyrolysis times of 1% <i>n</i> -propanol with 11 atm data scaled to 3.5 atm using $p^{-0.55}$ relation.	72
3.27 Comparison of ignition delay times ($\phi = 1$) with pyrolysis time scales of <i>iso</i> -propanol, including simulation results.	74
3.28 Comparison of ignition delay times ($\phi = 1$) with pyrolysis time scales of <i>n</i> -propanol, including simulation results.	74
3.29 Typical fuel time-history during fuel pyrolysis, indicating global first order kinetics. Model: Johnson et al. [110].	75
3.30 Simulated fuel time histories during ignition. A change in profile toward pyrolysis-type decay occurs as temperature increases. Model: Johnson et al. [110].	75

3.31	Reaction pathway for <i>n</i> -propanol ignition ($\phi = 1$, 1% fuel, $D = 21$, $p = 3$ atm) using the model by Sarathy et al. [119] at temperatures of 1475 K (top) and 1230 K (bottom).	77
3.32	Reaction pathway for <i>n</i> -propanol ignition ($\phi = 1$, 1% fuel, $D = 21$, $p = 3$ atm) using models by Sarathy et al.[119] with temperatures of 1510 K (top) and 1310 K (bottom).	78
3.33	Reaction pathway for <i>n</i> -propanol pyrolysis using model by Sarathy et al. [119] with three conditions. Condition 1(in bold): 1% fuel, 1450 K, and 3 atm; Condition 2 (in bold italic): 1% fuel, 1450 K, and 12 atm; Condition 3(in regular): 2% fuel, 1450 K, and 3 atm.	78
3.34	Reaction pathway for <i>iso</i> -propanol pyrolysis using model by Sarathy et al. [119] with three conditions. Condition 1(in bold): 1% fuel, 1450 K, and 12 atm; Condition 2(in bold italic): 1% fuel, 1450 K, and 12 atm; Condition 3(in regular): 2% fuel, 1450 K, and 12 atm.	79
3.35	Pressure effect on 2-MTHF at 3.3 and 12 atm.	81
3.36	Pressure effect on MTBE at 3.5 and 12 atm.	81
3.37	Comparison of measured 2-MTHF ignition delay times at 3.3 and 12 atm with model predictions [46, 49].	81
3.38	Comparison of measured MTBE ignition delay times at 3.5 and 12 atm with model predictions [67].	81
3.39	Comparison of measured 2-MTHF ignition delay times at three equivalence ratios with predictions of model by Fenard et al. [49].	82
3.40	Pyrolysis time scales of 2-MTHF at 3.3 & 11 atm.	84
3.41	Pyrolysis time scales of 2-MTHF and MTBE at different pressures.	84
3.42	Comparison of pyrolysis time scales of 2-MTHF at 3.3 & 11 atm with simulations [46, 49].	84

3.43	Comparison of pyrolysis time scales of MTBE at different pressures with simulation [67].	84
3.44	Comparison of ignition delay times ($\phi = 1$) with pyrolysis time scales for 3% of 2-MTHF at pressures of 11-12 atm.	85
3.45	Comparison of ignition delay times ($\phi = 1$) with pyrolysis time scales for 3% MTBE at pressures of 11-12 atm.	85
3.46	Comparison of 2-MTHF global kinetic times for mixtures with 3% fuel for the case of pyrolysis and ignition at equivalence ratios of $\phi = 1, 0.5$, and 3. . . .	86
3.47	Comparison of ignition delay times at $\phi = 1, 0.5, 3$, with pyrolysis time scales of 3% 2-MTHF based on kinetic model simulations.	87
3.48	Comparison of ignition delay times at $\phi = 1, 0.5, 3$ with pyrolysis time scales of 3% MTBE based on kinetic model simulations.	87
3.49	Ignition delay times of stoichiometric mixtures of fuel, oxygen, and argon for MP and CH_4 at scaled pressure of 7.4 atm. Solid lines represent Arrhenius fits	89
3.50	Experimental and model predictions of ignition delay times of MP, CH_4 and blend of both at scaled pressure of 7.4 atm. Solid lines: model by Zhang et al. [163] Dashed lines: model by Zhao et al. [164].	89
3.51	Experimental and model predictions of ignition delay times of MP, CH_4 and blend of both at scaled pressure of 4 atm. Solid lines: model by Zhang et al. [163] Dashed lines: model by Zhao et al. [164].	90
3.52	Experimental and model predictions of ignition delay times of MP, CH_4 and blend of both for mixtures with 3% fuel and $\phi = 0.5$ at a nominal pressure of 4 atm. Solid lines: model by Zhang et al. [163] Dashed lines: model by Zhao et al. [164].	91
3.53	Experimental ignition delay times of stoichiometric and lean mixtures of MP and CH_4 with fuel maintained at 3% at an average pressure of 4 atm. Solid lines: model by Zhang et al. [163] Dashed lines: model by Zhao et al. [164]. .	92

3.54	Experimental ignition delay times and model predictions of MP, CH ₄ and blend of both fuels with O ₂ maintained at 10% and at an average pressure of 10 atm. Solid lines: model by Zhang et al. [163] Dashed lines: model by Zhao et al. [164].	92
3.55	Reaction pathway for 3% CH ₄ ($\phi=1$, T=1500 K, p = 7.4 atm) using models by Zhang et al. [163].	93
3.56	Reaction pathway for 3% MP ($\phi=1$, T=1287 K, p = 7.4 atm) using models by Zhang et al. [163].	94
3.57	Reaction pathway for 90% CH ₄ and 10% MP ($\phi=1$, T=1311 K, p = 7.4 atm) using models by Zhang et al. [163]	95
3.58	a) Pyrolysis time scales of MP and its equal blend with CH ₄ . b) Comparison of pyrolysis time scales with simulations. Solid lines: model by Zhang et al. [163] Dashed lines: model by Zhao et al. [164]	97
3.59	Comparison of ignition delay times ($\phi=1$) with pyrolysis time scales of 1.5% MP with 1.5% CH ₄	98
3.60	Comparison of ignition delay times ($\phi=1$) with pyrolysis time scales of 3% MP.	98
4.1	a) Shock tube measurements of 2-MTHF absorption cross sections, $\phi=1$ and $D = 3.76$, before the incident shock and behind the reflected shock. b) Shock tube measurements of 2-MF absorption cross sections, $\phi=1$ and $D = 3.76$, before the incident shock and behind the reflected shock.	101
4.2	Summary of the interference correction method for a shock at 1257 K, 3 atm and stoichiometric mixture a) Absorbance time-histories due to six interfering species and their sum. b) Uncorrected experimental absorbance plotted against normalized time and absorbances obtained from simulations using model [219]. The simulations are with and without accounting for interference absorption.	102

4.3	a) Comparison of corrected 2-MTHF mole fraction against model simulations at three temperatures, pressure of 3 atm, and $\phi=1$. b) Comparison of corrected 2-MTHF mole fraction against model simulations at two temperatures, pressure of 12 atm, and $\phi=0.5$	103
4.4	Summary of the interference correction method for a shock at temperature of 1442 K, pressure of 3 atm and 3% fuel. a) Absorbance time-histories due to six interfering species and their sum. b) Absorbance profiles of 2-MTHF pyrolysis. Simulations are based on model by Moshhammer et al. [219] and the simulation time has been multiplied by a factor of 6.	105
4.5	Concentration profiles of 2-MTHF pyrolysis at 1442 K, pressure 3 atm and 3% fuel. Simulations based on model by Moshhammer et al. [219].	105
4.6	Concentration profiles of 2-MTHF pyrolysis at two temperatures, pressure of 3 atm and 3% fuel. Simulations based on model by Moshhammer et al. [219]. .	106
4.7	Absorbance of interfering species obtained from the ignition simulation of a stoichiometric mixture of 1,3-DMCH/O ₂ /Ar at 1249 K. The sum is used to correct the measured absorbance.	107
4.8	Fuel mole fractions based on uncorrected and corrected absorbance for three ignition experiments.	108
4.9	Comparison of corrected 1,3-DMCH concentration profiles with predictions of the 1,3-DMCH model at $\phi = 1.0$ and Ar/O ₂ ratio of 3.76 at average pressure of 4.2 atm.	109
4.10	Comparison of corrected 13DMCH concentration profiles with predictions of the 13DMCH model at $\phi = 1.0$ and Ar/O ₂ ratio of 10.0 at average pressure of 4.7 atm.	110
4.11	Absorbance of interfering species obtained from the simulation of 1.54 % fuel pyrolysis at 1406 K. The sum is used to correct the measured absorbance during pyrolysis at simulated conditions.	110

4.12	Fuel mole fractions based on uncorrected and corrected absorbance for two pyrolysis experiments.	111
4.13	Comparison of corrected 1,3-DMCH concentration profiles during pyrolysis with predictions of the 1,3-DMCH model for pyrolysis 1.54% fuel in argon at 4 atm.	111
4.14	Comparison of CO concentration with simulations using the Johnson et al. [110], Sarathy et al. [119] and Man et al. [112] mechanisms during pyrolysis of 1% <i>iso</i> -propanol in argon at two different temperatures.	113
4.15	Correlation functions (normalized by respective maxima) for pyrolysis of 1% <i>iso</i> -propanol in argon at 3.5 atm and 1489 K, showing times to maximum and decay rates.	114
4.16	CO time-history during 1% <i>n</i> -propanol pyrolysis (T=1476 K, p=3.3 atm) with comparison of three models.	114
4.17	CO time-history of 1% <i>n</i> -propanol at three different temperatures with the Sarathy et al. [119] mechanism.	114
4.18	Correlations functions (normalized by respective maxima) for pyrolysis of 1% <i>n</i> -propanol in argon at 1476 K and 3.5 atm, showing different times to maximum	115
4.19	Comparison of CO concentration during pyrolysis of 1% <i>n</i> -propanol and <i>iso</i> - propanol in argon at different temperatures.	116
4.20	CO time-histories during 2-MTHF pyrolysis at two different temperatures compared to predictions by two different models [46, 49].	117
4.21	CO time-histories during MTBE pyrolysis at two different temperatures in- cluding predicted time-histories using the model by the Curran et al. [67] model.	117
4.22	Comparison of CO concentration during pyrolysis of 3% 2-MTHF and MTBE in argon.	118

4.23	Comparison of CO time-history with simulation using Fenard et al. [49] model at both constant pressure (hp) and constant volume (uv) reactors for time to 90% of $x_{CO,eq}$.	119
4.24	Reaction pathway for CO production during 2-MTHF pyrolysis (3% fuel, 3.5 atm and 1450 K) from model by Fenard et al. [49] at 40 μ s.	119
4.25	Time histories of fuel, CO and key intermediates for CO production during pyrolysis of 2-MTHF, namely, CH_2O and CH_2CO using the model by Fenard et al. [49].	120
4.26	Reaction pathway for CO production during MTBE pyrolysis (3% fuel, 3.25 atm and 1497 K) from model by Curran et al. [67] at 40 μ s.	121
4.27	CO time-history during pyrolysis of two different MP concentration and its equal blend with CH_4 .	122
4.28	Comparison of CO histories with simulations using the Zhao et al. [164], Zhang et al. [163] mechanisms during pyrolysis of during pyrolysis of 3% MP and its equal blend with CH_4 .	122

Chapter 1. Introduction and literature review

1.1 Background and motivation

One of the primary causes of global climate forcing is the combustion of fossil fuels that leads to emissions of greenhouse gases such as carbon dioxide (CO_2). Over the past decade, greenhouse gas emissions produced by transportation sector have increased at a faster rate than any other energy sector (20% global CO_2 emissions), with predictable 80% higher energy use and carbon dioxide emissions by 2030 [1]. According to the 2017 International Energy Outlook prepared by the U.S. Energy Information Administration (EIA) [2], the world consumption of petroleum and other liquid fuels will increase from 95 million barrels per day in 2015 to 113 million barrels per day in 2040. As shown in Figure 1.1, petroleum and other liquids remains the largest source of energy. This growing demand for energy, increasing environmental problems and concerns for depletion of petroleum fuel motivate the development of advanced combustion systems and alternative sources of energy. Clean and efficient combustion systems are required and in order to design these, detailed combustion chemistry models as well as general understanding of trends of combustion properties are essential [3].

Developing these models from first principles is currently impossible because of many complexities; fundamental experiments are therefore needed to constrain proposed chemical kinetic models. One way to advance the characterization and modeling of combustion properties is the use of the shock tube to investigate high-temperature kinetic processes. Recently, global measurements in shock tube such as ignition times in shock tube have been extended to include species time-history measurement using mid infrared (IR) absorption. Application of

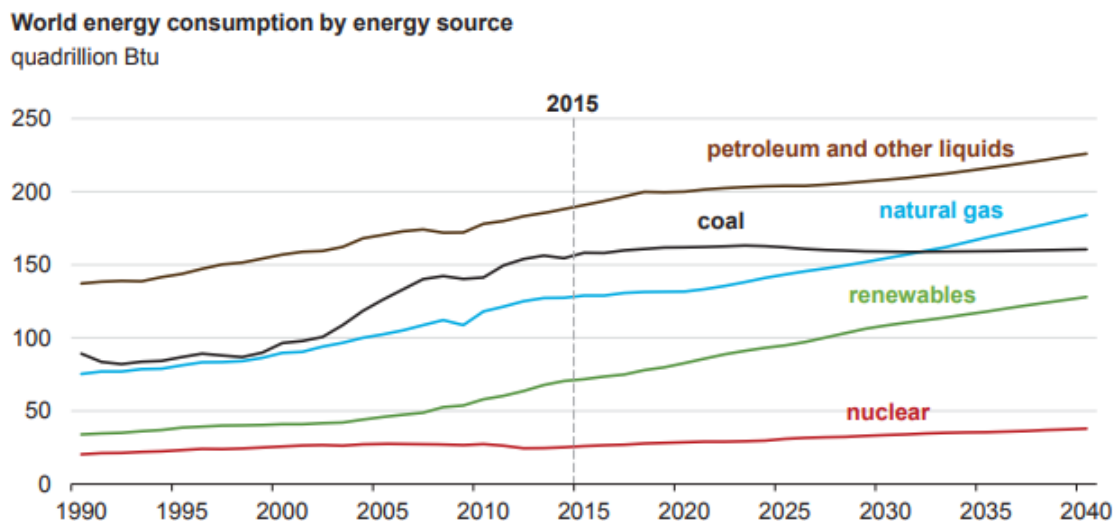


Figure 1.1: Annual world energy consumption by energy source [2].

mid-IR lasers to combustion research continue to show more impact and growth [4], because they provide sensitive, non-intrusive and time resolved measurements of important species time-histories.

In this thesis, the work is focused on using the shock tube technique and laser absorption diagnostics to measure global chemical kinetic times and time-histories of relevant species such as the fuel and carbon monoxide (CO). CO is a product of hydrocarbon combustion and knowledge of its concentration can indicate the amount of chemical energy not converted to final products at a point in time. In pyrolysis, CO production is a measure of the degree and rate of fuel conversion. The fuel profile can also indicate the absence or presence of first-order kinetics that is characteristic of a strong influence of pyrolysis in combustion.

Regarding the fuels to be studied, this work will focus on furans, propanol isomers, dimethylcyclohexane, methy tert-butyl ether, methyl propanoate and methane. These fuels are chosen based on considerations of the needs of combustion systems.

Furan-derived compounds such as 2-methylfuran (2-MF), and 2-methyltetrahydrofuran (2-MTHF) are possible alternative fuels for spark ignition (SI) engines that can be produced

from non-food biomass [5–8]. Unlike the limitations of ethanol such as low energy density and high volatility and limited solubility in gasoline, furan and its derivatives are more soluble in gasoline.

C_3 to C_5 alcohols such as iso-propanol have advantages over ethanol as fuels in terms of energy density. The use of oxygenates in fuel such as methyl tert-butyl ether (MTBE) is associated with reduced particulate emissions [9]. The combustion features of these fuels need to be characterized before their use in engine systems. A significant amount of cycloalkanes are included in transportation fuels. Thus, more attention needs to be paid to the kinetics of cycloalkanes such as 1,3-dimethylcyclohexane (1,3-DMCH) oxidation and pyrolysis.

Natural gas is one of the promising alternative fuel. Due to the abundance of natural gas and its combustion characteristics it is seen as a viable alternative fuel for both compression and spark ignition engines [10, 11]. The high methane content of natural gas leads to poor ignition characteristics in compression ignition engines. The use of natural gas in compression ignition engines can be completed by using biodiesel as a pilot. Biodiesel which is a mixture of saturated and unsaturated long-chain methyl and ethyl esters, has been used in diesel engines and provides many environmental advantages such as the renewability, low greenhouse effect, low sulfur content [12]. Biodiesel can be presented by methyl propanoate (MP). Fundamental studies of chemical kinetic interactions involved in natural gas and biodiesel blend ignition are needed.

1.2 Literature review

Previous work on the molecular systems targeted in this work will be reviewed first. This will be followed by a discussion of chemical kinetic modeling and the use of direct mid-IR laser absorption in studies of combustion kinetics.

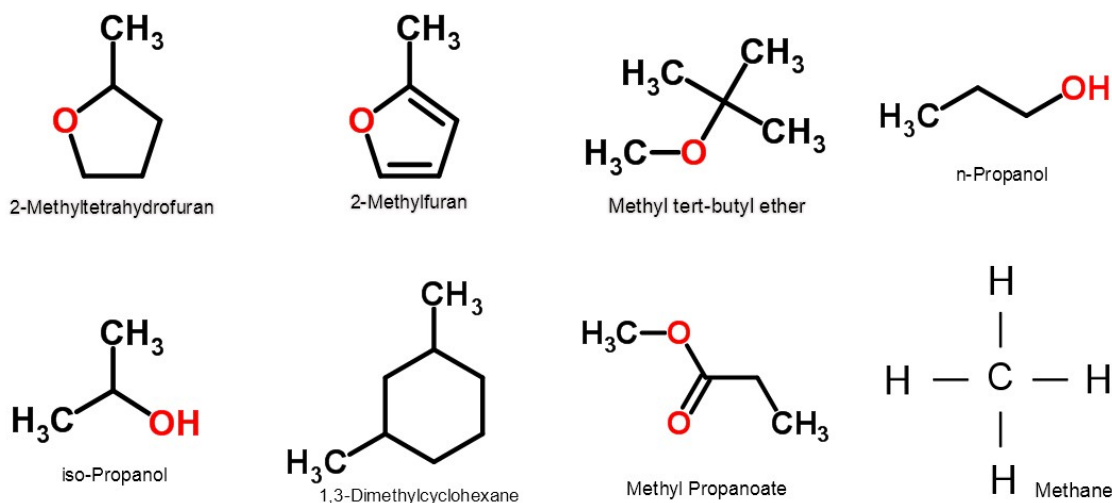


Figure 1.2: Chemical structure of the investigated fuels.

1.2.1 Previous work on the targeted fuels

As declared at the beginning furans, propanol isomers, MTBE, 1,3-DMCH, MP and methane are studied here. The chemical structure of the investigated fuels is shown in Figure 1.2. Biofuels are potential substitutes for fossil fuel [13]. Ethanol is produced in large quantities and has been discussed in many publications [14, 15]. However, it has many limitations such as low energy density, high boiling point, and high energy consumption during its production. Another biofuel class is biodiesel which is generally a fatty acid methyl ester produced from vegetable oils, animal fats, and grease. Biodiesel is an attractive alternative transportation fuel because of its lower emissions compared to petroleum diesel. However, biodiesel has high feedstock costs, poor storage and low oxidative stability, poor low-temperature operability compared to petrodiesel and lower volumetric energy content [16]. Biodiesel is also not well suited for use in the more popular SI engine. The search for alternatives to ethanol and biodiesel has become an important research area. Furan-derived compounds and longer chain alcohols ($C_3 \rightarrow C_5$) have more attractive features that make them worthwhile to explore. Furans and alcohols can be obtained from chemical processing of non-edible biomass.

The most widely investigated fuel from the furan class is 2,5-dimethylfuran (2,5-DMF). These investigations include mechanistic studies of reaction pathways, ignition delay measurements, and chemical kinetic model development [17–19]; speciation studies of low pressure flames [20]; and engine studies [21–24]. Review on production method and several experimental data have been presented by Xu et al. [25], showing the need for further research on furan derivatives. Further progress has recently been reviewed by Qian et al. [26] and Eldeeb and Akih-Kumgeh [27], highlighting many outstanding challenges such as the need for widely validated models. Apart from 2,5-DMF, 2-methyl furan (2-MF) has also been investigated. In a study by Thewes et al. [28] the impact of 2-MF on in-cylinder mixture preparation and combustion performance was investigated. The results indicated faster evaporation of 2-MF compared to ethanol and better combustion stability. Wang et al. [24] compared the combustion characteristics of 2-MF, 2,5-DMF, ethanol, and gasoline. The authors concluded that emissions during 2-MF combustion were comparable with those of the other fuels, whereas a faster burning rate of 2-MF could result in improved efficiency. At a fundamental level, autoignition behavior has been investigated. Eldeeb and Akih-Kumgeh [29] established the relative ignition behavior of furan, 2-MF, and 2,5-DMF, showing that 2-MF was the most reactive of the three furans. Other experimental investigations and detailed modeling of 2-MF have been carried out [30–32]. Similar to 2,5-DMF, more recent work is focused on the better understanding of the oxidation kinetics of 2-MF [33].

The saturated furans, tetrahydrofurans, are equally attractive as fuel additives or pure fuels. Although not as extensively studied as 2,5-DMF and 2-MF, there are increasingly more research activities on understanding tetrahydrofuran derivatives such as 2-methyltetrahydrofuran (2-MTHF).

2-MTHF can be produced from non-edible biomass [34, 35]. It has been shown to possess good antiknock characteristics, making it a good automotive fuel additive [36]. It has a high lower heating value (LHV) 28.5 MJ/L, that is closer to gasoline (31.6 MJ/L) compared to

the rather low value for ethanol (21.3 MJ/L). It also has a high energy density (0.85 kg/L) compared to gasoline (0.74 kg/L) and ethanol (0.79 kg/L) [37, 38]. 2-MTHF can also be used as a pure SI engine fuel without blending with gasoline [39]. Analysis of nitrogen oxides (NO_x), non-methane hydrocarbons, and carbon monoxide (CO) emissions from an SI engine fueled with a mixture of gasoline and 2-MTHF were carried out by Rodolph and Thomas [40] and compared with unleaded gasoline. The results showed that the fuel blend containing 10% MTHF is such that its power outputs, NO_x , non-methane hydrocarbons and CO emissions are similar to unleaded gasoline. Kar et al. [41] has suggested the class called P-series fuels with 2-MTHF as a component to be substituted for gasoline. The P-series fuels are blends of ethanol, 2-MTHF, pentanes and butane that can be used in severe cold-weather conditions to solve engine cold-start issues. Janssen et al. [42] recently reported a blend of 2-MTHF with di-n-butylether complies with ideal fuel properties in terms of emission performance and engine efficiency.

The mechanistic reaction pathways of 2-MTHF oxidation and pyrolysis have been explored using computational chemistry. The bond dissociation energies (BDEs) for carbon-hydrogen and carbon-methyl bonds, barrier heights and reaction enthalpies for all possible H abstraction reactions by H atoms and CH_3 have been computed using the model chemistries of CBS-QB3 and G3 by Simmie et al. [43]. Further, Sudholt et al. [39] has also calculated BDEs for (hydro) furanic species including 2-MTHF by employing CBS-QB3 and these later results show good agreement with Simmie et al. [43]. Recently, Chakravarty et al. [44] calculated the rate parameters for reaction of 2-MTHF with HO_2 using CBS-QB3 and CCSD(T)/cc-pVTZ//B3LYP/cc-pVTZ level of theory. These results are recommended by the authors for model development.

With respect to kinetic modeling and fundamental experiments, Moshhammer et al. [45] studied low pressure premixed laminar flames of 2-MTHF with an equivalence ratio of 1.7 and at a pressure of 40 mbar using molecular beam mass spectrometry. The results of this study

were used to support the development of a detailed kinetic model for its high-temperature combustion. This model needs further validation with other experiments. Ignition delay times of 2-MTHF at high-temperatures have been reported by Wang et al. [46] and the authors also developed a new kinetic model based on the model of Moshhammer et al. [45] and Tran et al. [47]. The improved model accorded well with their experimental results. The combustion chemistry of 2-MTHF in premixed laminar flames and its pyrolysis in a plug flow reactor has also been investigated by De Bruycker et al. [48] who also developed a kinetic model. Recently, Fenard et al. [49] equally studied the oxidation of 2-MTHF in a rapid compression machine. In addition, Fenard et al. [49] have developed a detailed kinetic model with 507 species involved in 2425 reactions. The sub mechanism of Moshhammer et al. [45] is included in the Fenard et al. [49] mechanism with some updated thermochemical data and other improvements. This makes the model more widely validated but still in need of further validation.

The structural differences between unsaturated furans and tetrahydrofurans suggest that their fundamental combustion properties may differ such that the results can be used to further refine chemical kinetic models or to develop generalized correlation for key combustion properties. Further, species concentration measurements during shock tube ignition and pyrolysis have been identified as further validation targets for combustion chemistry models [50]. However, efforts geared toward characterization of furan combustion have not yet made use of this additional shock tube capability. This work comparatively studies kinetics of saturated and unsaturated furans to identify structure-activity trends including species time histories for further model validation.

Some of the selected fuels are focused on identifying ignition-resistant fuels. Highly branched oxygenated hydrocarbons, such as tert butyl ethers can be added to gasoline to increase its ignition resistance while also reducing emissions such as CO. The furans discussed above are also ethers but of the cyclic type. Among specific ethers of interest to SI engines are methyl tert-butyl ether (MTBE) and 2-methyltetrahydr-ofuran (2-MTHF). These are both

C5 ethers, such that the first is aliphatic while the second is cyclic. Being of the same ether class but structurally different, one might seek to understand similarities and differences in their combustion kinetics in connection with their ignition resistance. We might also want to contrast the kinetics of their ignition and pyrolysis.

The combustion properties of MTBE have been investigated in the past, following its introduction as an antiknock replacement of tetraethyl lead in gasoline. The chemical kinetics of its oxidation in static reactor was studied by Brocard et al. [51] over the temperature range of 300-500 °C and at pressures up to 1000 Torr. They confirmed by comparing to other hydrocarbons that MTBE has an inhibiting effect on other hydrocarbon oxidation. Studies of the high-temperature oxidation of MTBE in flow reactors have been reported by Norton et al. [52, 53]. They observed that isobutene is the major intermediate product during oxidation of stoichiometric mixtures at atmospheric pressure and temperatures above 1000 K. The analysis of Norton et al. [53] showed that MTBE decomposes directly to isobutene and methanol. Using jet-stirred reactors [54–56] and a rapid compression machine [57], MTBE oxidation was studied at higher pressures. Further, the effect of MTBE on engine performance and exhaust emissions have been explored [58, 59]. Another study of MTBE kinetics is one by McEnally et al. [60], where the focus is on the hydrocarbon growth pathway of some oxygenated hydrocarbon fuels in nonpremixed flames. With regards to the behavior of MTBE in flames, Van et al. [61] used a molecular beam mass spectrometry in different equivalence ratios to deduce the rate coefficients of H atom abstraction.

Regarding ignition of MTBE, the ignition delay times of the fuel in mixture with oxygen and argon have been measured behind reflected shock waves by Dunphy et al. [62] over the temperature range of 1040-1880 K with pressures of 2, 3 and 4.5 bar. Dunphy et al. [62] found that ignition delay times decrease with increasing fuel concentration. Fieweger et al. [63] studied the shock tube ignition of MTBE-air mixture at conditions similar to those of SI engines. They observed slow initiation of ignition without rapid pressure increase at low

temperatures compared to the rapid pressure increase at higher temperatures. Fieweger et al. [64] considered a classification of ignition into strong initial deflagration at high pressure and mild ignition.

With respect to MTBE as an additive, Gray et al. [65] investigated the high temperature shock tube ignition of propane with MTBE as an additive. He combined MTBE and its decomposition reactions with a propane mechanism to explain the kinetic interaction of MTBE with a typical hydrocarbon fuel. He observed that both the experiments and model demonstrate oxidative inhibition of propane ignition by the MTBE addition.

A detailed kinetic model of MTBE oxidation was presented by Brocard et al. [51, 66] for temperatures below 800 K. Curran et al. [67] then extended the model to higher temperatures resulting in a model with 214 species and more than 400 elementary reactions. Curran et al. [67] also measured ignition delay times for a set of fuel, oxygen and argon mixtures, over the temperature range of 1100-1900 K and equivalence ratios of 0.15-2.4. Under these conditions, they concluded that MTBE decomposes via a unimolecular elimination reaction to form isobutene and methanol. They found that H atom abstraction had only a minor effect on ignition of MTBE. Yasunaga et al. [68] have recently constructed a kinetic mechanism of MTBE for pyrolysis and oxidation [68], comprising of 1051 reactions and 215 species. From their analysis, they also concluded that MTBE decomposes via unimolecular decomposition to produce methanol and isobutene. Isobutene is found to slowly react with reactive atoms and radicals, producing relatively unreactive methyl radicals. Thus, at high temperatures, isobutene formed by MTBE decomposition retards the reactivity of the overall chemical system.

The decomposition mechanism of MTBE has also been studied using quantum chemical calculations at the G3B3 level of theory by Zhang et al. [69]. They calculated the primary and secondary pyrolysis pathways of the main fuel molecule. The primary pyrolysis pathways include formation of isobutene and methanol, CH_4 elimination, H_2 elimination and C-H,

C–C and C–O bond cleavage reactions. Formation of isobutene and methanol is found to have the lowest energy pathway and is characterized by a four-member-ring transition state. The energy barrier for this channel is 62.70 kcal/mol. The secondary pathways show further decomposition of tert-butyl radical, isobutene, methanol and acetone.

From an experimental perspective, Zhang et al. [70] investigated the pyrolysis of MTBE at a pressure of 267 Pa over a temperature range of 700–1420 K, using the tunable synchrotron Vacuum Ultraviolet Photoionization and Molecular-Beam Mass Spectroscopy. Major pyrolysis products such as H_2 , CO, CH_4 , CH_3OH and C_4H_8 were detected. Also identified were radicals such as methyl, methoxy, propargyl, allyl, C_4H_5 and C_4H_7 and isomers of pyrolysis products such as propyne, allene, 1,2,3-butatriene, vinylacetylene, isobutene, 1-butene, propanol, and acetone. Two major pathways for CO formation were identified. One pathway is through the loss of two H atoms from CH_2O at low temperature and the second one is through two steps of CH_3 abstraction from C_3H_6O at high temperatures.

Although MTBE has the ability to retard fuel ignition, its widespread use has been implicated in surface and ground water contamination [71–73]. Therefore, the use of MTBE is being banned or limited in USA. In connection with this, the bioremediation of MTBE has become an active area of research. It is suggested that aerobic biodegradation can decrease the impact of MTBE on water contamination [74, 75]. Combustion research has turned to the exploration of other tert butyl ethers with possibly similar chemical reactivity. The advent of cyclic ethers or furans has expanded the range of possible oxygenated fuel additives [43, 76]. These cyclic ethers can be derived from biomass processing. Among these promising cyclic ethers, tetrahydrofuran derivatives such as 2-MTHF are attractive fuel components. No experimental study has addressed the pyrolysis of 2-MTHF in a shock tube. Further, oxidation and pyrolysis kinetics need to be contrasted for further insight. In addition, there are no studies on the relative kinetic behavior of representative cyclic and aliphatic ethers. These gaps could be filled by comparing the behavior of the two C5 ethers, 2-MTHF and

MTBE.

The furans discussed above are new fuels with complicated processing pathways. There is interest in alcohols from biomass. More mature biomass processing techniques yield alcohols. These alcohols can improve the sustainability of transportation and they present attractive combustion properties such as low emissions and high ignition resistance [77–79]. The short-chain alcohols, methanol and ethanol, often referred to as "first-generation" bioalcohol fuels, have been extensively studied [80, 81]. Drawbacks of these short-chain alcohols are their low energy content and their ability to cause corrosion in engine fuel supply systems [81, 82]. On the other hand, higher molecular weight alcohols, including propanol and butanol, have shown better properties; they are significantly less toxic and less volatile than methanol [83]. Therefore, there is growing interest in higher molecular weight alcohols [84–91]. For optimal performance in engines, some physical properties of the higher alcohols (e.g. boiling point) should be comparable with those of gasoline. Butanol is less volatile than gasoline, while the volatility of propanol is closer to that of gasoline. As a result, propanol isomers are attractive to combustion engines due to their appropriate energy density and favorable fuel volatility. Propanol isomers can be commercially produced via processing petrochemical feed stocks and from fermentation of biomass [92, 93]. In terms of octane numbers as a standard measure of resistance to uncontrolled ignition, conventional gasoline has a research octane numbers (RON) less than 100 while, some bioalcohols have higher RON: for example, ethanol - 108 [94] or 109 [95]; methanol - 109 [95]; *n*-propanol - 105 [94]; and *iso*-propanol - 113 [94].

The engine performance of propanol isomers as potential gasoline additives has been investigated by different research groups in both spark ignition and homogeneous charge compression ignition (HCCI) engines. Results show that propanol isomers can be used in spark ignition engines and lower CO and HC emission could be achieved with them as additives [96, 97]. Combustion of alcohols, such as propanol isomers, have the drawback that they increase aldehyde and ketone emissions [98, 99]. The inhibition effects of a *iso*-propanol additive on

n-heptane HCCI combustion was investigated by Lu et al. [100], and showed that increasing volume fraction of *iso*-propanol addition to 30 - 40% would lead to incomplete combustion. There are some studies showing the potential of *n*-propanol, as a diesel fuel additive [101, 102].

In spite of the many attractive features of propanols, there are a few kinetic studies of their oxidation and pyrolysis. Some of the studies have shown the relative reactivities of the two isomers, establishing the expected trend that *n*-propanol because of the weaker secondary C-H bonds, is more reactive than *iso*-propanol.

A number of experimental studies have reported the oxidation studies of propanol isomers. The structures of counterflow non-premixed flames of *n*- and *iso*-propanol were investigated by Frassoldati et al. [83]. They developed a chemical kinetic model capable of describing the observed profiles. Recently, the intermediate species profiles of premixed flames of propanol isomers were measured [103, 104], determining key differences in their combustion chemistry. Propanol oxidation in a jet-stirred reactor (JSR) at 10 atm over the temperature range of 770 K - 1190 K and equivalence ratios, $\phi = 0.35 - 4.0$ investigated by Togbe et al. [105] and Galmiche et al. [106]. Premixed laminar flames at pressures of 1 - 10 atm were also studied. They found that the two isomers have substantially different major intermediates.

Afterward, Veloo and Egolfopoulos [107] studied counterflow laminar premixed and non-premixed flames of both *n*- and *iso*-propanol to determine isomer effects on their burning velocities and extinction strain rates. Results showed that *n*-propanol premixed flames are faster than those of *iso*-propanol and that the extinction strain rates of *n*-propanol are consistently higher than those of *iso*-propanol in both premixed and non-premixed flames. Some differences were found in analysis of the underlying chemical kinetics such as in *iso*-propanol/air flames, relatively non-reactive allyl radicals formed from higher concentrations of propene, resulted in retarding the overall reactivity of *iso*-propanol. It was found that higher concentrations of formaldehyde in *n*-propanol/air flames lead to the formation of

formyl radicals, thereby enhancing the reactivity. Beeckmann et al. [108] and Gong et al. [109] also studied further laminar burning velocities of *n*-propanol.

With respect to auto-ignition study of the isomers, Johnson et al. [110] measured the ignition delay times of propanol isomers behind reflected shock waves at temperatures of 1350-2000 K, equivalence ratios of 0.5, 1.0 and 2.0, and pressures of 1.2 atm. They found that *n*-propanol is more reactive than *iso*-propanol. The ignition delay times of *n*- and *iso*-propanol under pressures of 1.0 - 12 atm measured by Noorani et al. [84] and Akih-Kumgeh et al. [111], in their comparative investigations of ignition of C1 - C4 primary alcohols and C3 oxygenated hydrocarbons. Man et al. [112] extended the range of test conditions for both isomers and measured the ignition delay times behind reflected shock waves at pressures of 1.2 to 16 atm and temperatures of 1100 - 1500 K. Their study showed that the H-abstraction reactions are mainly responsible for propanol consumption. *n*-Propanol produces ethanol, propene and ethane, while *iso*-propanol produces propene and acetone. The authors also proposed a modified chemical kinetic model based on the earlier model by Johnson et al. [110]. Yang et al. [113] has compared ignition delay times of propanal and propane with those of Man et al. [112].

Little research has been devoted to the pyrolysis of propanol isomers. Among the few studies available, Barnard et al. [114, 115] measured the decomposition rate and products of *n*- and *iso*-propanol using batch reactors. They postulated that fission of the C - C bond is the chain initiation step for *n*-propanol and the primary products are methane and acetaldehyde. It is also suggested that the initial step of *iso*-propanol decomposition involves the splitting the C-H bond adjacent to the C-O bond and the resulting acetone then decomposes into methane and ketene.

More recently, the kinetics and mechanisms for the unimolecular decomposition of *iso*-propanol were studied by Bui et al. [116] using computational chemistry calculations over a wide range of reaction conditions. It was found that at low pressures (below 1 atm), thermal decomposition

proceeds mainly through the concerted dehydration reaction producing $\text{CH}_3\text{C}(\text{H})\text{CH}_2$ and H_2O . At the high-pressure limit and over 1000 K, direct C-C bond scission to produce CH_3 and $\text{CH}_3\text{C}(\text{H})\text{OH}$ becomes dominant.

Later, the pyrolysis of several alcohols, including *iso*-propanol with acetylene, was investigated by Esarte et al. [117] using a flow reactor to examine the effects of alcohol on soot reduction. Measurements and analysis of the detailed chemical kinetic mechanism revealed that *iso*-propanol partially leads to reduction of PAH formation because of alternate favorable decomposition channels that lead to CO and CH_4 formation. Although the resulting C2 and C3 hydrocarbons can possibly contribute to increased PAH and soot formation at the intermediate level, the overall effect of blending with alcohols is a reduction in soot formation.

Heyne et al. [118] carried out decomposition studies of *iso*-propanol and determined the rate parameters of dehydration and C-C bond scission reactions with the goal of validating the theoretical predictions of Bui et al. [116]. The experiments were performed at 12.5 atm pressure and over a temperature range of 976-1000 K in a Variable Pressure Flow Reactor. The study showed that the experimentally determined dehydration rate constants were significantly higher than the predictions of Bui et al. [116]. The pre-exponential factor of Bui et al. [116] was then adjusted to reconcile the discrepancy with their experiment.

Combustion features of propanol and other alcohols as alternative transportation fuel, from renewable sources, have been reviewed by Sarathy et al. [119]. A number of detailed combustion models that are enable to describe the combustion chemistry of both propanol isomers during oxidation and pyrolysis have been developed, such as the models by Johnson et al. [110], Man et al. [112], and Sarathy et al. [119]. However, there are still significant problems in terms of the performance of these chemical kinetic models over a wide range of conditions. The interaction of fuel pyrolysis and oxidation kinetics are not well known. This knowledge could improve the predictions of existing models which have noted differences with measurements at a number of test conditions.

Alkanes: Also of interest in this work is a cycloalkane, which is not well characterized. Various proportion of cycloalkanes exist in transportation fuels, such as conventional diesel ($\sim 30\%$), jet fuel ($\sim 20\%$), automotive gasoline ($\sim 10\%$), and aviation gasoline (20-30%) [120, 121]. Many experimental and modeling studies have been reported for mono-alkylated cyclohexanes such as methylcyclohexane (MCH) [122, 123] and ethylcyclohexane (ECH) [122, 124]. Previous studies on DMCH included the isomerization of *cis*-1,2-DMCH in a single-pulse shock tube by Rosado-Reyes and Tsang [125]. Recently, Kang et al. [126] investigated the ignition process of the isomers, 1,3-DMCH and 1,2-DMCH, as well as ECH in a modified Cooperative Fuel Research engine. This study revealed that both 1,3-DMCH and 1,2-DMCH are less reactive than ECH. The unimolecular decomposition of 1,3-DMCH and 1,2-DMCH in nonpremixed flames was investigated by McEnally and Pfefferle [127]. The study revealed that these dimethylcyclohexanes decompose slower than similar cycloalkanes with unsaturated side-chains. More recently, the pyrolysis of various DMCH structures was studied through theoretical simulations of thermal cracking by Sun et al. [128]. A number of studies have focused on the investigation of dimethylcyclohexane ring opening [129–131] and H-abstraction reactions [132]. However, there are no experimental data and chemical kinetic models for alkylated cycloalkanes with multiple side-chains such as dimethylcyclohexane (DMCH). Improved understanding of the combustion behavior of these cycloalkanes will improve surrogate modeling of fuel blends.

The other group of interest is biodiesel surrogate, represented in this work by methyl propanoate (MP), which can be used to modify the ignition of natural gas. The relative abundance of natural gas and its potential to emit less combustion emissions motivate the development of more combustion systems fueled with natural gas [10, 11, 133]. Methane is the main component in natural gas, thus the fuel is characterized by a higher H/C ratio than other fossil fuels, so that natural gas combustion generally yields comparable thermal energy with less CO₂ emissions than the other fossil fuels characterized by a lower H/C ratio.

Although most transportation systems use spark-ignition engines, their efficiencies are limited by the early onset of uncontrolled auto-ignition of most fuels. In order to increase the efficiencies of transportation engines, advanced compression-ignition engines are considered as a viable solution. Although most natural gas engines used for transportation are spark-ignited, using it in compression-ignition engines will increase the overall efficiency. For effective use of natural gas in compression-ignition engines, combustion initiation poses a problem since the predominant component in natural gas, methane, is resistant to ignition [134]. The ignition propensity can be boosted by blending natural gas with another more reactive fuel.

The interest in natural gas for combustion engines also supplements existing and growing interest in biofuels for combustion systems. Biofuels are of interest because of the possibility to recycle the CO_2 generated during combustion as feedstock for the production of new fuels through photosynthesis. Among biofuels, biodiesel, which can be derived from vegetable oils and animal fat [135, 136], is of interest. Biodiesel can be used in compression-ignition combustion systems where their higher reactivity proves to be an advantage. Blending biodiesel with natural gas can therefore result in a more dependable compression-ignition fuel. Combustion systems designed to use both natural gas and biodiesel can thus be seen as responsibly making the shift from more pollutant fossil fuels to a sustainable energy economy. Compression-ignition engines using natural gas and diesel have been investigated in several studies [137–139]. The studies show stable combustion compared to pure natural gas and reduced emissions compared to diesel. However, this fossil-fuel based solution to the natural gas ignition problem does not promote energy sustainability.

The influence of diesel or biodiesel on natural gas combustion can be investigated directly in engine systems or in fundamental experiments. The latter experiments support the development and validation of models of the controlling chemical kinetics. Compression-ignition engine studies of natural gas and biodiesel have been carried out in the past [10, 113, 140–143]. They also generally point to more stable ignition compared to pure natural gas and

reduced emission levels compared to diesel or biodiesel. There are very limited fundamental experiments aimed at understanding the chemical kinetic interactions involved in natural gas and biodiesel blend ignition. Such fundamental studies would first proceed by using surrogates for natural gas and biodiesel. Small esters have been used to unravel the kinetics of biodiesel combustion [144, 145] and in this work, MP, shown to be a very reactive methyl ester [145], has been chosen to represent biodiesel.

Although each of the two fuels, methane and MP, has been the subject of many chemical kinetic studies, fundamental studies of their chemical interactions and ignition behavior are not sufficiently addressed in the literature. One of the fundamental combustion properties relevant to compression-ignition engines is the auto-ignition behavior which can be studied in shock tubes.

Surrogates and their blends have each been the subject of several experimental and chemical kinetic modeling studies. The use of natural gas in spark-ignition engines has been investigated [11, 146], establishing that with the appropriate logistic modifications, natural gas can be used without problems. In terms of the fundamental combustion properties, such as ignition, the studies of natural gas combustion kinetics has relied on extensive studies of methane [134, 147–155].

Other studies involving methane have examined the effect of composition on natural gas combustion by including other C2-C5 hydrocarbons. The effects of ethane and propane addition on ignition of methane blends has been investigated by Naber et al. [156], demonstrating that the higher hydrocarbons lead to shorter ignition delay times. A chemical kinetic model was also provided. Petersen et al. [149, 157] and de Vries et al. [158] also investigated the effect of propane on methane ignition under lean and stoichiometric conditions, establishing the methane ignition enhancement abilities of propane. The study by Petersen et al. [157] also proposed a chemical kinetic model. In subsequent studies by Petersen’s group and collaborators [159–162], the effect of various C2-C5 alkanes on methane ignition have been investigated,

culminating in an extensively validated chemical kinetic model for C1-C5 hydrocarbons [162]. These studies indicate that adding these higher alkanes to methane leads to reduction in the ignition delay times.

Experimental studies on the autoignition of methyl propanoate have been limited. Akih-Kumgeh and Bergthorson [145] measured autoignition delay times of C1-C4 methyl esters, investigating the structure reactivity trends. In another study, Zhang et al.[163] measured ignition delay times of MP in a shock tube a various conditions. A kinetic model was developed and validated against the ignition delay and the pyrolysis data of Zhao et al.[164]. Recently, Kumar et al.[165] studied the ignition of MP at high pressure and low-to-intermediate temperature conditions in a rapid compression machine. Comparisons of the reactivity of MP to methyl ethanoate and methyl butanoate were made. There are no fundamental studies which explore the chemical influence of MP on the combustion of natural gas or its main component, methane.

One way to examine the mutual kinetic effects of methane/MP blends is to compare the pyrolysis of MP with that of methane/MP blend to see if the presence of methane slows down the kinetics of MP decomposition. Such a study has not been done and studies of pure MP pyrolysis are also limited. Zhao et al. [164] studied the pyrolysis of MP in a laminar flow reactor at low pressures and from this data developed a kinetic mechanism for MP pyrolysis. Farooq et al. [166] measured species time-histories in pyrolysis of MP and ethyl propanoate in a shock tube at temperatures between 1250- 1750 K and proposed a kinetic mechanism. Ning et al. [167] conducted pyrolysis measurements of MP behind reflected shock waves at temperatures between 1292 - 1551 K at 1.6 atm, as well as chemical kinetic modeling to refine the chemical kinetic model of Felsmann et al. [168]. Although these pyrolysis studies yield species time histories, they do not provide global kinetic parameters that can capture the complex pyrolysis kinetics and their dependence on thermodynamic conditions of the reactor. The mail deficiency is the lack of studies of MP and methane kinetics.

1.2.2 Combustion chemistry modeling

To assess the interplay of fluid mechanics and heat release during combustions, chemical kinetic models are needed. Such analysis of chemically reacting flows help in the development of clean and efficient combustors that utilize alternative fuels or their blends with conventional fuels. A chemical kinetic model for methane oxidation [169, 170] was the first detailed hydrocarbon fuel model followed by a model for methanol [171]. Development of kinetic models for larger hydrocarbon have followed, including models for ethene [172], ethane [173] and propane [174]. Development of kinetic models for larger hydrocarbon fuels lead to models of very large sizes in terms of species and elementary reactions. While the early model for methane included about 20 chemical species, models for propane and n-butane [175] included about 100 chemical species and a recent model for iso-octane and heptane has about 1000 chemical species [176].

Implementation of these models in reacting flow analysis is difficult because of these large sizes [177]. So there is a need to develop highly reduced version of these kinetic models. Accurate measurement of concentration time histories of key intermediate species formed during combustion can be facilitate kinetic model development efforts that seek to capture essential kinetic features [178]. A new approach to provide small kinetic models has been proposed by Wang [179]. The proposed hybrid modeling scheme breaks down the combustion of large fuel molecules into a sub-mechanism for pyrolysis and an oxidation mechanism of small molecules. In order to implement this, kinetic features of pyrolysis and how they differ from oxidation need to be well understood. The effects of thermodynamic conditions such as pressure and temperature also need to be studied. This work seeks to provide insight that can facilitate this size-conscious model development.

Apart from the prediction of species time histories, the complexity of chemical kinetic models can be captured in global kinetic properties such as ignition delay times for oxidation in

homogeneous reactors and laminar burning velocities in freely propagating flames. There is no established global kinetic property that can capture the kinetics of pyrolysis. Such a property would be useful given the importance of pyrolysis to combustion processes. The chemical reactions that control pyrolysis are generally also included in oxidation processes such as ignition. Pyrolysis is therefore a limiting case that can be used to isolate the model subset that is controlled by non-oxidative kinetics. Characteristic pyrolysis times can therefore be used to compare pyrolysis and ignition processes in order to determine conditions under which predominantly pyrolytic processes control fuel consumption in ignition. This distinction could also have a bearing on the development of highly reduced chemical kinetic models for realistic transportation fuels, where the kinetic model is supposed to consist of sub models for pyrolysis of large hydrocarbons to form smaller hydrocarbon species and subsequent more elaborate kinetic schemes for the oxidation of these smaller pyrolysis products [180, 181].

1.2.3 Fuel and species concentration using shock tube

Modern combustion research relies on diagnostics that can resolve the associated complex transient phenomena. Using laser-based diagnostics is attractive because they are sensitive, non-intrusive and can have fast response time. While hundreds of species appear during combustion, a few of them are actually crucial to the observed kinetic effects.

It has been recognized in some standard combustion experiments (flow reactors, stabilized flames, etc.) that laser diagnostics can enhance the investigation of fundamental combustion properties [182, 183]. Recent developments in shock tube techniques have therefore expanded the capabilities of the shock tube reactor to include concentration measurements by direct laser absorption [184, 185]. Direct laser absorption relies on signature rotational, vibrational, and rovibrational motions to translate observed laser absorbance to specific species concentrations.

Fuel is one of the major species whose quantification is of kinetic interest. Fuel measurements

rely on the strong absorption feature near $3.39\ \mu\text{m}$ associated with the C-H stretch vibration. A fixed wavelength mid-infrared (IR) HeNe laser is used to diagnose the hydrocarbon fuels at this wavelength.

Tomita et al. [186, 187] used this absorption method to measure iso-octane concentration profiles near the spark plug in a spark ignition engine. They reported the dependence of the absorption coefficient on the temperature and pressure. Klingbeil et al. [188] used this wavelength to investigate the temperature and pressure dependence of the absorption cross sections of a number of fuel representatives including methane, ethylene, propane, n-heptane, iso-octane, n-decane, n-dodecane, JP-10, gasoline and jet-A at temperature of 298 to 673 K and pressure from 500 to 2000 Torr. Haylette et al. [189] and Davidson et al. [190, 191] also used the wavelength to measure concentration time-histories during hexadecane, n-dodecane and n-heptane oxidation behind reflected shock waves. Methane concentration during n-heptane pyrolysis was equally measured by Pyun et al. [192].

A main challenge to fuel concentration measurement is a mid-IR HeNe laser at $3.39\ \mu\text{m}$ is absorbed by fuel and other species containing C-H bonds and interfere with the fuel measurement [193]. This interference is usually accounted for or minimized which will be explained later.

CO is a simple molecule of interest in fuel oxidation as well as in the pyrolysis of oxygenated fuels, such as the propanol isomers considered here. By means of a Quantum Cascade Laser (QCL) system emitting near $4.6\ \mu\text{m}$, the concentration of CO can be measured on the basis of its rovibrational transitions. This laser-based concentration measurement capability makes it possible to investigate high-temperature fuel pyrolysis which is not accompanied by abrupt pressure changes or signature chemiluminescence signals as in the case of ignition. Pyun et al. [194] used Quantum Cascade Laser (QCL) to measure CO time histories during the investigation of dimethyl ether (DME) pyrolysis behind reflected shock waves. Also, CO time-histories during the pyrolysis and oxidation of methyl formate have been measured by

Ren et al. [195]. Ren et al. [196] studied the decomposition of methyl formate and measured five major species including CO at $4.6\text{ }\mu\text{m}$. Camou et al. [197] measured CO time-histories near $4.5\text{ }\mu\text{m}$ using a distributed feedback quantum cascade laser (DFB-QC).

In terms of the fuels investigated with these enhanced shock tube methods, the focus has so far been mostly on non-oxygenated hydrocarbons that feature in conventional transportation fuels. Among bioalcohols, only butanol isomers have received considerable attention [198, 199].

These databases can be used to identify reaction pathways and optimize rate constants in proposed detailed mechanisms for fuel oxidation and pyrolysis. However, there is still a need for species time histories for other relevant fuels, especially biofuels. These data can be used to develop or improve kinetic mechanisms.

1.3 Objectives and organization of thesis

The above review has established the state of research in the chosen area and also revealed some gaps which need to be addressed.

The study of reactivity differences between furans is needed. Similarly kinetic experiments are needed to aid the development of kinetic models for alkylated cycloalkanes, important fuel components.

With respect to other alternative fuels, reactivity differences between propanol isomers need to be brought out. Further, given the abundance of natural gas and its observed ignition resistance, the practice of blending it with more reactive fuels needs experimental support. In this case, the interaction kinetics of methane, and a biodiesel surrogate would be an important contribution. These needs motivate the specific objectives of this thesis.

The specific objectives of the proposed work are to:

- Study the ignition behavior of the target fuels using measured ignition delay times of

2-methyl furan, 2-methyl tetrahydrofuran, dimethylcyclohexane, propanol isomers, and methyl tert butyl ether.

- Develop a database of fuel time-histories during ignition and pyrolysis of tetrahydrofurans, and dimethylcyclohexane.
- Develop and apply CO absorption system and introduce a pyrolysis time based on concentration profiles. Subsequently, demonstrate measurement of pyrolysis times of selected oxygenated fuels: propanol isomers, 2-methyl tetrahydrofuran, methyl tert butyl ether, and methyl propanoate.
- Distinguish between oxidation and pyrolysis kinetics with respect to their temperature dependence.
- Establish the relative ignition behavior of methane (main component of natural gas) and MP (biodiesel surrogate) as well as ignition behavior of blends of the two fuels. This is intended to verify that the ignition of methane can be enhanced by adding MP.
- Analyze and validate literature chemical kinetic models with respect to predictions of ignition delay times, pyrolysis times, and time-histories of selected species.

The dissertation is organized as follows:

Chapter 2 describes the shock tube facility and laser absorption diagnostics, that are used in this work to measure fuel and *CO* time-histories. The associated gas dynamics, determination of reactor conditions, experimental setup description and data processing are then discussed. Furthermore, a characteristic pyrolysis times is defined, based on the laser absorption measurements. Finally, experimental uncertainties are discussed.

Chapter 3 presents global chemical kinetic times measurements. In this chapter the ignition delay times of 2-methyl furan, 2-methyl tetrahydrofuran and dimethylcyclohexane are measured. This chapter also presents pyrolysis times of propanol isomers, methyl tert butyl ether

and 2-methyl tetrahydrofuran in addition to their ignition delay times by means of direct laser absorption. The ignition times of methane, MP and their blend are also presented in this chapter.

Chapter 4 provides fuel and CO time-histories. The first and second parts focus on fuel time-histories during ignition and pyrolysis of 2-methyl tetrahydrofuran and dimethylcyclohexane. The third and fourth parts demonstrate CO time-histories during pyrolysis of propanol isomers, methyl tert-butyl ether and 2-methyl tetrahydrofuran. It ends with CO time-histories during pyrolysis of MP and its blend with methane.

Finally, chapter 5 summarizes the major findings of this thesis and makes suggestions for future work.

Chapter 2. Experimental Methods

2.1 Introduction

This work uses a shock tube reactor equipped with various laser absorption accessories. The shock tube reactor can be used to study chemical kinetics relevant to combustion. Global kinetic properties such as ignition delay times can be measured using the basic set up. By adding laser diagnostic techniques, species time histories can also be measured. In this section, the shock tube technique is presented. The data acquisition and processing procedures are described. Then the relevant fundamentals of laser absorption spectroscopy are presented. This is followed by a discussion of the chemical kinetic simulations used in this work. A consideration of the experimental uncertainties is also presented.

2.2 Shock tube reactor

A shock tube reactor provides precise high pressure and temperature conditions for studying the evolution of chemical systems. The reactor is essentially a long tube divided into driver and driven sections by a diaphragm. The driven or test section is filled with the test gas and the driver section is then pressurized with an inert gas such as helium until the diaphragm bursts. The initial pressure in the shock tube before the experiment is illustrated in Figure 2.1. After the diaphragm ruptures, two waves travel in opposite directions. The first wave is a shock that travels into the low pressure region while the second, the expansion wave, propagates toward the high pressure region. The incident shock wave in the driven section increases the pressure and temperature of the mixture. The pressure and temperature are further increased when the incident shock wave reflects from the end wall of the driven section. Measurements are usually carried out close to the endwall of the driven section, for instance,

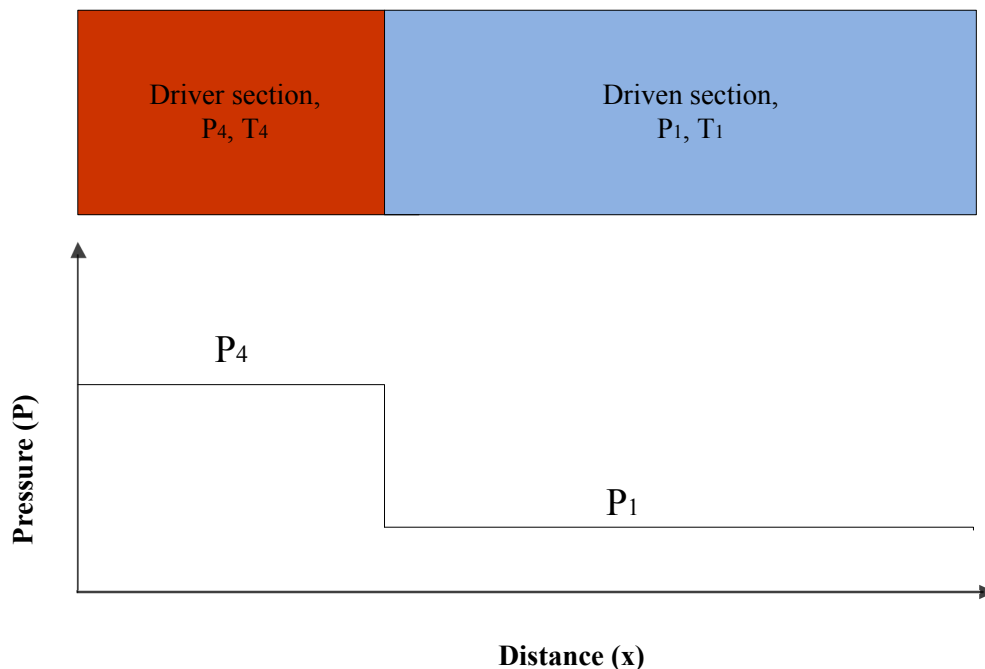


Figure 2.1: Conditions in a shock tube before the diaphragm ruptures.

about 1-2 cm from the endwall in our shock tube, where the established observation time is maximum.

2.2.1 Experimental setup and procedure

The shock tube used in this study has an internal diameter of 10 cm, a driven section of 6.0 m and a driver section of 3.0 m. Research- grade samples of 2-MF, 2-MTHF, DMCH, *n*-propanol, *iso*-propanol, MTBE, methane, and MP are obtained from Sigma-Aldrich, (at least 99 %). The oxygen, argon, and helium used in mixture preparation and shock generation are ultra high purity gases (> 99.999 %) supplied by Airgas.

A 150-liter mixing tank at room temperature (298 K) is used to prepare pyrolysis and oxidation test mixtures based on partial pressures. The tank is first evacuated by a vacuum pump (Edwards, RV12). The tank is equipped with a 100-Torr high-precision MKS Baraton pressure transducer that is accurate to 0.12% of reading. The fuel is then delivered using a

gas-tight syringe and it instantly vaporizes. To avoid fuel condensation, the partial pressure of the fuel in all mixtures is kept at less than 50% of their vapor pressure. For ignition studies, the fuel is mixed with oxygen based on the required equivalence ratio, ϕ , and diluted with argon to obtain the desired argon/oxygen ratio, D. For pyrolysis studies, the fuel is diluted with argon. The mixture is then left to mix by molecular diffusion for at least 12 hours.

To start the experiment, a polycarbonate diaphragm of proper thickness is placed between the driven and driver sections. To remove possible residual impurities, the shock tube is vacuumed out to ultimate pressure of 2×10^{-3} mbar before shock experiments. The leak rate of the tube is very low, typically below 1 Pa/min. For low initial pressure experiments, residual air in the driven section is minimized by flushing this section with the test gas mixture. Afterwards, the test gas mixture is introduced to the driven section to a pressure that is likely to lead to the desired pressure, p_5 . This is estimated based on empirical calculations from validated experiments.

After filling the driven section with the desired amount of the test gas, the valves controlling the driven section are closed. Then, the driver section is filled gradually with helium gas until the pressure difference between the two tube sections causes rupture of diaphragm. A shock wave rapidly forms and propagates to the driven section, increasing the temperature and pressure of the test gas. The shock wave reaches the endwall and reflects toward the driver section, stagnating the test gas, and further increasing the gas temperature and pressure. This provides almost an ideal test environment for combustion kinetics studies. Typical test times of shock tube experiments are on the order of a few milliseconds. The test times are ended by the arrival of the reflection of the rarefaction wave from the end wall of the driver section at the contact surface, causing the decay of the shock. Test times can also be terminated by reflected compression waves from the interaction of the reflected shock wave and the contact surface between the driver and test gas.

2.2.2 Determination of reactor conditions

Accurate determination of pressure and temperature in the reflected shock wave region is very important since reaction rates are sensitive to these. This determination relies on a theoretical consideration of shock tube gas dynamics.

The distance-time diagram of the waves in the shock tube reactor is shown in Figure 2.2. The various regions are indicated by the numbers 1 to 5. Region 1 indicates the initial test gas (T_1 , p_1), region 4 is the initial driver gas at a high pressure and room temperature (T_4 , p_4), region

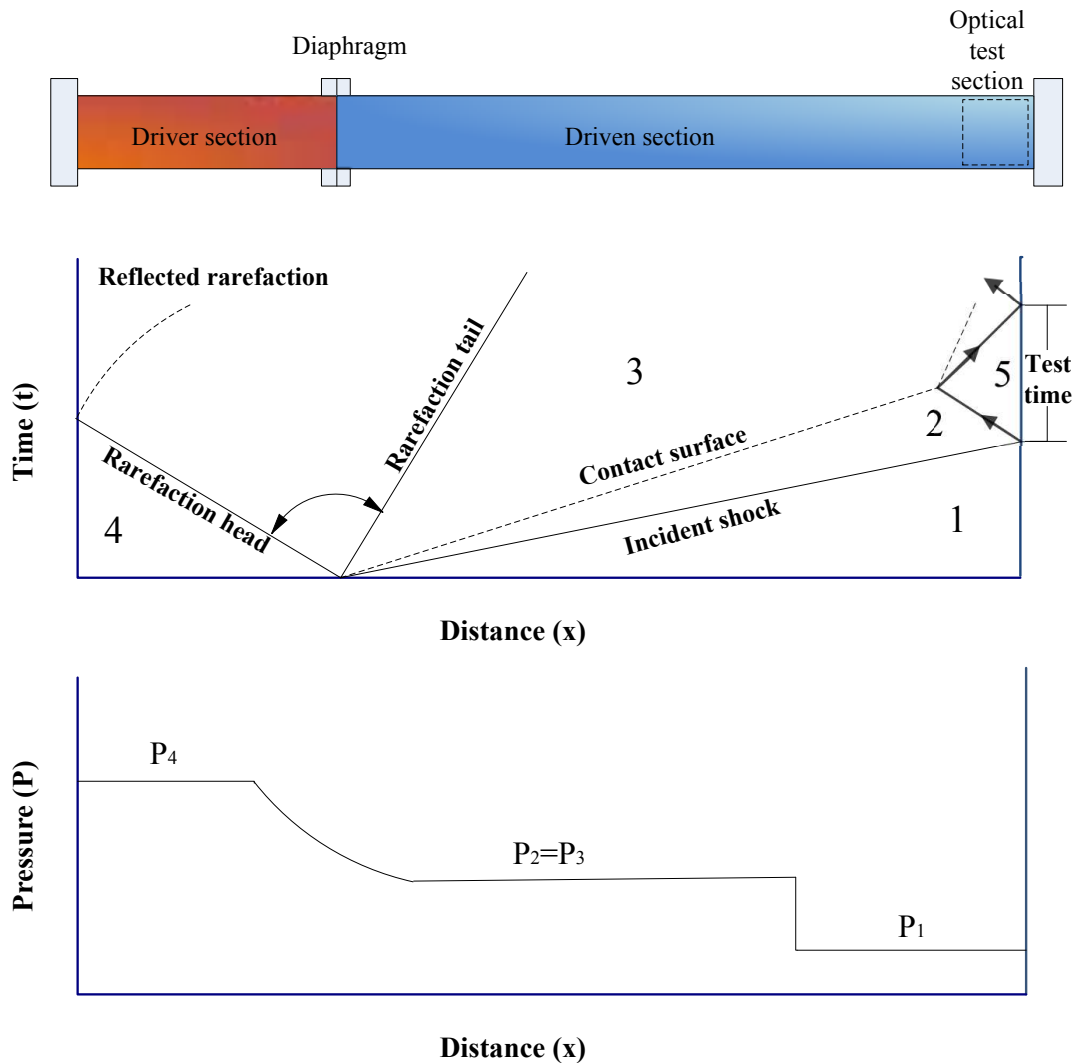


Figure 2.2: Wave processes in the various regions of shock tube after the diaphragm ruptures.

2 is the test gas behind the incident shock (T_2, p_2), region 3 is the driver gas expanding into the driven section (T_3, p_3) and region 5 is the test gas at reflected shock conditions (T_5, p_5). The test time is determined as the time between the reflection of the incident shock wave and the arrival of waves produced by interactions of the reflected shock wave with the contact surface of the driven gas and driver gas as illustrated in Figure 2.2.

The conditions of regions are the initial conditions of a homogeneous constant volume reactor. p_5 can be measured while, measuring T_5 is not easy because of the short test duration (few *ms*). Therefore, the test temperature can be determined using the gas dynamic model of a one-dimensional shock wave. T_2 can be calculated accurately if we know the initial conditions and using conservation equations of mass, energy, and momentum as well as an appropriate equation of state [200] :

$$\rho_1 u_1 = \rho_2 u_2 \quad (2.1)$$

$$h_1 + \frac{1}{2}u_1^2 = h_2 + \frac{1}{2}u_2^2 \quad (2.2)$$

$$p_1 + \rho_1 u_1^2 = p_2 + \rho_2 u_2^2 \quad (2.3)$$

$$p = \rho R_g T = \frac{R_g T}{v} \quad (2.4)$$

Where ρ is density, u is relative velocity, p is pressure, h is specific enthalpy and v is specific volume. The subscripts 1 and 2 denote the low pressure gas and the gas immediately behind the incident shock wave, respectively. At region 5 for temperature above 1000 K and pressure less than 100 atm, where real gas behavior can be neglected, the ideal gas equation of state is appropriate to close the system of equations [201]. Assuming constant specific heat, the shock parameters such as p_2/p_1 and T_2/T_1 can be obtained from the following relations [200]:

$$\frac{p_2}{p_1} = \frac{2\gamma M_1^2 - (\gamma - 1)}{\gamma + 1} \quad (2.5)$$

$$\frac{T_2}{T_1} = \frac{(\gamma M_1^2 - \frac{\gamma-1}{2})(\frac{\gamma-1}{2} M_1^2 + 1)}{(\frac{\gamma+1}{2})^2 M_1^2} \quad (2.6)$$

where T_1 and p_1 are initial temperature and pressure of the test gas, T_2 and p_2 are the temperature and pressure behind the incident shock, γ is the specific heat ratio, and M_1 is the incident Mach number.

The same procedure can be applied to the reflected shock wave between regions 2 and 5 to find p_5/p_2 and T_5/T_2 . Then, the pressure p_5 and temperature T_5 behind the reflected shock can be determined in terms of the initial pressure, temperature, and incident Mach number in the form [200]:

$$\frac{p_5}{p_1} = \left[\frac{2\gamma M_1^2 - (\gamma - 1)}{\gamma + 1} \right] \left[\frac{(3\gamma - 1)M_1^2 - 2(\gamma - 1)}{(\gamma - 1)M_1^2 + 2} \right] \quad (2.7)$$

$$\frac{T_5}{T_1} = \frac{[2(\gamma - 1)M_1^2 + (3 - \gamma)][(3\gamma - 1)M_1^2 - 2(\gamma - 1)]}{(\gamma + 1)^2 M_1^2} \quad (2.8)$$

The relations above are true for gases with constant specific heats, which is not the case. For a real polyatomic gas the specific heats are temperature dependent. In this case, a system of shock equations (2.1 to 2.3) is solved implicitly to calculate T_5 . The NASA polynomial coefficients are used to store and calculate the constant pressure specific heat capacity (c_p), enthalpy (h), and entropy (s) of a fuel:

$$\frac{c_p}{R} = a_1 + a_2 T + a_3 T^2 + a_4 T^3 + a_5 T^4 \quad (2.9)$$

$$\frac{h}{RT} = a_1 + \frac{a_2}{2} T + \frac{a_3}{3} T^2 + \frac{a_4}{4} T^3 + \frac{a_5}{5} T^4 + \frac{a_6}{T} \quad (2.10)$$

$$\frac{s}{RT} = a_1 \ln T + a_2 T + \frac{a_3}{2} T^2 + \frac{a_4}{3} T^3 + \frac{a_5}{4} T^4 + a_7 \quad (2.11)$$

Where the coefficients a_1 to a_7 are provided for each species in thermodynamic files.

The reflected shock temperature and pressure are calculated from equations of motion for the 1D shock wave with known initial pressure, temperature, incident shock speed and mixture composition.

The shock velocity is determined from the shock arrival times at four piezoelectric pressure transducers accurate to 0.12% of reading, distributed at 40-cm interval over the last 1.5 m of the shock tube. A pressure transducer located at 1.0 cm from the end wall is used to measure the pressure of the test gas. For these purposes, a MATLAB code is used. Figure 2.3 shows the determination of the shock arrival time at a pressure transducer. The shock velocity is calculated as the ratio of transducer separation to the arrival time differences between the sensors. The shock velocity at the test located is obtained by extrapolating measured shock velocities to the test cross section, as shown in Figure 2.4 . The shock attenuates because of the boundary layer and other non-ideal effects. Typical shock attenuation rates are about 1%/m. Post-reflected temperatures are determined using the CalTech detonation and shock tool kit [202], embedded in the CANTERA software [203]. It solves the conservation equations of mass, momentum, and energy for the incident and reflected wave as discussed previously.

Uncertainty in the calculated pressure and temperature behind reflected shock wave are related to the determination of shock velocity and initial thermodynamic conditions of the mixture. These uncertainties are addressed below.

2.2.3 Uncertainties in ignition delay times

Uncertainties in measured delay times at a given test conditions depends on the uncertainties of the conditions. Assuming a dependence of ignition delay time (τ) on pressure (p), equivalence ratio (ϕ), and temperature (T) of the form:

$$\tau \propto p^a \phi^n \exp\left(\frac{E_a}{RT}\right) \quad (2.12)$$

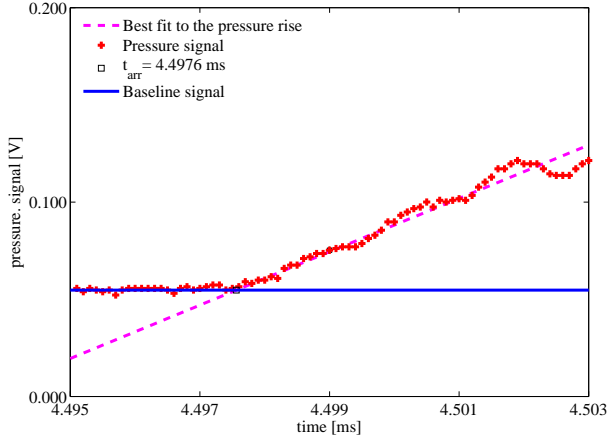


Figure 2.3: Representative shock wave arrival time determination. Shown is the pressure signal near the endwall with corresponding arrival time for a MTHF/O₂/Ar mixture with $\phi = 0.5$, argon/oxygen ratio, $D = 3.76$, $p = 4.7$ atm and $T = 1243$ K.

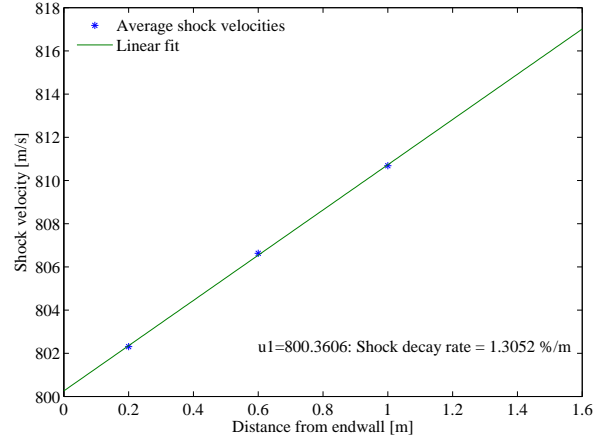


Figure 2.4: Representative shock velocity profile. Shown are shock velocities at midway locations between pressure transducers with a linear fit, for a MTHF/O₂/Ar mixture with $\phi = 0.5$, argon/oxygen ratio, $D = 3.76$, $p = 4.7$ atm and $T = 1243$ K.

Because of its exponential dependence on temperature, the delay time is more sensitive to changes or uncertainties in the calculated post-reflected shock temperature. The calculated temperature is in turn strongly dependent on the incident shock velocity. Hence, uncertainties in the shock velocity which is determined by the distances and time intervals between pressure transducers, are very critical in uncertainties estimation of reflected shock temperature.

Another source of uncertainty in the reflected shock temperature are viscous effects. These viscous effects include the interaction between the reflected shock wave and the incident shock boundary layer. This interaction can cause the reflected shock temperature to increase slowly during the test times. Viscous effects also cause the deceleration of the incident shock velocity. So the observed temperature rise becomes more significant at longer test times and at higher shock attenuation rates. A typical shock attenuation rate is usually about 1% per meter for this shock tube [204]. This means, that the ignition data reported here are less impacted by the temperature rise during induction.

The reflected shock temperature uncertainty analysis is carried out according to the work

by Petersen et al. [205]; assuming that the incident shock speed, V_s , is constant. Based on the 1D shock equations, the reflected shock temperature is a function of the unshocked gas temperature, T_1 , the driven gas specific heat ratio, γ , and the incident-shock Mach number, M , as follows [200]:

$$T_5 = \frac{T_1[2(\gamma - 1)M_1^2 + (3 - \gamma)][(3\gamma - 1)M_1^2 - 2(\gamma - 1)]}{(\gamma + 1)^2 M_1^2} \quad (2.13)$$

In this thesis, argon is used in the driven gas as the main bath gas. It has a specific heat ratio, γ , of 1.67. At an initial temperature of 300 K, equation (2.13) can be approximated as [205]:

$$T_5 = 225.1M_1^2 + 149.85 - 74.99M_1^{-2} \quad (2.14)$$

The Mach number which is a function of the shock velocity, V_s , and the speed of sound in the driven gas is calculated as follows:

$$M_1 = \frac{V_s}{\sqrt{\gamma RT_1}} \quad (2.15)$$

Where R is the specific gas constant. The shock velocity, V_s , can be determined from:

$$V_s = \frac{\Delta x}{\Delta t} \quad (2.16)$$

Δx and Δt are the distance and time between pressure transducers, respectively. The transducer spacing can be measured to 1 mm while the resolution of the fast-response PCB pressure sensor is 1 μ s. The standard root-sum-squares (RSS) method can be used to calculate the uncertainty of shock velocity, δV_s . This means that it is a function of Δx and Δt , and the uncertainty of the temperature behind the reflected shock wave that is only a function of

the Mach number for the driven gas as follows [205]:

$$\begin{aligned}\delta V_s &= \sqrt{\left(\frac{\delta V_s}{\delta(\Delta x)}\delta_{\Delta x}\right)^2 + \left(\frac{\delta V_s}{\delta(\Delta t)}\delta_{\Delta t}\right)^2} \\ &= \sqrt{\left(\frac{1}{\Delta t}\delta_{\Delta x}\right)^2 + \left(\frac{-\Delta x}{\Delta t^2}\delta_{\Delta t}\right)^2}\end{aligned}\quad (2.17)$$

$$\delta_{T_5} = \frac{\partial T_5}{\partial M_1}\delta_{M_1} = (450.19M_1 + 149.98M_1^{-3})\frac{\delta_{V_s}}{\sqrt{\gamma RT_1}} \quad (2.18)$$

Then, uncertainty analysis is performed for ignition delay time. Based on the equation (2.12), ignition delay time correlation can be expressed as follows:

$$\tau = Ap^a\phi^n \exp\left(\frac{b}{T}\right) \quad (2.19)$$

Thus, the uncertainty of ignition delay times from temperature and pressure uncertainties using the standard root-sum-squares (RSS) method, can be calculated from:

$$\delta_\tau = \sqrt{\left(Ae^{\frac{b}{T}}ap^{a-1}\delta_p\right)^2 + \left(Ae^{\frac{b}{T}}p^a\frac{b}{T^2}\delta_T\right)^2} + f(\phi) \quad (2.20)$$

Where δ_p and δ_T are pressure and temperature uncertainties, respectively. The last term accounting for uncertainty in ϕ can be neglected for a mixture of given ϕ used in a series of experiments.

2.2.4 Simulation of the shock tube reactor

An appropriate gas-dynamic model of the chemical reactor is needed to represent shock tube experiments so that the experimental data can be used to validate chemical kinetic

simulations. In this work a homogeneous, constant volume and constant internal energy model will be used for modeling all shock tube experiment. This is contrasted in some cases by a constant pressure and constant enthalpy reactor. One-dimensional analyses anticipate that the gas behind the reflected shock wave has uniform thermodynamic properties and is stationary during the experiment. The mathematical problem is therefore one of the solving a system of coupled ordinary differential equations, yielding time histories of the state variables such as T , p and species concentrations. Here, simulations are carried out using the CANTERA software package. Chemical kinetic simulations using appropriate mechanisms enable us to simulate ignition delay times and species concentration profiles in order to compare predictions with observations.

2.3 Laser absorption diagnostic

The fuel and CO time histories pursued in this work, use direct laser absorption spectroscopy. Laser absorption spectroscopy relies on the quantized nature of atomic and molecular motion. Regarding the species to be monitored and the laser wavelength, a database research has been carried out. Figure 2.5 illustrates a part of the spectrum in the mid-IR region with the location of strong absorption bands of selected species. Laser absorption measurements in this thesis are focused on fuel and species concentration measurements using a fixed wavelength He-Ne laser at $3.39 \mu\text{m}$, and CO using a QCL at $4.56 \mu\text{m}$. The fuel measurement at $3.39 \mu\text{m}$ focuses on C-H bond stretch absorption bands in this wavelength region. Since C-H bond activities are a general feature of hydrocarbons, substantial interference poses a challenge to specific species measurement. Correction are required for fuel measurement at $3.39 \mu\text{m}$.

Absorption occurs when there is transition from a low quantum level to a higher level as a result of energy transfer from the radiation field to the molecule or atom, as described in the Planck's law:

$$\Delta E = E_{upper} - E_{lower} = h\nu = \frac{hc}{\lambda} \quad (2.21)$$

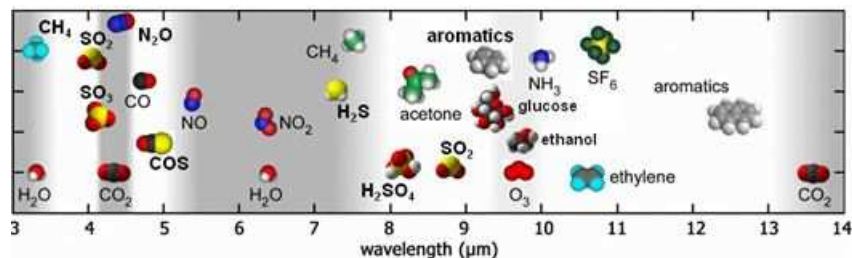


Figure 2.5: Strong absorption bands of various molecules in the IR wavelength range.

Selection rules determine which transitions are physically allowed. There are three basic types of motion: translations, vibrations and rotations. The type of transition depends on the wavelength of the light: electronic transitions occur in the UV and visible light, vibrational transitions occur in the Infrared (IR) and pure rotational transitions in the microwave region. Combined rotational and vibrational transitions are possible in the IR region.

Absorption of IR radiation leads to the vibrational excitation of the atoms of a molecule. This excitation results in the stretching and compressing of bonds length. The bond vibration is similar to spring in classical harmonic oscillator. The quantized energy of a vibration is given by:

$$E_\nu = h\nu \left(n + \frac{1}{2} \right) \quad n = 0, 1, 2, \dots \quad (2.22)$$

Where n is the vibrational quantum number, h is Planck's constant ($6.626 \times 10^{-34} \text{ J.s}$), and ν is the frequency of the vibration given by:

$$\nu = \frac{1}{2\pi} \left(\frac{k}{\mu} \right)^{\frac{1}{2}} \quad (2.23)$$

Where k is the force constant and μ is the reduced mass of two vibrant parts with masses m_1 and m_2 , given by:

$$\mu = \frac{m_1 m_2}{m_1 + m_2} \quad (2.24)$$

The transition between the vibrational levels are governed by a selection rule requiring that

$\Delta n = \pm 1$. For absorption experiments, $\Delta n = 1$.

Rotational motion can also absorb energy. A rotating molecule can be treated as a rigid rotator, consisting of two point masses m_1 and m_2 at fixed distances from their center of mass. The quantized energy of a rotation is given by:

$$E_J = \frac{h^2}{8\pi^2 I} J(J+1) \quad J = 0, 1, 2, \dots \quad (2.25)$$

Where J is the rotational quantum number, I is moment of inertia given by:

$$I = \mu r^2 \quad (2.26)$$

Where μ is the reduced mass. The energy can be more conveniently expressed in wavenumber units as:

$$\bar{E}_J = \frac{E_J}{hc} = \frac{h}{8\pi^2 I c} J(J+1) \quad (2.27)$$

This rotational energy also can be written as:

$$\bar{E}_J = \bar{B} J(J+1) \quad (2.28)$$

Where B is the rotational constant of the molecule. The barred symbol is used to emphasize the unit of wavenumber, cm^{-1} . The transition among the rotational levels are subject to a selection rule requiring that $\Delta J = \pm 1$.

In this work, we will focus on the mid infrared (mid-IR) region, where combined rotational and vibrational transitions occur and relevant fixed wavelength lasers can be found with reasonable energies. Within the transition for the rigid rotor-harmonic oscillator model, the

total energy of combined rotational and vibrational energy of a molecule is given by:

$$E_{vib,rot} = h\nu \left(n + \frac{1}{2} \right) + hc\bar{B}J(J+1) \quad (2.29)$$

In absorption spectroscopy, a beam of light at a frequency, ν , is passed through the gaseous media, where target gas species can absorb some of it, if the wavelength is adjusted to an absorption feature of the species of interest. Quantification of the population density of interest can be achieved by using the Beer-Lambert's Law:

$$-\ln \left(\frac{I}{I_0} \right)_{\nu} = \alpha_{\nu} L = \sigma(\lambda, P, T) N L \quad (2.30)$$

Where I is the transmitted laser intensity through the shock tube in the presence of absorbing species and I_0 the transmitted laser intensity without the presence of the absorbing species, α is the absorption coefficient with units of inverse length. The quantity, αL , is known as the absorbance and L is path length. Expressing the absorption coefficient in terms of the absorption cross-section, σ [$cm^2/molecule$], number density of the absorbing species, N [$molecule/cm^3$], defined in terms of the mole fraction x , total pressure, p , and temperature, T , $N = \frac{xp}{RT}$, gives a direct relation between the concentration of the absorbing species in the medium and the absorbance.

For fuel measurement, we start with a mixture in which the concentration is known. If pressure and temperature are constant then cross-section can be calculated. On the other hand, for species formed with unknown concentration at any time, theory can be used to determine cross-section needed to convert absorbance to concentration.

For this the Beer-Lambert's law can also be expressed as:

$$-\ln \left(\frac{I}{I_0} \right)_{\nu} = S(T) N \phi_{\nu} L \quad (2.31)$$

Where S [$cm^{-1}/molecule\ cm^{-2}$] is the line-strength of the specific transition and ϕ_ν is the line-shape function [cm]. Thus, the absorption cross-section can be inferred from equations (2.30) and (2.31) as:

$$\sigma = S(T) \phi_\nu \quad (2.32)$$

The line-strength is a function of the temperature as:

$$S(T) = S(T_0) \frac{Q(T)}{Q(T_0)} \left(\frac{T_0}{T}\right) \exp\left[-\frac{hcE''}{K} \left(\frac{1}{T} - \frac{1}{T_0}\right)\right] \left[1 - \exp\left(\frac{-hc\nu_0}{KT}\right)\right] \left[1 - \exp\left(\frac{-hc\nu_0}{KT_0}\right)\right]^{-1} \quad (2.33)$$

where $Q(T)$ is the partition function of the absorbing molecule, E'' [cm^{-1}] is the lower-state energy, and ν_0 [cm^{-1}] is the line-center frequency,

The line-shape function is determined by various spectrum broadening process. The line-shape function is often calculated with a Voigt function that captures Doppler and collisional broadening of the spectrum as:

$$\phi_\nu(\nu_0) = \frac{2\sqrt{\ln 2}}{\Delta\nu_D\sqrt{\pi}} \exp(a^2) \operatorname{erfc}(a) \quad (2.34)$$

a (a non-dimensional parameter) is expressed as:

$$a = \sqrt{\ln 2} \frac{\Delta\nu_c}{\Delta\nu_D} \quad (2.35)$$

The full-width of the Doppler-broadened spatial frequency spectrum at half of the maximum line strength is given by:

$$\Delta\nu_D, cm^{-1} = \nu_0 \sqrt{\frac{8kT\ln 2}{mc^2}} \approx 7.1623 \times 10^{-7} \nu_0 \sqrt{\frac{T}{M}} \quad (2.36)$$

Where c [cm/s] is speed of light, and k [J/K] is the Boltzmann constant, and M [g/mol] is the molecular weight of the absorbing species. The full-width of the collisional-broadened spatial frequency spectrum at half of the maximum line strength is given by:

$$\Delta\nu_c, cm^{-1} = p \sum_i x_i 2\gamma_i \quad (2.37)$$

Where p is the total pressure, x_i is the mole fraction of the i th bath gas collision partner and γ is the broadening coefficient for collisions of the i th bath gas with the absorbing species. The collisional broadening coefficient is defined as:

$$\gamma_i(T) = \gamma_i(T_0) \left(\frac{T_0}{T} \right)^{n_i} \quad (2.38)$$

where T_0 is the reference temperature (296 K) and n is the collisional temperature coefficient for collisions of the i th bath gas with the absorbing species.

2.3.1 Uncertainties in direct laser absorption measurements

The uncertainty of direct laser absorption measurements, is estimated using standard root-sum-squares (RSS) method [206]. The result, y , of the experiment is assumed to be determined from other input quantities represented by:

$$y = y(x_1, x_2, x_3, \dots, x_n) \quad (2.39)$$

Then, the uncertainty could be calculated as following:

$$\delta y = \sqrt{\left(\frac{\partial y}{\partial x_1} \right)^2 dx_1^2 + \left(\frac{\partial y}{\partial x_2} \right)^2 dx_2^2 + \left(\frac{\partial y}{\partial x_3} \right)^2 dx_3^2 + \dots + \left(\frac{\partial y}{\partial x_n} \right)^2 dx_n^2} \quad (2.40)$$

In this work, fuel and CO time histories were measured using direct laser absorption spectroscopy. The primary sources of fuel measurement uncertainty, are laser noise and uncertainty in initial fuel mole fraction. A band-pass filter is used to reduce the noise by preventing signals at unwanted frequencies from getting through as well as optimizing the signal-to-noise ratio. To eliminate the effect of fuel adsorption, the partial pressure of the fuel is kept at less than 50% of their vapor pressure.

As per Beer's law equation (2.30) and having $X = \frac{A}{\sigma L \frac{p}{RT}}$, the fuel mole fraction is a function of absorbance (total absorbance and absorbance of interfering species), absorption cross-section, pressure, temperature and path length. Therefore, the uncertainty in fuel mole fraction is calculated by the same method described in equation 2.40. The error in the cross section obtained in shock tube experiments also, is calculated from propagated uncertainties in the measured quantities:

$$\delta\sigma = \sqrt{\left(\frac{\partial\sigma}{\partial I}\right)^2 dI^2 + \left(\frac{\partial\sigma}{\partial I_0}\right)^2 dI_0^2 + \left(\frac{\partial\sigma}{\partial T}\right)^2 dT^2 + \left(\frac{\partial\sigma}{\partial p}\right)^2 dp^2 + \left(\frac{\partial\sigma}{\partial L}\right)^2 dL^2} \quad (2.41)$$

The uncertainty of CO concentration time histories comes from several sources including the initial reactor temperature, initial reactor pressure, absorption cross-section, absorbance, and absorption path length. The total CO mole fraction uncertainties, is also calculated by the propagation and **the estimated uncertainties in the reported data will be discussed later.**

2.4 Data processing

2.4.1 Ignition delay time measurements

During the ignition process, the concentration of radical species such as CH significantly increase. Thus, one way of measuring the ignition delay time is to identify the sudden increase

in CH concentration. This can be obtained by measuring the emission light of excited CH radicals as they deactivate toward ground state CH radicals.

In this work, photodiodes equipped with 430 ± 10 nm narrow band filters are used to obtain CH chemiluminescence signals for ignition delay time determination. The ignition delay time in the shock tube is defined as the time between the pressure rise due to the arrival of the shock wave at the endwall and the maximum gradient of the photodiode signal, which is located at the end wall. An example of the pressure and CH chemiluminescence signals utilized to determine the ignition delay times is shown in Figure 2.6 for the ignition delay time of a stoichiometric mixture of 2-MTHF/ O_2 /Ar at a pressure of 3.35 atm and temperature of 1179 K.

By varying the fill pressure, different strengths of the shock wave, hence reactor temperatures can be established with fairly comparable final reactor pressures. The temperature sensitivity of the ignition can then be judged by plotting ignition delay time (τ) vs. $1/T$ to reveal Arrhenius behavior. This is usually done by plotting τ on a logarithmic scale.

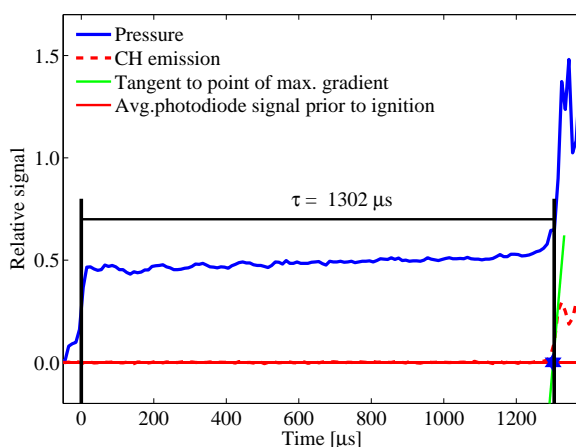


Figure 2.6: Representative ignition delay time measurement. Shown are the sidewall pressure and CH emission signals, for a 2-MTHF/ O_2 /Ar mixture with $\phi = 1.0$, $p = 3.35$ atm, $T = 1179$ K and ratio of argon to oxygen, D , is 3.76.

2.4.2 Species time-history measurements

Fuel concentration time histories during ignition and pyrolysis are measured by direct mid-infrared laser absorption using a fixed wavelength He-Ne laser at $3.39 \mu\text{m}$ as discussed before. The laser used in this study is a He-Ne laser from Newport and the intensities are measured using 1 MHz photovoltaic detectors (PVI-4TE-5-1X1) from Vigo systems.

A schematic of the experimental setup is shown in Figure 2.7a while a representative recording of the reference and transmitted laser intensities is shown in figure 2.7b for a stoichiometric ignition event of the 2-MTHF at a pressure of 3 atm and temperature of 1179 K. A monochromatic source with wavelength λ passes through the window of the shock tube of length L , and the incident light, I_0 , and transmitted light, I , are measured with photo detectors as shown in 2.7a. The amount of light attenuation can be associated with the mole fraction, X , of the absorbing species using Beer's law (2.30).

The intensity of the HeNe laser fluctuates over the time. Common mode rejection (CMR) is used to minimize uncertainty related to laser stability and noise. CMR is achieved by

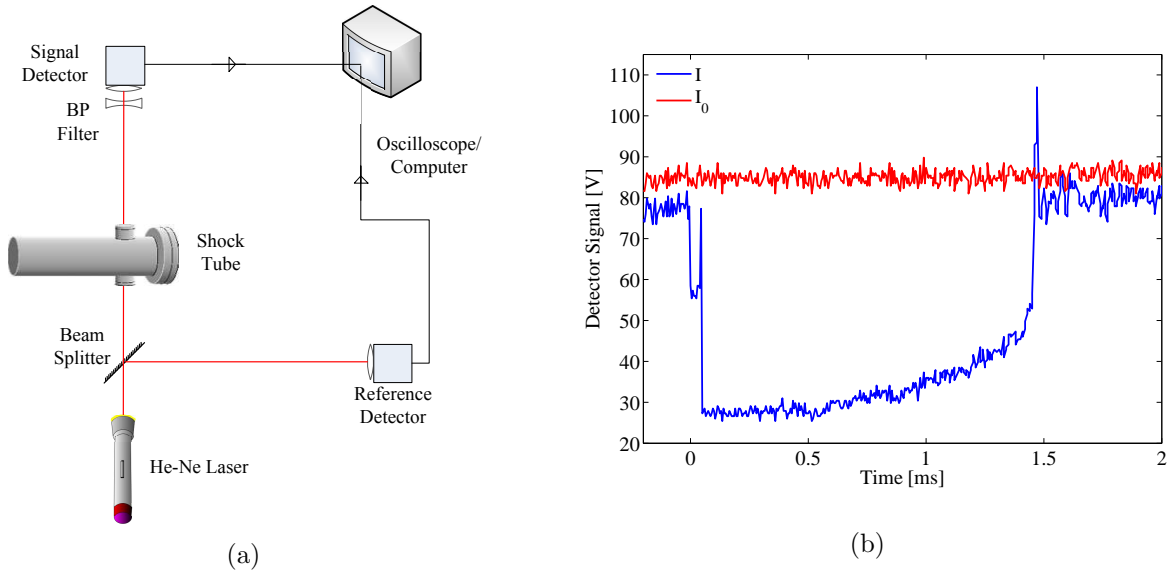


Figure 2.7: a) Laser absorption experimental setup. b) Representative photo detector signals for a 2-MTHF ignition experiment at pressure 3 atm and $T=1179 \text{ K}$.

using a beam splitter to direct 50% of the laser to the reference detector and the rest to the transmitted signal detector. Assuming a constant ration between the two detector signals, the absorbance now become:

$$A = \ln \left(\frac{I_{ref} \times I_{sig,0}}{I_{sig} \times I_{ref,0}} \right) \quad (2.42)$$

Where I_{sig} and I_{ref} refer to signal and reference intensity. For fuel measurements, since the initial concentration is known and both pressure and temperature remain fairly constant during the experiments, the required cross-section for fuel absorption is measured. This is achieved by passing a laser beam at a single wavelength through the tube where the species mole fraction, temperature, pressure and path length are known.

The absorption cross-section, σ , is determined under similar pressure and temperature conditions before it is used to deduce species mole fractions from absorbance measurements. Accurate species concentration measurements require that absorption of the laser beam by interfering species be minimized or correctly accounted for. In this work, absorption cross-section measurements are carried out in the shock tube at different conditions of pressure and temperature (before experiments, after the incident wave, and after reflected shock wave), making use of the known composition of the test mixtures which are prepared by partial pressures. For fuel concentration measurement during ignition or pyrolysis, the absorption cross-section measured behind the post-reflected shock wave is used to determine the concentration profile.

It should be noted that separate measurements of absorption cross-sections in a heated gas cell prior to shock tube experiments can not be used for these high-temperature measurements. Since most absorption cross-sections are temperature-dependent, such measurements are only useful for low-temperature diagnostics (<400 K) where there is no danger of the fuel rapidly decomposing during absorption cross-section measurements. Above 400 K, the reference mixture needs to be heated instantaneously and the absorbance needs to be measured before

the onset of thermal decomposition. This rapid heating is achieved in shock tubes and cross-sections are determined by taking advantage of the fact that the concentration is known from prior mixture preparation by partial pressures.

The cross-sections, as observed in previous work on a number of hydrocarbons [207–209], can decrease as the shock pressures and temperature increase. In previous studies, it was observed that the cross-sections of cyclohexane, naphthene and aromatic hydrocarbons decreased with jointly increasing temperature and pressure. This contrasts with *iso*-octane that shows a complex dependence on pressure and temperature [208].

Because of species interference in absorbance of mid-IR HeNe laser at $3.39\ \mu\text{m}$ [193], there are two ways in which the measured absorbance can be used for model validation. The first would be to determine all hydrocarbons with non-negligible concentrations and high absorption cross-sections at each time, determine their cross-sections and compute the combined absorbance based on simulated concentrations. This absorbance can then be compared directly with the measurements. Such comparison can only establish that the induced hydrocarbons are possibly well predicted. The second option is to assume that the temporal chemical structure of the reactor displays a certain similarity and use the simulated concentrations of interfering species to correct the raw absorbance. The case against this method is that the method is circular. One can admit the circularity but point to the pragmatic value of such comparison. It can be shown here that such corrections based on the assumption of a self-similar chemical structure of the reactor does not mask cases where models fail to capture the global reactivity time scale. The raw absorbance data is made available to modelers who may prefer the first approach to validation.

In this second approach, a chemical kinetic model is used to predict the mole fraction of most important interfering species as successfully done in other studies [193, 210]. While this may be seen to inadmissible if one seeks to validate said model, it has the virtue of reducing the otherwise high uncertainty that would result from assuming that interferences are negligible.

This is particularly important during fuel pyrolysis where such intermediates are expected to accumulate to a greater extent.

The other species time-history measured in this work is CO. Measurement of CO near $4.6\ \mu\text{m}$ is carried out using a Thorlabs QCL system (Model QD4580CM1) powered by a Thorlabs diode laser driver (Model ITC4005QCL). The laser injection current is adjusted to effect emission at $2179.8\ \text{cm}^{-1}$, corresponding to the R9 line of CO rovibrational transition. Absorption near this fundamental band, similar to that at other bands near $4.6\ \mu\text{m}$, is orders-of-magnitude stronger than at the overtone bands [211, 212]. From literature review and exploration of the HITRAN database, it has been ascertained that there are no strong interfering absorption bands near the chosen wavelength. To ensure stability of the laser beam, a beam splitter is used to focus a reference beam onto a photo detector in front of the shock tube while the other beam is transmitted through the reactor. Since there is no CO in the shock tube prior to the start of fuel pyrolysis, laser stability is confirmed through constant profiles of the reference and transmitted laser beams prior to arrival of the reflected shock wave at the test location.

The absorbance of CO is obtained from the experiments. The concentration of CO is unknown. With the equations given in section 2.3, the line shape function can be evaluated and together with the line strength at the central frequency, the measured absorbance can be converted into CO concentration. The line strength at this frequency and at a given reactor temperature is obtained from online HITRAN resources [213]. For the collisional broadening, self broadening and air broadening coefficients are also taken from online HITRAN resources [213] while collisional broadening parameters for CO–Ar taken from Thibault et al. [214] and used to determine the collisional broadening at given reactor pressure and temperature. The Doppler broadening FWHM is determined for the given reactor temperature. The required line shape is then determined from equation (2.34).

2.4.3 Characteristic chemical kinetic time scale of pyrolysis

It is necessary to capture the global kinetics of fuel decomposition in a characteristic kinetic time. In this thesis, it is demonstrated that a pyrolysis time can be obtained from the measurement of the absorbance of a single stable product of pyrolysis. Target product species can be any small stable molecule of the C0-C2 systems, such as C_2H_4 for non-oxygenated and oxygenated fuel pyrolysis or CO in the case of oxygenated fuel pyrolysis. This pyrolysis time can serve as a global assessment of the kinetics of non-oxidative fuel breakdown. It also enables the investigation of effects of thermodynamic conditions (pressure, temperature, and fuel concentration) and chemical structure on the rate of fuel breakdown. Compared to ignition delay times, the pyrolysis time can further enable us to distinguish between regimes of predominantly oxidative and predominantly non-oxidative fuel consumption kinetics. The proposed global kinetic characterization of pyrolysis through a pyrolysis time is demonstrated here by investigating the pyrolysis of propanol isomers using CO absorbance measurements. It is later used in studying the pyrolysis of MTBE, MTHF, and MP.

CO emerges from the pyrolysis of oxygenated fuel as a result of a chain of reactions. Figure 2.8 is a representative reaction pathway for CO production during pyrolysis of *n*-propanol, based on the chemical kinetic models by Sarathy et al. [119] and Johnson et al. [110]. Both models are analyzed at the instance where 20% of the initial fuel mole fraction is consumed. It is observed that both models display three main channels leading to CO production from the initial fuel molecule. Among these channels, fuel decomposition is initiated by direct C-C bond scission and H-abstraction by atomic hydrogen and other radicals, such as CH_3 and OH. At the considered instant, the contribution from C-C bond fission (7 - 18%) is less than contributions from H-abstraction (with over 30%). The three channels from the fuel lead to the formation of formaldehyde from which CO emerges after further intermediate reactions. This analysis indicates that during propanol pyrolysis there is a correlation between the fuel left in the system and the CO produced.

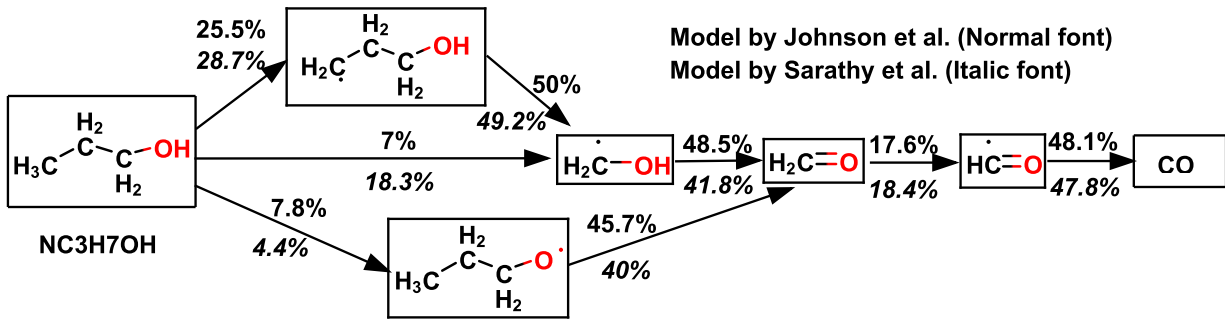


Figure 2.8: Reaction pathway for CO production during *n*-propanol pyrolysis (1% fuel, 3 atm and 1450 K) from models by Johnson et al. [110] and Sarathy et al. [119]. Instant at which 20% fuel is consumed.

To arrive at the definition of a pyrolysis time scale, we may first define the concept of a concentration correlation function, f_{cc} , choosing two chemical species such that one is being formed while the other is consumed. It is motivated by the observation that there are no signature species time histories which feature distinct maxima by means of which characteristic times can be defined. During ignition, on the contrary, excited CH and OH emission signals are used to clearly determine ignition delay times. The proposed correlation function involving a species being consumed and one that is being formed, will necessarily feature a maximum which can be used to determine a time scale that is representative of the underlying complex chemical kinetics.

The f_{cc} for species i and j is simply the time-dependent product of their mole fractions:

$$f_{cc} = X_i X_j \quad (2.43)$$

To use this function for combustion analysis, a good candidate for the species being consumed is the fuel and for oxygenated fuels, that being formed could be CO. Measurement of fuel concentration by direct laser absorption generally relies on C-H bond stretch activity at 3.39 μm . This process of fuel concentration measurement is complicated at later times owing to increasing interfering absorption by other hydrocarbon intermediates as discussed previously.

An appropriate correction method is needed. Although there are proposed methods for correcting these interferences [215–217], adopting one of them could complicate the process of obtaining a simple chemical time scale as pursued in this work. Regarding the species being formed, one can focus on C1-C2 species such as CO and C_2H_4 which can exhibit strong absorption bands without significant interference from other species. A possible way out of the fuel measurement problem is to focus on the species being formed and postulate a relation between its rate of formation and the unknown fuel concentration. For instance, we can postulate a proportional relation between fuel concentration and the rate of CO formation:

$$\frac{dX_{CO}}{dt} \propto X_{fuel}$$

Thus, we can redefine f_{cc} and associate the maximum of this function with a characteristic pyrolysis time. That is, f_{cc} is now approximated through:

$$f_{cc} = const. X_j \frac{dX_j}{dt} \quad (2.44)$$

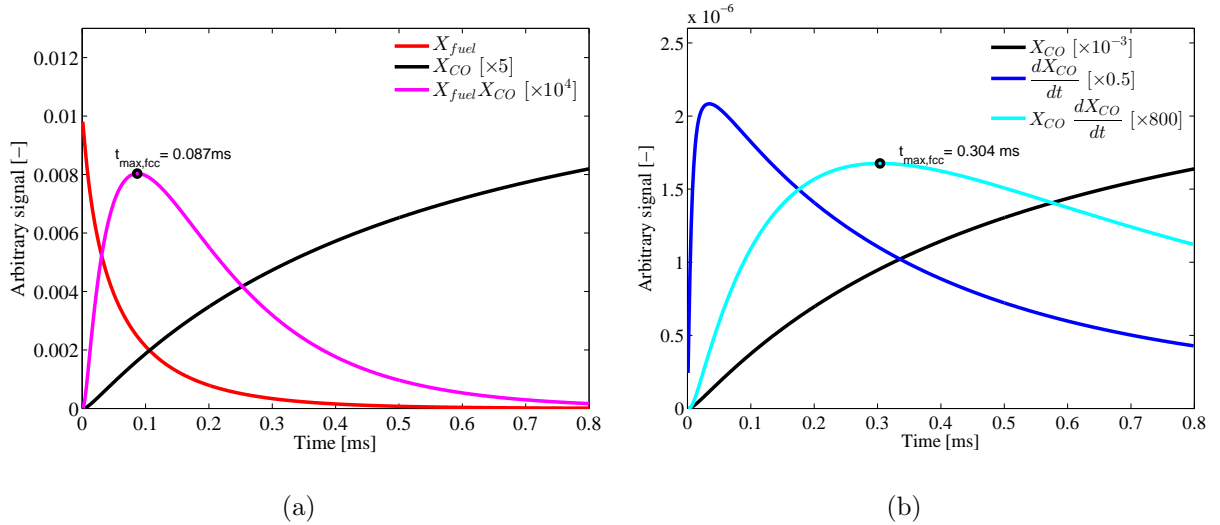


Figure 2.9: Pyrolysis time definition on the basis of product species time-histories during pyrolysis. Shown are results from simulations of 1% iso-propanol in argon at 1450 K and 12 atm using the model by Johnson et al. [110]. In 2.9a, the time is based on maximum of $X_{fuel} X_{CO}$, whereas in 2.9b, it is based on product of X_{CO} and its rate of production.

A suitable chemical time scale that captures the global kinetics of pyrolysis is then obtained as the maximum of concentration correlation function in Eqs. 2.44. By means of this chemical time, we can investigate the effects of temperature, pressure, and fuel concentration on pyrolysis. This is illustrated in Figure 2.9, where the pyrolysis of *iso*-propanol is considered at a pressure of 12 atm and a temperature of 1450 K. The figure is based on a simulation using the model by Johnson et al. [110]. Figure 2.9a is the case where the time could be determined as the time to maximum of f_{cc} based on fuel and the pyrolysis product, CO. This can be contrasted with Figure 2.9b where the fuel concentration is represented through $\frac{dX_{CO}}{dt}$. The two characteristic times are not quantitatively the same, the latter being longer; but if the method is applied to study parametric effects on pyrolysis, they yield the same sensitivities to temperature, pressure, and fuel concentration as would be obtained with the original fuel-based f_{cc} .

Since the emphasis is on a chemical time, the measured absorbance can be used to determine the time without necessarily converting the absorbance to the associated mole fraction. This conversion requires an accurate absorption cross section but the time to the maximum of the

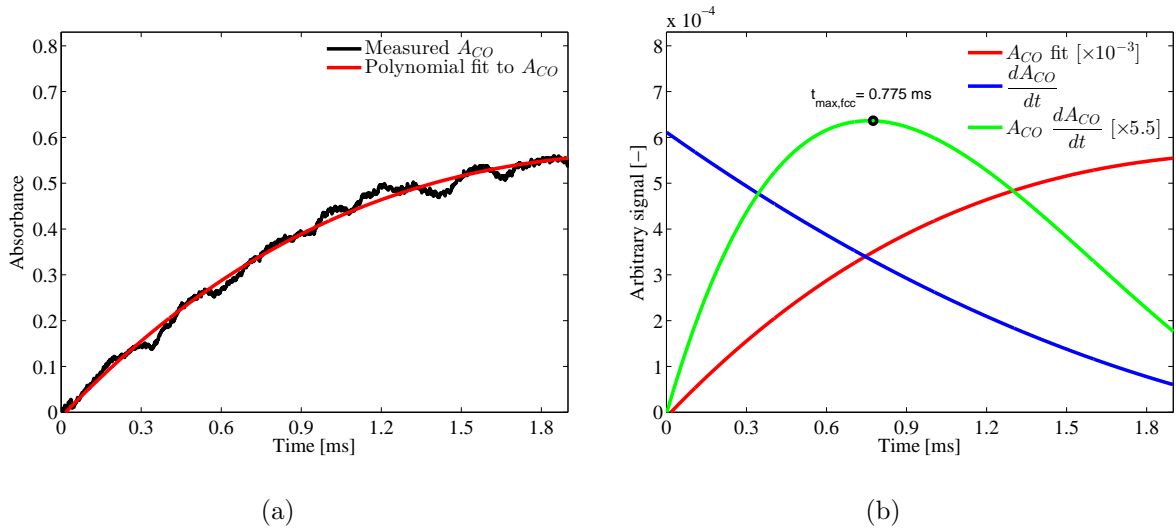


Figure 2.10: Determining a pyrolysis time scale from an experimental realization of *iso*-propanol pyrolysis in the case of 1% *iso*-propanol in Ar at 1395 K and 3.6 atm. a) Absorbance time-histories of CO (A_{CO}) with its polynomial fit b) Time-histories of $\frac{dA_{CO}}{dt}$ and $A_{CO} \frac{dA_{CO}}{dt}$, indicating respective pyrolysis times.

resulting correlation function is not dependent on whether the correlation function is based on the absorbance or on the mole fraction. This arises from the relation $N = \frac{\ln\left(\frac{I_0}{I}\right)}{\sigma L} = X \frac{p}{RT}$, so that we have $X = \frac{\ln\left(\frac{I_0}{I}\right)}{\sigma L \frac{p}{RT}}$. Assuming σ and $\frac{p}{RT}$ to be fairly constant during the pyrolysis process we have $X \propto \ln\left(\frac{I_0}{I}\right)$. We note that $\frac{p}{RT}$ may be fairly constant despite combined decrease or increase of p and T . Therefore, f_{cc} can be approximated in terms of the absorbance ($A = \ln\left(\frac{I_0}{I}\right)$) of the product species as:

$$f_{cc} = \text{const.} \cdot A_j \frac{dA_j}{dt} \quad (2.45)$$

From an experimental realization, the necessary time scale can be obtained as illustrated in Figure 2.10. A polynomial is first fitted to the measured absorbance and from it, a derivative can be obtained to calculate f_{cc} and the time to its maximum. As mentioned before, although this pyrolysis time is not exactly the same as that which would be obtained from the fuel and CO f_{cc} , a parametric study of pressure and temperature effects on the pyrolysis time based

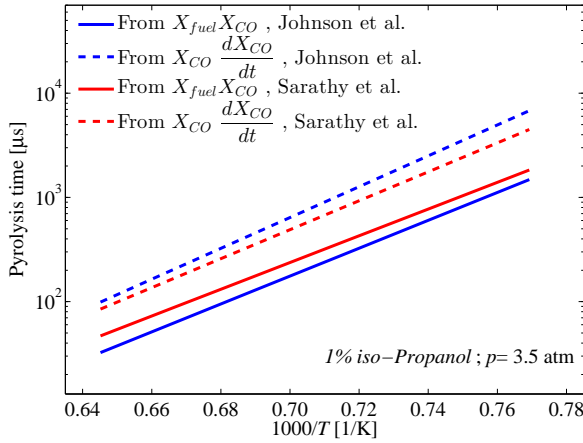


Figure 2.11: Simulated pyrolysis times of iso-propanol based on correlation of fuel and CO compared with times based on correlations of CO and its rate of production for 1% fuel in argon at 3.5 atm. Models: Johnson et al. [110] and Sarathy et al. [119].

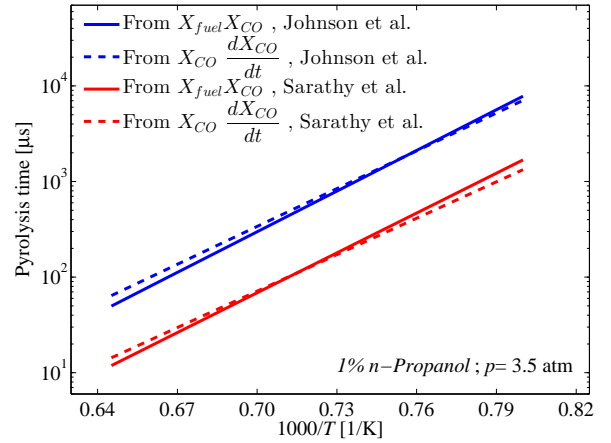


Figure 2.12: Simulated pyrolysis times of n-propanol based on correlation of fuel and CO compared with times based on correlations of CO and its rate of production for 1% fuel in argon at 3.5 atm. Models: Johnson et al. [110] and Sarathy et al. [119].

on model simulations shows that they preserve the temperature and pressure sensitivities of the global pyrolysis kinetics.

Concrete examples of the relation between pyrolysis times obtained from correlations of fuel and product and those obtained from correlations of product concentration and their rate of formation have been examined for pyrolysis of 1% fuel in argon at 3.5 atm. For *iso*-propanol, in line with the previous example, the pyrolysis time obtained on the basis of fuel and CO is shorter than that obtained on the basis of CO and its rate of production, as shown in Figure 2.11, using two models. Although quantitatively different, the pyrolysis times show similar temperature-sensitivity. In the case of *n*-propanol, Figure 2.12 shows that the two times are comparable. Successful use of the method for pyrolysis time determination therefore needs a clear definition and the use of a single product as adopted here offers additional simplicity.

Chapter 3. Measurement of global chemical times

In this chapter results of the global chemical time measurements are presented. They are compared with predictions of available chemical kinetic models and previous data, where these are available at the same conditions. The first section is devoted to the measurements of ignition delays for 2-methyl furan and 2-methyl tetrahydrofuran, where the effect of saturated molecular structure is brought out.

The second presents ignition delay times of 1,3-dimethylcyclohexane. The study is carried out to aid the development of a chemical kinetic model for this fuel and to establish the effect of branching on the kinetics of cyclohexanes.

The third section is devoted to the global kinetic times for ignition and pyrolysis of propanol isomers, where the usefulness of the pyrolysis time introduced in this work is brought out. The further sections, focus on global chemical time measurements by contrasting the ignition and pyrolysis times of the ignition-resistant methyl tert-butyl ether with those of 2-methyl tetrahydrofuran.

The ignition delay times of methane, MP and their blend are also presented. Pyrolysis times of MP and its blend with methane are also reported.

3.1 Ignition delay times of 2-methyl tetrahydrofuran and 2-methyl furan

Ignition delay times of 2-MTHF are compared with 2-MF data. The experimental results are then compared with predictions using chemical kinetic models from the literature. The relative ignition behavior of stoichiometric mixtures of 2-MF and 2-MTHF are studied at a nominal pressure of 3 atm and the mixtures are such that the argon to oxygen ratio,

D , is 3.76. Ignition data of 2-MF mixtures are taken from previous work by Eldeeb and Akih-Kumgeh [29]. Further ignition delay times of 2-MF and 2-MTHF are measured at lean and rich conditions and D of 3.76 at nominal pressure of 12 atm. The primary contributions to uncertainties in the measured delay times as estimated by propagating are: temperature uncertainties (1.0 - 1.5%), pressure uncertainties (1.0-1.5%), fits to ignition signal and ignition delay measurements (1%). As a result of these, actual ignition delay time uncertainties range from 10% to 20%.

Figure 3.1 shows ignition delay times of stoichiometric mixtures of 2-MF and 2-MTHF at a pressure of 3 atm over a range of temperatures. Deviations from the nominal pressure are accounted for using a power law, $\tau \propto p^\beta$, for which the exponent, β , is obtained from data regression. Arrhenius fits to the data are included for improved legibility. It is observed that the ignition delay times of the saturated furan, 2-MTHF, are longer than those of the unsaturated 2-MF up to a factor of 2 at 3 atm. Thus, 2-MTHF is less reactive than 2-MF when both are subjected to the same initial thermodynamic conditions. The higher reactivity of methyl furan relative to furan is thought to be mostly related to the weaker C–H bonds on the methyl group in 2-MF. It was shown in earlier work by Simmie and Curran [218] that

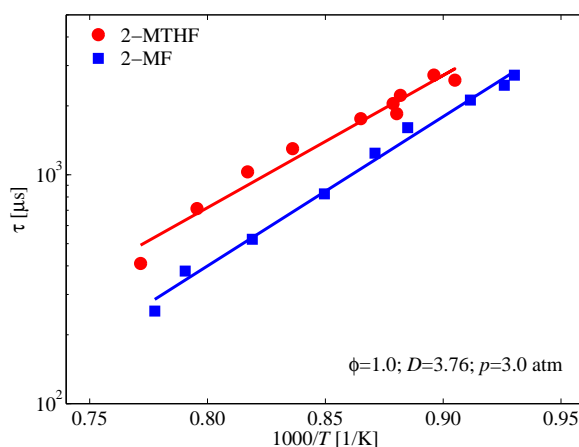


Figure 3.1: Ignition delay times of 2-MF and 2-MTHF for stoichiometric mixtures at a nominal pressure of 3 atm.

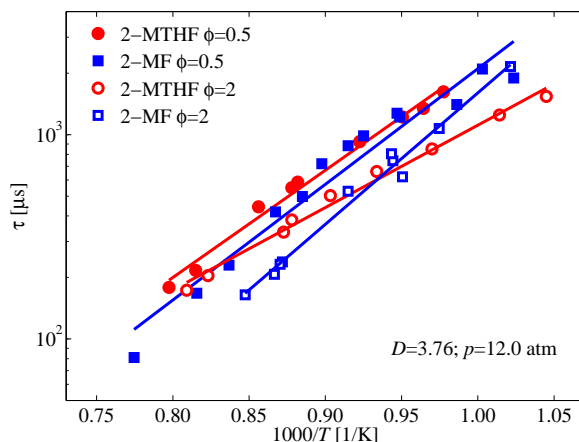


Figure 3.2: Ignition delay times of 2-MF and 2-MTHF at a nominal pressure of 12 atm under lean and rich conditions.

ring C-H bonds in furans are exceptionally strong, so that oxidation initiation through these sites is limited. The observed differences between 2-MF and 2-MTHF suggest that reactivity differences could be localized on the methyl groups of these furans, as will be discussed later in detail. A second possibility for the observed reactivity is that the addition of radicals on the 2-MF C=C bonds, and subsequently ring-opening reactions are faster whereas this possibility is absent in 2-MTHF.

In Figure 3.2, 2-MTHF still shows slightly longer ignition delay times than 2-MF at lean conditions and higher pressure of 12 atm. For the rich mixtures, 2-MTHF has longer ignition delay times at higher temperatures but the trend is reversed at lower temperatures, indicating a weaker temperature sensitivity of 2-MTHF under these conditions.

Figure 3.3 shows the effect of equivalence ratio on 2-MTHF ignition. Within the investigated temperature window, it is observed that ignition delay times decrease as the equivalence ratio increases. This is similar to observed trends for 2-MF [29] and other hydrocarbons. As suggested by the data, if the temperature is further increased, stoichiometric mixtures can ignite more readily than the richer mixtures.

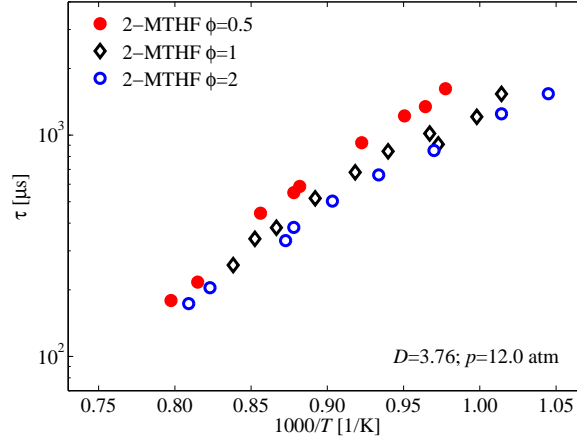


Figure 3.3: Effect of equivalence ratio on 2-MTHF ignition delay times at a nominal pressure of 12 atm.

The measured ignition delay times are next compared to model predictions using a 2-MF model by Somers et al. [18] and a 2-MTHF model by Moshhammer et al. [219]. For stoichiometric mixtures at an average pressure of 3 atm, the comparison is shown in Figure 3.4, where it is observed that both models under-predict the measured ignition delay times by approximately a factor of 2. The observed reactivity trend is reproduced qualitatively at

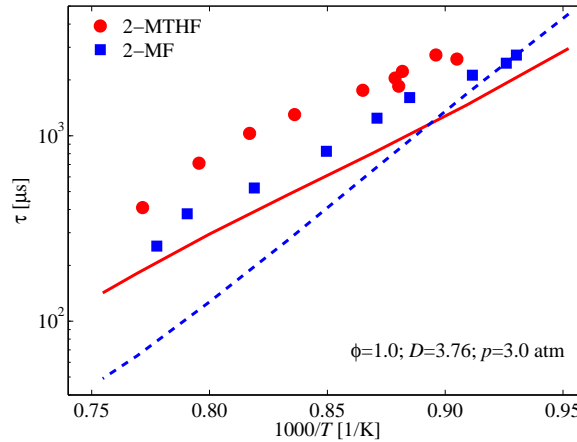


Figure 3.4: Ignition delay times of 2-MF and 2-MTHF at a nominal pressure of 3 atm. Model predictions: solid line is 2-MTHF model by Moshhammer et al. [219] and dash line is 2-MF model by Somers et al. [18].

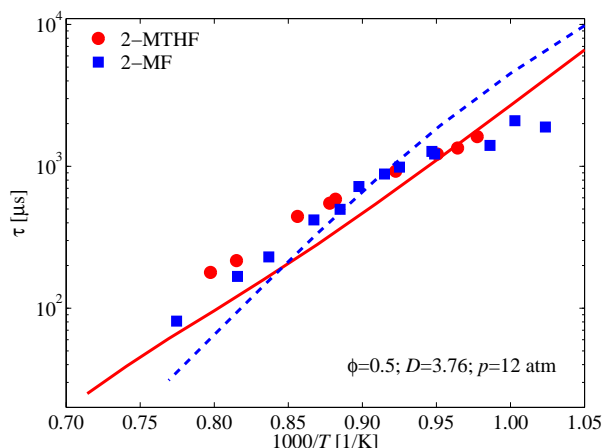


Figure 3.5: Ignition delay time of 2-MTHF at a nominal pressure of 12 atm, $\phi = 0.5$. Model predictions: solid line is 2-MTHF model by Moshhammer et al. [219] and dash line is 2-MF model by Somers et al. [18].

the higher temperature end and temperature sensitivity of the 2-MTHF model is comparable with that of the experiment.

Further comparison of model predictions with measured ignition data for lean and rich mixtures at 12 atm are shown in Figures 3.5 and 3.6. In Figure 3.5, it is observed that model predictions are in closer agreement with the experimental data at $\phi = 0.5$, compared to the stoichiometric case at 3 atm. In case of 2-MF, greater deviation is observed between the measured and predicted delay times. Similarly, Figure 3.6 shows that model predictions and measured data agree only over a narrow temperature range, indicating that the main modeling challenge is to accurately capture the temperature dependence of the ignition delay times.

As observed in the results presented above, reactivity differences are clearly established for stoichiometric mixtures, such that 2-MTHF is more difficult to ignite. The differences are less pronounced for lean mixtures at 12 atm, while for rich mixtures at lower temperatures, 2-MTHF can become more reactive than 2-MF. One approach to shed light on these differences is to examine the molecular structures with respect to the various bond dissociation energies

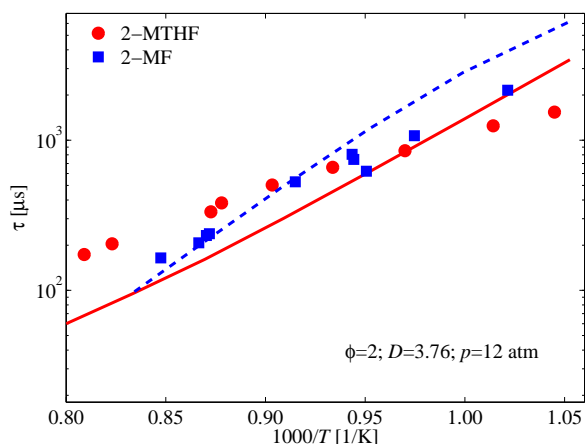


Figure 3.6: Ignition delay time of 2-MTHF at a nominal pressure of 12 atm, $\phi = 2$. Model predictions: solid line is 2-MTHF model by Moshhammer et al. [219] and dash line is 2-MF model by Somers et al. [18].

(BDEs). These have been computed here by direct atomization (CBS QB3 method) using the Gaussian software package [220] and the results are shown in Figure 3.7. It shows that in 2-MF the C-H bond in the methyl group (BDE of 86.3 kcal/mol) is weaker than the corresponding bond in 2-MTHF (BDE of 102.9 kcal/mol). In 2-MF, as a result of the much stronger C-H bonds directly on the ring, radical or O_2 attack on the molecule is much easier at the methyl site as shown by Davis et al. [221], thus leading to the observed higher reactivity since the corresponding bond in 2-MTHF is stronger. The calculated BDEs are in close agreement with previous 2-MF calculations by Simmie and Curran [218]. The reactivity of the various 2-MTHF C-H sites have been investigated by Chakravarty et al. [222], focusing on H-abstraction by HO_2 radicals. The authors show that the lowest activation energy is observed for H abstraction from the C-H bond on the ring carbon to which the methyl group is attached. H abstraction from the methyl group is the most difficult, even compared to the ring C-H bonds. These structural differences translate to differences in reactivity such that 2-MF is generally more reactive because of the relative ease with which its initial fuel radicals can be generated. Further, as previously mentioned, low activation barrier addition of radicals to the ring C=C bonds in 2-MF would subsequently lead to ring-opening and

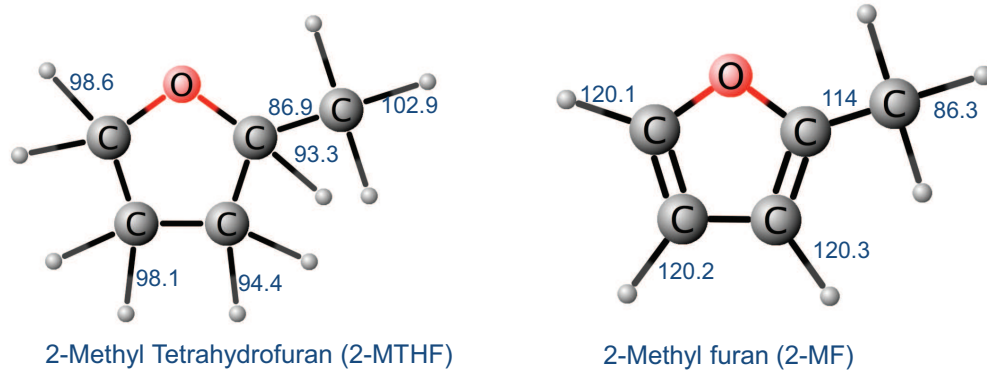


Figure 3.7: Comparison of bond dissociation energies calculated by direct atomization (CBS QB3 method) using the Gaussian 09 software package.

more rapid consumption of the fuel than in 2-MTHF where such C=C bonds are absent.

It has been shown above that while the two chemical kinetic models qualitatively predict the observed trends, they generally underpredict the ignition delay times. The newer model, that of 2-MTHF by Moshhammer et al. [219], is further analyzed to identify the most sensitive reactions and species. Figure 3.8 shows the 20 most important reactions during ignition of a stoichiometric mixture of 2-MTHF. The main observation is that the key reactions are those of

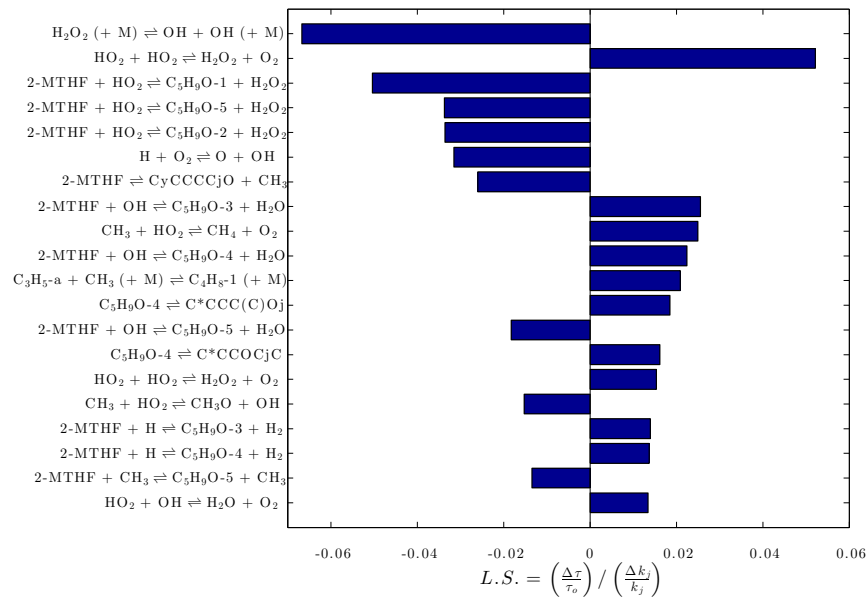


Figure 3.8: Most important reactions from the sensitivity analysis of the 2-MTHF mechanism by Moshhammer et al. [219].

hydrogen abstraction from various sites of the saturated furan. Among radicals, abstraction by HO_2 is the most important. In addition to these abstraction reactions, are reactions from the hydrogen oxidation system involving HO_2 , OH , and H_2O_2 . The decomposition of H_2O_2 is found to be more important than the familiar chain branching reaction in hydrocarbon oxidation, $\text{H} + \text{O}_2 \rightleftharpoons \text{OH} + \text{O}$. This is related to the more rapid production of H_2O_2 through hydrogen abstraction by HO_2 radicals. The sensitivity analysis suggests that the high reactivity of the model with respect to ignition prediction could be improved by revisiting the initial rate assignment for the hydrogen abstraction reactions. For instance, in the original paper, the authors indicate that the rate parameters for abstraction by HO_2 were assigned based on analogous reactions in tetrahydrofuran oxidation.

Apart from reaction sensitivity analysis, species sensitivity analysis can indicate which species play an important role in the mechanism. Figure 3.9 shows the 20 most important species in the oxidation process. These are in addition to the fuel, O_2 , CO_2 , and H_2O which are generally not included in the analysis. The normalized changes are evaluated based on the

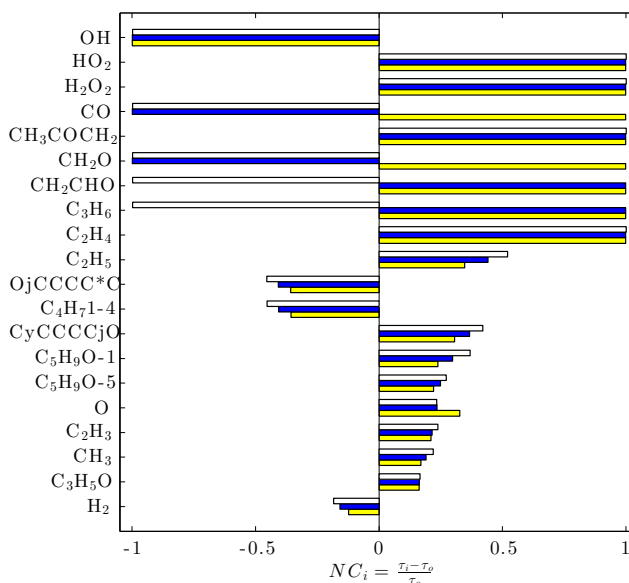


Figure 3.9: Most important species from the sensitivity analysis of the 2-MTHF mechanism by Moshammer et al. [219]. The fuel, O_2 , CO_2 , and H_2O are considered indispensable for oxidation and are therefore not part of the analysis.

alternative species elimination as discussed in previous work [223]. The results confirm the importance of OH, HO₂, and H₂O₂ as well as other radicals and molecules that are central to the C0-C2 oxidation chemistry. Fuel radicals and other intermediates associated with ring-opening also appear on the list. Improving the kinetic parameters of the production and consuming channels of these species are most likely to impact the overall performance of the model.

In summary, this subsection established the lower reactivity of 2-MTHF compared to 2-MF. Under stoichiometric conditions, 2-MTHF has longer ignition delay times than 2-MF, with differences of about a factor of 2 at 3 atm. The differences are less pronounced for lean mixtures at 12 atm and a complex behavior is observed for rich mixtures where 2-MTHF can be more reactive at lower temperatures. For 2-MTHF it is observed that as the equivalence ratio increases, ignition delay times decrease. The reactivity difference is attributed to differences in the rates of radical attack on side methyl groups, such that they are faster for 2-MF.

3.2 Ignition delay times of 1,3-Dimethylcyclohexane

This section is based on collaboration with my former colleague Dr. Mazen A. Eldeeb. On the basis of the results obtained in this work, a new chemical kinetic model was developed for 1,3-DMCH through a research collaboration between the Thermodynamics and Combustion Lab (TCL) at Syracuse University and Dr. Sarathy's group at the Clean Combustion Research Center (CCRC) at KAUST. Ignition delay times of 1,3-DMCH in oxygen and argon mixtures are measured at nominal pressures of 5.0 and 12 atm, equivalence ratios of 0.5, 1.0, and 2.0, and Ar/O₂ ratios of 3.76 and 10.0. Also measured are delay times of ethyl cyclohexane, an isomer of 1,3-DMCH. As noted before, the main source of uncertainties in ignition delay times is the temperature uncertainty. The temperature uncertainties in this study are estimated to be in the range of 12-22 K, corresponding to about 1.0-1.5% of the reflected shock temperature.

The starting point for 1,3-DMCH chemical model is the recent work of Wang et al. [224–226]

on the combustion chemistry of cyclohexane, methylcyclohexane (MCH) and ethylcyclohexane (ECH). The thermochemical data of the species in 1,3-DMCH sub-mechanism was estimated using the THERM software [227] with new group values from Burke et al. [228]. The 1,3-DMCH kinetic model was developed by adding the 1,3-DMCH sub-mechanism into the existing cycloalkane models. The resulting model contains 540 species and 2929 reactions. Only a subset of experimental data was used to constrain the model. The resulting model is then validated against all data sets. The experiments are also designed to bring out isomer effects by looking at the ignition of ECH in comparing to 1,3-DMCH.

The results of the stoichiometric cyclohexane studies are shown in Figure 3.10, where it can be seen that the ethylated cyclohexane isomer ignites more readily than the 1,3-dimethyl isomer at a pressure of 5.0 atm. Less pronounced differences are observed at 12 atm. A possible explanation for the observed reactivity differences is that, whereas ECH has weak secondary C–H bonds, 1,3-DMCH has only terminal C–H bonds that are generally more resistant to radical attack. Also, direct initiation in ECH can result from C–C bond scission, liberating more reactive C_2H_5 radicals, compared to the less reactive CH_3 radicals in the case of 1,3-DMCH.

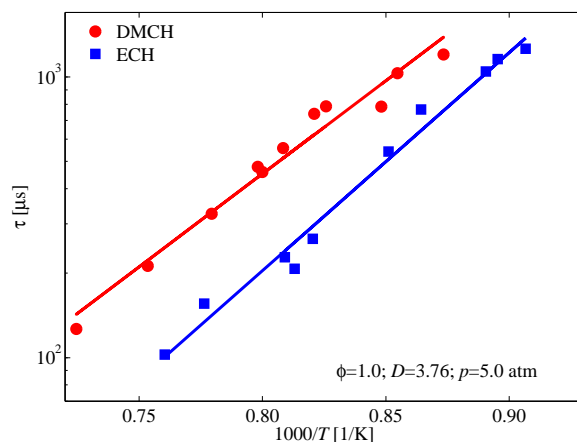


Figure 3.10: Ignition delay times of stoichiometric mixtures of fuel, oxygen, argon for 1,3-DMCH and ECH with an argon/oxygen ratio of 3.76 at a pressure of 5.0 atm. Solid lines represent Arrhenius fits.

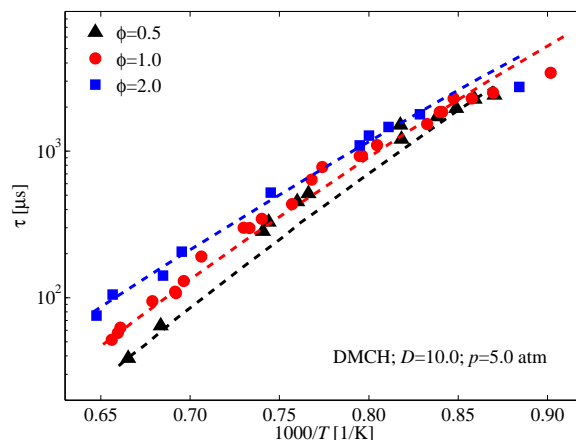


Figure 3.11: Ignition delay times of 1,3-DMCH at a pressure of 5.0 atm, an Ar/O₂ ratio of 10.0, and equivalence ratios of 0.5, 1.0, and 2.0. Dashed lines: model predictions.

Figure 3.11 shows the effect of equivalence ratio based on measurements at a pressure of 5.0 atm, an Ar/O₂ ratio of 10.0, and equivalence ratios of 0.5, 1.0, and 2.0. Within the investigated temperature window, rich mixtures are observed to have the longest ignition delay times, lean mixtures ignite most readily, while the delay times of stoichiometric mixtures fall between the two. The reason for this trend is that there is a competition between pyrolysis and oxidation. At higher temperatures pyrolysis contributes more significantly to fuel consumption compared to dominant oxidation kinetics at lower temperatures. At lower temperatures, pyrolysis is less important and oxidation is such that rich mixtures ignite more readily. Figure 3.11 suggests that at temperatures below 1150 K, the observed equivalence ratio trend reverses. It is also seen that the 1,3-DMCH model predict the experimentally observed effect of equivalence ratio. However, some deviations are observed at the low temperature end, especially at stoichiometric and rich conditions.

The equivalence ratio effect is also compared at the higher pressure of 12 atm, an Ar/O₂ ratio of 10.0, and equivalence ratios of 0.5 and 1.0, as shown in Figure 3.12. Good agreement between the experimental data and the predictions of the kinetic model is observed for the stoichiometric case. At the lean conditions, predictions of the model agree reasonably well with the experimental data, with the model under-predicting ignition delay times at the lower

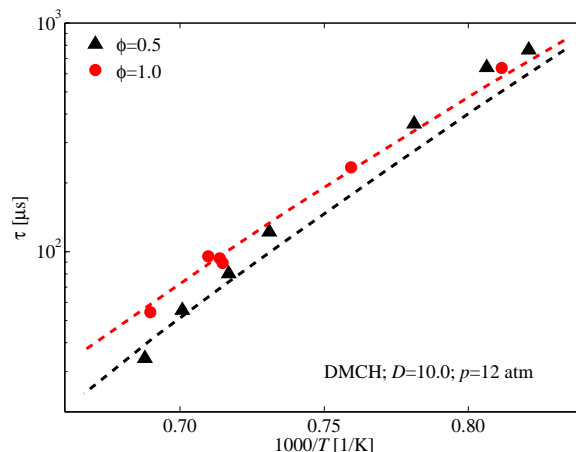


Figure 3.12: Ignition delay times of 1,3-DMCH at a pressure of 12 atm, an Ar/O₂ ratio of 10.0, and equivalence ratios of 0.5 and 1.0. Dashed lines: model predictions.

temperature end. The observed agreement at this high pressure of 12 atm and an Ar/O₂ dilution ratio of 10.0 is different from that observed at the same pressure and a dilution of 3.76, shown in Figure 3.13, where the model significantly over-predicts ignition delay times. This suggests that the predictions of the 1,3-DMCH model are more accurate for highly diluted mixtures.

Figure 3.13 compares model predictions of ignition delay times with measured data for stoichiometric 1,3-DMCH/O₂/Ar mixtures with an Ar/O₂ ratio of 3.76 and pressures of 3.0,

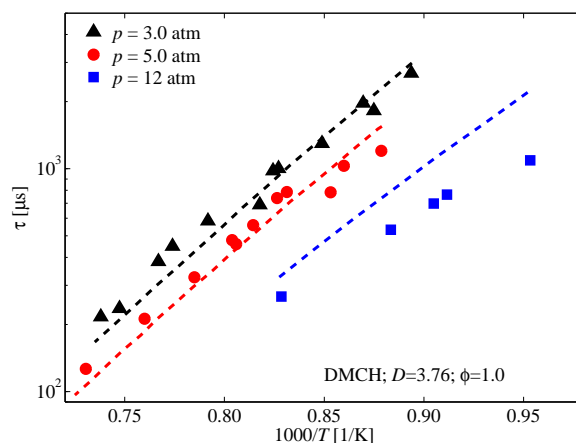


Figure 3.13: Effect of pressure on ignition delay times of 1,3-DMCH for $\phi = 1.0$, Ar/O₂ ratio of 3.76, and pressures of 3.0, 5.0, and 12 atm. Dashed lines: model predictions.

5.0, and 12 atm. It is observed that the model captures the experimentally observed pressure effect on ignition delay times and predicted delay times are generally in good agreement with the experimental data at pressures of 3.0 and 5.0 atm, with some deviations at the low temperature end, especially at 5.0 atm. However, the model predicts longer ignition delay times at the higher pressure of 12 atm, with deviations up to a factor of 2.

In summary, a chemical kinetic model of 1,3-DMCH has been established using measured ignition delay times from this study. The prediction of proposed kinetic model has overall good agreement with additional ignition delay times, except at low dilution levels and high pressures. Also, the model predicts reasonably well the effects of equivalence ratio and pressure on ignition delay times.

3.3 Global kinetic times of propanol isomers

The method of pyrolysis time developed in this work is applied to study the global kinetics of propanol isomers. The pyrolysis times are contrasted with ignition times. The measurements are also compared with model predictions.

3.3.1 Ignition delay times

Ignition delay times for stoichiometric fuel/O₂/Ar mixtures are measured under various pressure conditions to establish isomer and pressure effects. Lean ($\phi=0.5$) and rich ($\phi=2$) mixtures are also studied at average pressures of 3.5 atm to explore the equivalence ratio effect. A fixed argon to oxygen ratio, $D = 21$, is adopted such that the fuel molar fraction lies in the range of 0.5% - 2.0%, depending on the corresponding equivalence ratio. A further set of ignition delay measurements are obtained for less dilute stoichiometric mixtures ($D=3.76$) at 12 atm.

The shock tube ignition data are first compared with experimental ignition correlations

developed by Noorani et al. [84] and Man et al. [112]. Uncertainties in measured delay times are estimated by propagating major uncertainty contributions: temperature uncertainties (1.0 - 1.5%), pressure uncertainties (1.0-1.5%), fits to ignition signal and ignition delay measurement (1%). Ignition delay time uncertainties range from 10% to 20% and are indicated in the plots below. Uncertainties of ignition delay times calculated from the literature correlations are of a comparable magnitude (not shown for clarity). The results for *n*-propanol ignition at pressures of 3.5 atm are shown in Figure 3.14. It is observed that the correlation predictions agree with the current measurements within experimental uncertainties. The correlation by Noorani et al. [84] shows a lower activation energy such that longer delay times are predicted at higher temperatures.

With respect to *iso*-propanol, Figure 3.15 shows that the measured delay times accord with calculated times from the correlation by Man et al. [112], with the latter showing slightly shorter delay times at 3.5 atm.

The isomer effect is established by carrying out ignition experiments using mixtures of similar compositions and at similar test conditions. The results are shown in Figure 3.16 and Figure

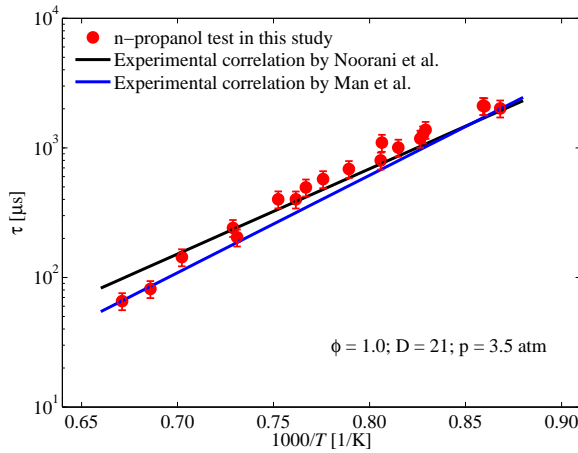


Figure 3.14: Comparison with *n*-propanol experiment correlations [84, 112] at 3.5 atm.

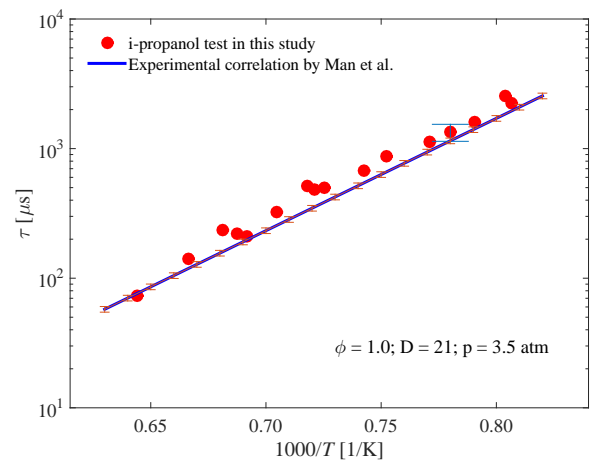


Figure 3.15: Comparison with *iso*-propanol experiment correlation [112] at 3.5 atm.

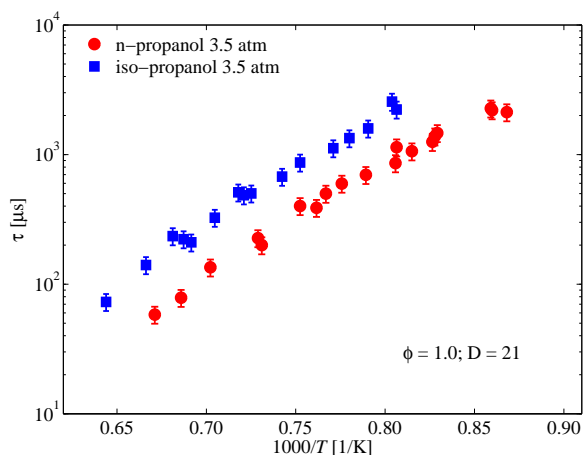


Figure 3.16: Isomer effect on propanol ignition (3.5 atm).

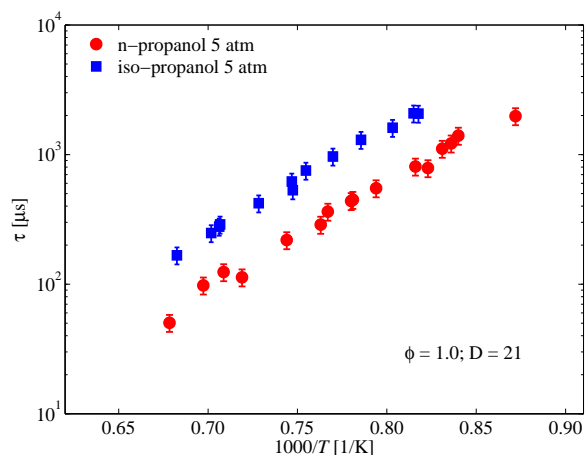


Figure 3.17: Isomer effect on propanol ignition (5 atm).

3.17 for pressures of 3 atm and 5 atm, respectively. As would be expected from the chemical structure of these isomers and in accordance with previous studies, *iso*-propanol has longer ignition delay times than *n*-propanol. This difference in reactivity is partially attributed to weaker secondary C-H bonds in *n*-propanol. Another reason for the observed difference is that *n*-propanol oxidation leads to formation of the highly reactive formaldehyde species whereas the less reactive acetone is more readily formed during *iso*-propanol oxidation. These differences correlate with higher H atom formation rates in *n*-propanol than in *iso*-propanol, which further result in more rapid fuel consumption in *n*-propanol.

The observed ignition delay times are also compared with predictions obtained using three chemical kinetic models from the literature [110, 112, 119]. Figure 3.18 shows the comparison of model predictions with measured ignition delay times for stoichiometric mixtures of *n*-propanol at 3.5 atm. It is observed that the model by Johnson et al. [110] predicts much longer delay times than measured, while the predictions of the models by Sarathy et al. [119] and Man et al. [112] are in closer agreement with the experimental observations. As discussed by the authors, the model by Man et al. [112] is an improved version of that by Johnson et al. [110]. It is also worth noting that the Man et al. and Sarathy et al. models predict ignition

delay times in close agreement albeit with slightly different global temperature sensitivities. A similar level of agreement is observed for *iso*-propanol as shown in Figure 3.19.

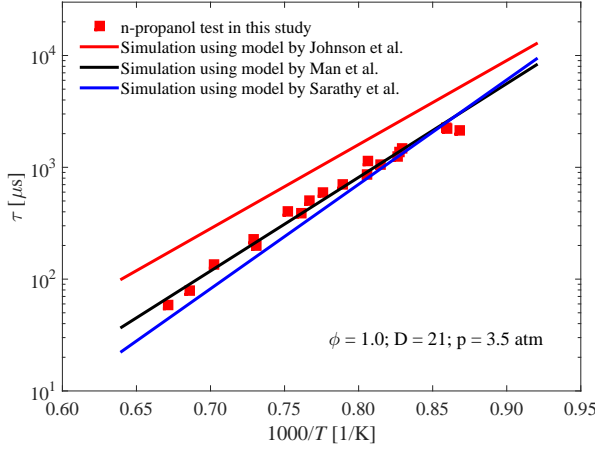


Figure 3.18: Comparison of measured *n*-propanol ignition delay times at 3.5 atm with model predictions.

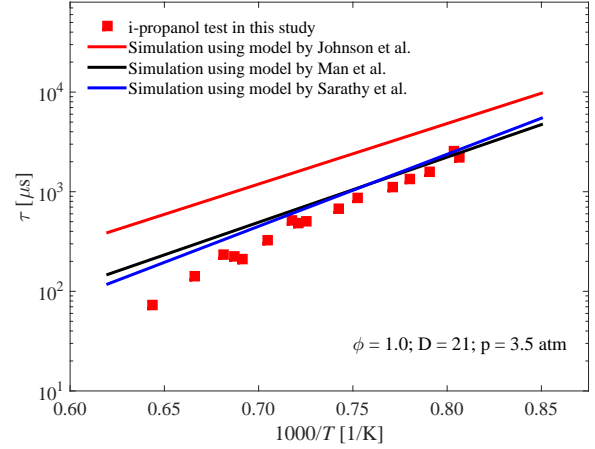


Figure 3.19: Comparison of measured *iso*-propanol ignition delay times at 3.5 atm with model predictions.

The equivalence ratio effect on ignition delay times is also examined by measuring ignition delay times under rich, lean, and stoichiometric conditions with a fixed D of 21 at 3.5 atm and the results are compared with predictions of the model by Sarathy et al. [119]. This model is chosen to examine the equivalence ratio effect on account of the close agreement between simulations and measured delay times at stoichiometric conditions, discussed above. In the case of *n*-propanol, Figure 3.20 shows that under the chosen conditions, there is a weak dependence on equivalence ratio. Ignition delay times decrease with increasing equivalence ratio but are more insensitive to equivalence ratio effects at higher temperatures. This relative behavior is captured by the model even though its predictions are slightly shorter than the measured data.

Figure 3.21 shows the results of equivalence ratio effects for *iso*-propanol. The trend observed for *n*-propanol is seen here at lower temperatures while a reversal occurs around 1300 K, with the rich mixture becoming more reactive. As will be discussed more under pyrolysis,

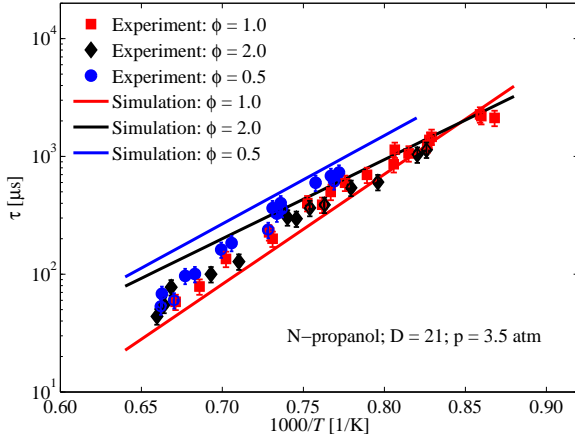


Figure 3.20: Comparison of measured *n*-propanol ignition delay times at three equivalence ratios with predictions of model by Sarathy et al. [119].

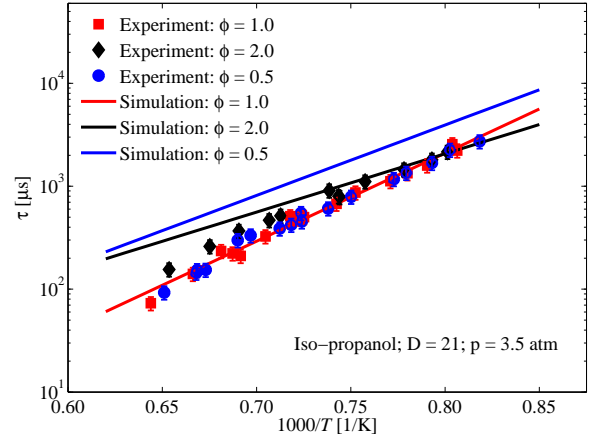


Figure 3.21: Comparison of measured *iso*-propanol ignition delay times at three equivalence ratios with predictions of model by Sarathy et al. [119].

during ignition, there is competition between oxidative processes and purely pyrolysis kinetics, however, pyrolysis kinetics have a higher apparent activation energy. The oxidative processes in *iso*-propanol are slower than in *n*-propanol, and so the competition between pyrolysis and oxidative processes is reached at lower temperatures in *iso*-propanol than in *n*-propanol.

The ignition results above have been obtained under very dilute conditions. Figure 3.22 shows

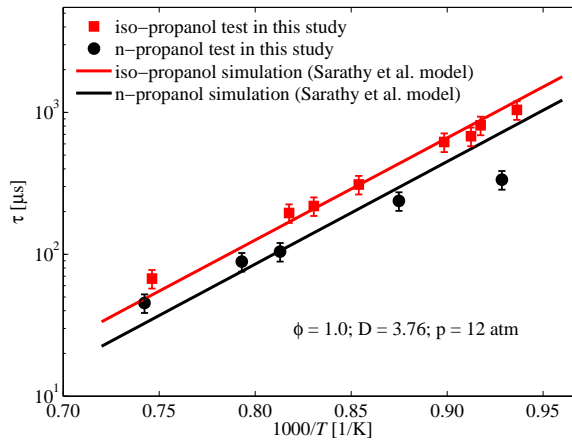


Figure 3.22: Isomer effect on ignition of stoichiometric mixtures at a higher average pressure of 12 atm and less dilute condition ($D = 3.76$). Model simulations: Sarathy et al. [119].

that the established isomer effect is consistently realized at the higher average pressure of 12 atm for less dilute mixtures with a ratio of argon to oxygen, D , of 3.76, reflective of the nitrogen to oxygen ratio in air. The experimental data are compared with predictions of the model by Sarathy et al. [119], showing reasonable agreement.

To Summarize, this subsection has shown the higher reactivity of *n*-propanol compared to *iso*-propanol based on ignition delay measurements. Comparison of experimental results with predictions using literature models show that models by Sarathy et al. [119] and Man et al. [112] predict ignition delay fairly well.

3.3.2 Pyrolysis times of propanol isomers

As previously defined, pyrolysis times are obtained as the time required to attend the maximum of f_{cc} based on CO absorbance and its time derivative (Figure 2.10). Different fuel concentrations (1% and 2%) and pressures (3.5 and 11 atm) are chosen to investigate the effect of concentration and pressure.

The main contributions to uncertainties in the measured pyrolysis times are: temperature (estimated at 1.0%), pressure (1.0%), correlation function fit parameters (10%). Pyrolysis times depend strongly on temperature as evidenced by their global activation energies and the overall uncertainty estimates after error propagation are in the range of 22-26%. Simulations of the shock tube pyrolysis experiment as a constant volume reactor shows that the endothermic nature of the process leads to a drop in temperature and pressure of up to 8% as the products approach their equilibrium concentrations. This drop is found to affect mostly mole fraction calculations but not the pyrolysis times obtained from the correlation functions.

Figure 3.23 shows the dependence of *n*- and *iso*-propanol pyrolysis time scales on temperature for mixtures of 1% fuel in argon. An Arrhenius-type dependence with a global activation energy greater than 60 kcal/mol is observed. This is in contrast to global activation energies

of ignition process which generally lie in the range of about 20-45 kcal/mol [84, 229], with the lower activation energies typically being observed for oxygenated fuel ignition. This difference in temperature sensitivity will be shown to impact the competition between oxidation-controlled ignition processes and pyrolysis kinetics. Figure 3.23 also shows that the reactivity difference between *n*- and *iso*-propanol ignition is also borne out in global pyrolysis kinetics. The pyrolysis time scales of *iso*-propanol are found to be longer than those of *n*-propanol under similar conditions.

The effect of fuel concentration on the pyrolysis times is shown in Figure 3.24, where the time scale is observed to be fairly insensitive to *n*-propanol concentration. It is possible that a very weak effect of fuel concentration exists but it cannot be discerned from the concentration doubling used here. This weak dependence is observed in simulations and it is such that a higher fuel concentration leads to longer pyrolysis times. A similar pyrolysis time insensitivity to fuel concentration is observed for *iso*-propanol.

Pyrolysis times are found to decrease with increasing pressure, similar to the effect of pressure on ignition delay times. This can be seen in Figure 3.25 for the pyrolysis of *n*-propanol at

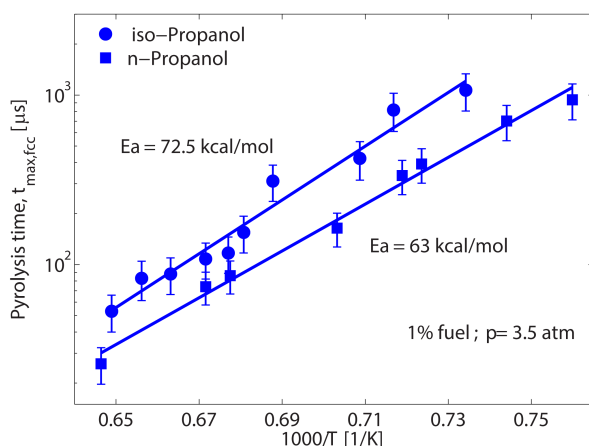


Figure 3.23: Pyrolysis time scales of *n*- and *iso*-propanol for 1% in argon at 3.5 atm.

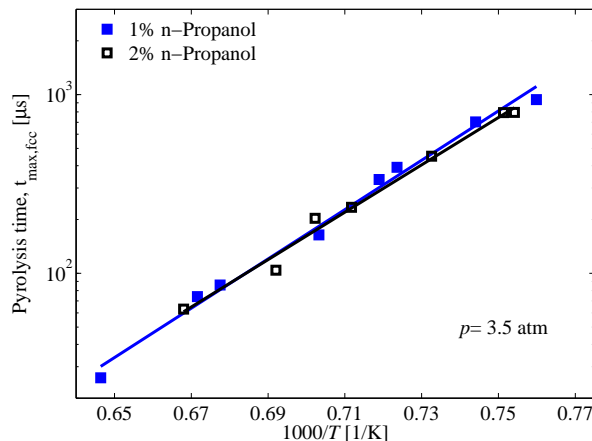


Figure 3.24: Effect of fuel concentration on pyrolysis time scales of *n*-propanol. No distinct influence is observed.

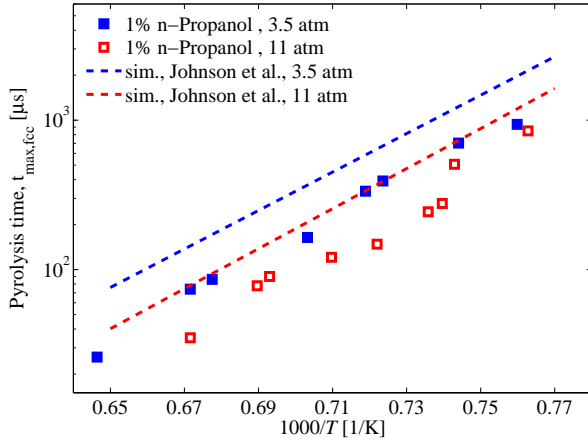


Figure 3.25: Pyrolysis times of 1% of *n*-propanol at 3.5 atm and 11 atm.

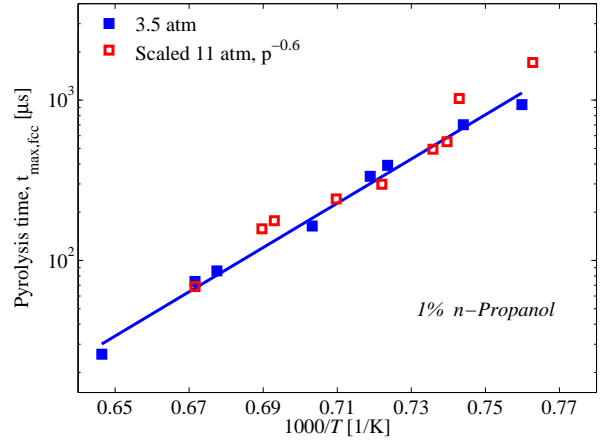
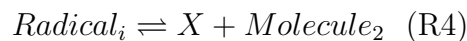
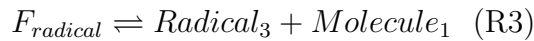
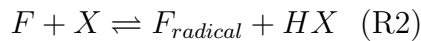
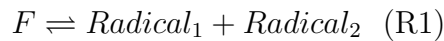


Figure 3.26: Pyrolysis times of 1% *n*-propanol with 11 atm data scaled to 3.5 atm using $p^{-0.55}$ relation.

average pressures of 3.5 atm and 11 atm. It is generally considered that the pressure effect arises from the higher number density and increased frequency of collisions which promote bimolecular reactive collisions. Figure 3.26 shows the pyrolysis times at 11 atm scaled to 3.5 atm using a pressure exponent of -0.55. This pressure exponent is lower than that used for pressure scaling of moderate temperature ignition delay times (typically in the range -0.6 to -1.0). When ignition delay times are studied at much higher temperatures, a weaker pressure effect is observed, closer to that observed here for pyrolysis time scales.

In order to understand the reasons for the observed temperature and pressure trends, we can consider pyrolysis to generally proceed according to the scheme:



where F is the fuel, X - a generic radical capable of further H abstraction from the fuel, $Radical_i$ - a generic radical, and $Molecule_i$ - a generic stable molecule. Reaction R1 is characterized by an activation energy of the order of a C-C bond dissociation energy (about 80 kcal/mol). This contributes significantly to the observed global pyrolysis kinetics that is characterized by an activation energy of more than 60 kcal/mol. Typical activation energies of H-abstraction reactions of generic type R2 are often in the range of 0-15 kcal/mol, while reactions R3 and R4 typically have activation energies in the range of 20-40 kcal/mol, closer to the global activation energy of ignition events. At very early times when the radicals, X , are absent or in very low concentration, fuel decomposition is dominated by R1 which typically involves direct C-C bond scission (with activation energies above 80 kcal/mol). While this scheme is similar to what may be observed for oxidation processes, it differs in that reactions such as R2 only involve H and CH_3 radicals as compared to the additional O_2 , HO_2 , and OH radicals in the case of oxidation. H-abstraction by O_2 is characterized by activation energies in the range 40-50 kcal/mol while abstraction by OH is almost barrier-less. During ignition, in addition to direct decomposition of the fuel radicals as in R3 and R4, addition of O_2 to the first generation fuel radicals occur, leading to low- or high-temperature pathways, depending on the prevailing conditions. It should be noted that in the case of oxygenated fuel pyrolysis (e.g. propanol isomers), OH, O, HO_2 radicals can appear during the process and react with the fuel. However, they occur in concentrations that are over three orders of magnitude lower than those observed during oxidation processes. They are also over four orders of magnitude lower than H and CH_3 . As a result, they do not significantly lower the global activation energies to levels typical of oxidation.

The complex competition between R1 and R2 and their subsequent reactions, R3 and R4, result in global kinetics whose activation energies lie between activation energies of R1 and R2, albeit closer to those of R1.

The difference in temperature sensitivity of pyrolysis and ignition leads to differences in the

relative contribution of purely pyrolytic reactions to the fuel consumption process during ignition. This can be illustrated more clearly by comparing the ignition and pyrolysis time scales of a given fuel at fixed fuel percentage. In the case of ignition, the fuel is mixed with O_2 and Ar, leading to reactions with oxygen-mediated radicals. The chemical times can also be compared to model predictions to determine whether the temperature sensitivities and relative competition are in line with experimental measurements.

Figure 3.27 shows the comparison between pyrolysis times of 1% *iso*-propanol and ignition delay times of a stoichiometric mixture with 1% *iso*-propanol at 3.5 atm. At low temperatures, ignition delay times are shorter than pyrolysis times but the trend reverses at higher temperatures on account of the stronger temperature sensitivity of the pyrolysis process. The experimental trend reversal occurs at about 1450 K. At temperatures above 1450 K, the ignition process is dominated by reactions of the pyrolytic scheme. Direct C–C bond scission and subsequent production of H and CH_3 predominate fuel attack by molecular oxygen and oxygenated radicals that are more important at lower temperatures. Both chemical kinetic models predict pyrolysis times in close agreement with the experimental data, although the predicted pyrolysis times are generally longer. The measured ignition delay times are only

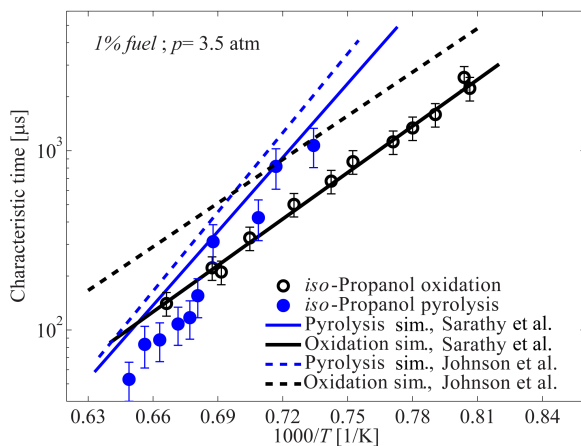


Figure 3.27: Comparison of ignition delay times ($\phi = 1$) with pyrolysis time scales of *iso*-propanol, including simulation results.

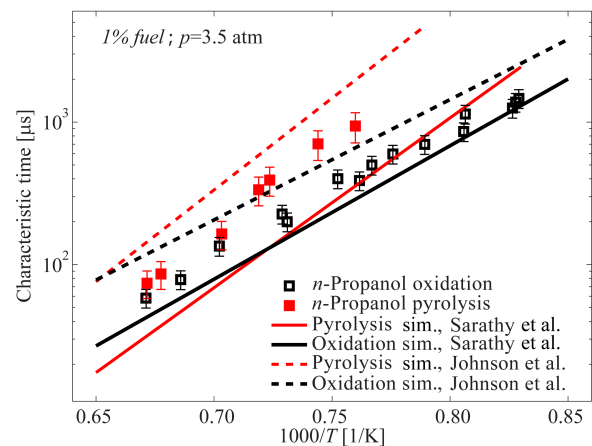


Figure 3.28: Comparison of ignition delay times ($\phi = 1$) with pyrolysis time scales of *n*-propanol, including simulation results.

well predicted by the Sarathy et al. model [119]. The model by Johnson et al. [110] predicts much longer ignition delay times than experimentally observed.

In the case of *n*-propanol, the experimental trend reversal in measured chemical times is observed at a higher temperature, 1490 K as shown in Figure 3.28. Here both chemical kinetic models predict shorter ignition delay times. The model by Sarathy et al. [119] also predicts a weaker temperature sensitivity of the pyrolysis process while the model by Johnson et al. [110] is in closer agreement with the measured pyrolysis times.

Through this comparison of the two time scales, we gain better understanding of the changes in fuel concentration profiles during ignition at different reactor temperatures as shown in Figures 3.29 and 3.30. They are such that at higher temperatures the fuel decays in a manner comparable with the fuel time-history during pyrolysis. This means, simplification of the oxidation kinetics of large hydrocarbons as sub models of pyrolysis of large hydrocarbons, to obtain small chemical species. Their subsequent oxidation is only well supported at temperatures higher than those characteristic of the trend reversal. At lower temperatures, the simplification must properly account for reactions of radicals from oxidative processes

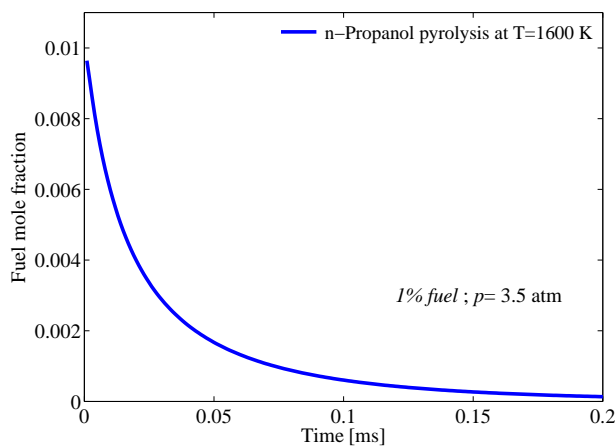


Figure 3.29: Typical fuel time-history during fuel pyrolysis, indicating global first order kinetics. Model: Johnson et al. [110].

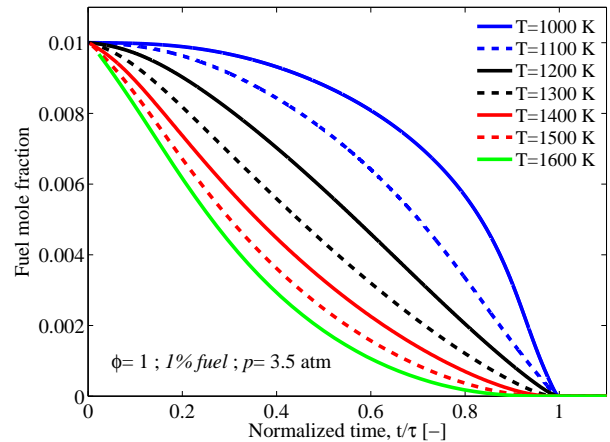


Figure 3.30: Simulated fuel time histories during ignition. A change in profile toward pyrolysis-type decay occurs as temperature increases. Model: Johnson et al. [110].

with the original fuel molecules, which lead to fuel time-history curvatures similar to those observed around 1000 K.

In Summary, this subsection has shown that by means of the newly developed pyrolysis time, the effects of reactor temperature, pressure, and fuel concentration on pyrolysis can be established. It also reveals a distinctly higher global temperature sensitivity of the pyrolysis process (global activation energy > 60 kcal/mol) compared to the typical global activation energy of ignition (global activation energy in the range of 20-40 kcal/mol). This difference leads to a cross-over effect at a characteristic reactor temperature between ignition that is controlled by pyrolysis and one that is controlled by predominantly oxidative kinetics. The measured pyrolysis times are also compared with predictions of three chemical kinetic models from the literature, showing relative strengths and weakness of the models.

3.3.3 Chemical kinetic model analysis

Reaction pathway analyses are carried out to better understand some of the kinetic reasons for the observed behavior in the propanols.

Reaction pathway analyses of representative oxidation and pyrolysis processes are carried out using the model by Sarathy et al. [119] on account of its overall better agreement with measurements. The purpose is to gain insight into the competing reaction channels and their relative importance. All analyses are carried out at the instance where 20% of the initial fuel molar fraction has been consumed.

Figures 3.31 shows the pathways during ignition of a stoichiometric mixture of 1% *n*-propanol at two temperatures. It is observed that fuel is primarily consumed through H-abstraction and unimolecular reactions, with the former accounting for more than 70% under both conditions, while the unimolecular decomposition accounts for about 13 % at the lower temperature and increases to about 23 % at the higher temperature. Concerted elimination of H₂O contributes

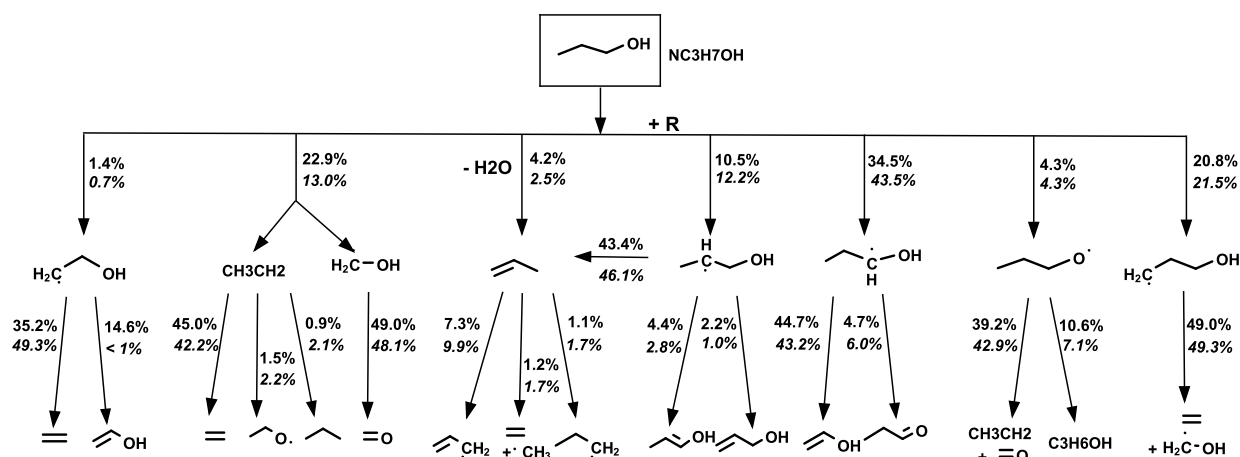


Figure 3.31: Reaction pathway for *n*-propanol ignition ($\phi = 1$, 1% fuel, $D = 21$, $p = 3$ atm) using the model by Sarathy et al. [119] at temperatures of 1475 K (top) and 1230 K (bottom).

less than 5 % and is higher at higher temperatures. At higher temperatures, the increasing role of pyrolysis is thus observed. It should also be noted that a proportion of the H-abstracting radicals are derived from further decomposition of products of the unimolecular decomposition and the fuel radicals obtained from earlier abstractions. The role of unimolecular reactions is stronger at even earlier times than considered in this analysis. A majority of the initial radicals react by β -scission to form smaller radicals and stable molecules.

In the case of *iso*-propanol ignition process (see Figure 3.32), H-abstraction from methyl C-H sites and the C-H site adjacent to the OH group is dominant at both temperatures (over 80 %). Their further reactions lead to the formation of propenol and acetone, with same carbon number as the fuel and in need of further radical and unimolecular reaction possibilities. Unimolecular reactions include direct C-C bond scission and concerted elimination of H_2O , with the latter being slightly more important than the direct scission.

For pyrolysis, reaction pathway analyses are carried out at three conditions to explore the effects of pressure, temperature, and fuel concentration. The results for *n*-propanol are shown in Figure 3.33. Under the three conditions, the primary fuel consumption pathways and their respective contributions do not change remarkably. H-abstraction reactions from the

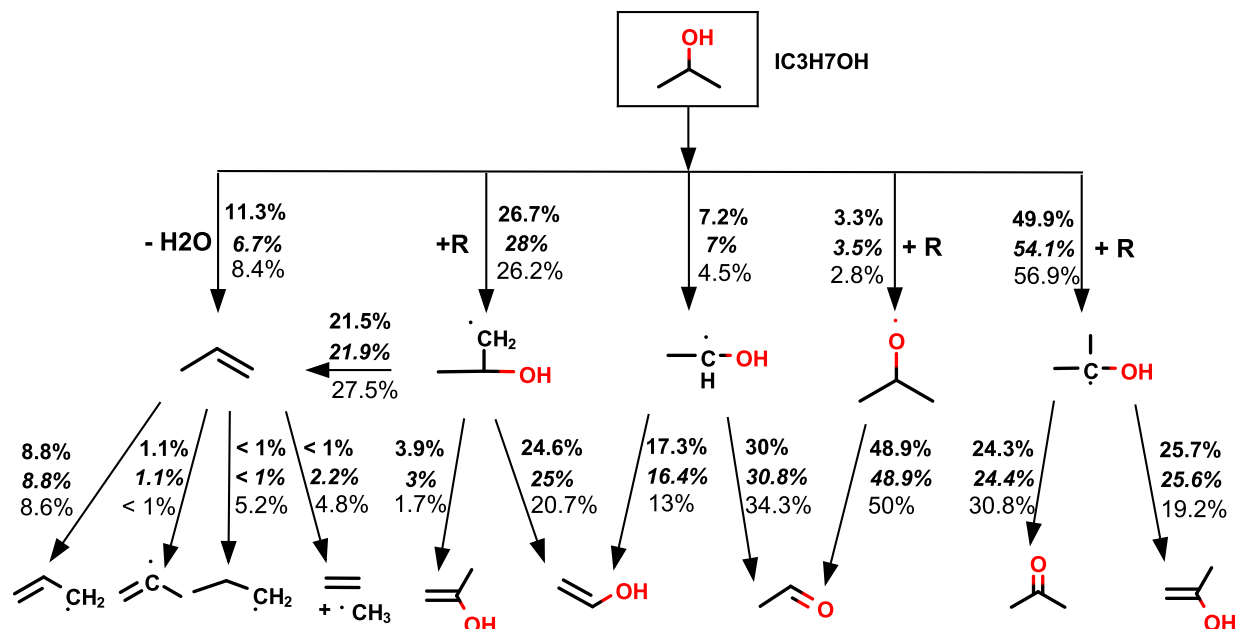


Figure 3.32: Reaction pathway for n -propanol ignition ($\phi = 1$, 1% fuel, $D = 21$, $p = 3$ atm) using models by Sarathy et al.[119] with temperatures of 1510 K (top) and 1310 K (bottom).

fuel account for approximately 77% of the total fuel consumption, while the unimolecular reactions make up about 22 %. Moreover, subsequent reactions from the fuel radicals are similar. It confirms our finding before that the concentration has no significant effect on

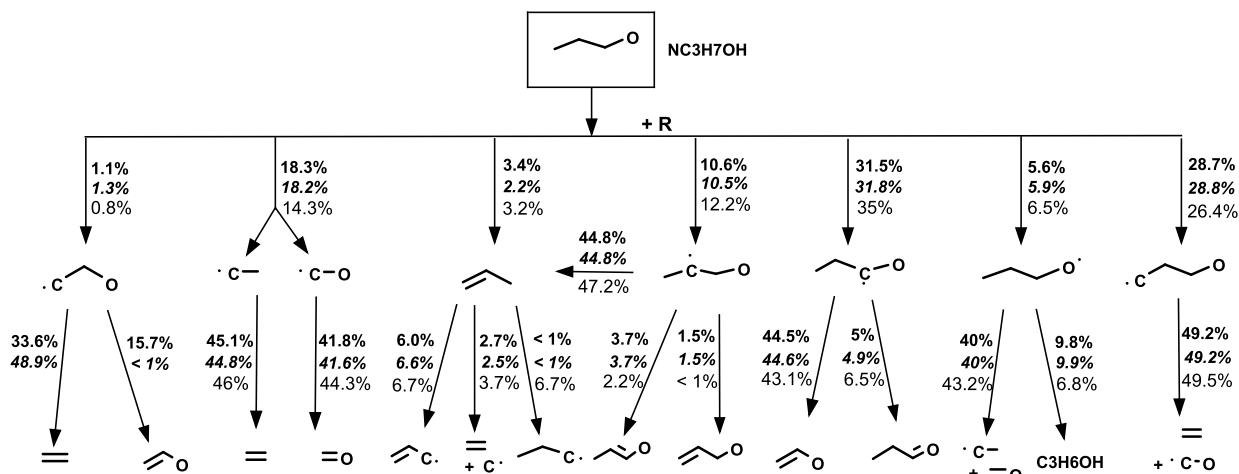


Figure 3.33: Reaction pathway for n -propanol pyrolysis using model by Sarathy et al. [119] with three conditions. Condition 1(in bold): 1% fuel, 1450 K, and 3 atm; Condition 2 (in bold italic): 1% fuel, 1450 K, and 12 atm; Condition 3(in regular): 2% fuel, 1450 K, and 3 atm.

pyrolysis time scales for these small percentages of fuel in a diluent gas. It also shows that the observed pressure effects are not associated with changes in the pathways, rather, they involve increased reaction rates either through number densities or pressure-dependent reaction rate parameters.

Figure 3.34 illustrates the main pathway for *iso*-propanol pyrolysis under the same condition as described for *n*-propanol above. It is observed that fuel consumption through H-abstraction accounts for over 80% of the total consumption rate, while unimolecular decomposition accounts for less than 20%. Similar to the results for *n*-propanol, no significant changes are observed among these three conditions. Similar results for reaction channels during pyrolysis are obtained with the model by Johnson et al. [110], although the pressure effect is evident through 14% increase in H-abstraction at the higher pressure. The model by Johnson et al. over-emphasizes concerted elimination of H₂O from the initial fuel molecule. This possibly also accounts for the observed slower CO formation, since the fuel-bound oxygen initially

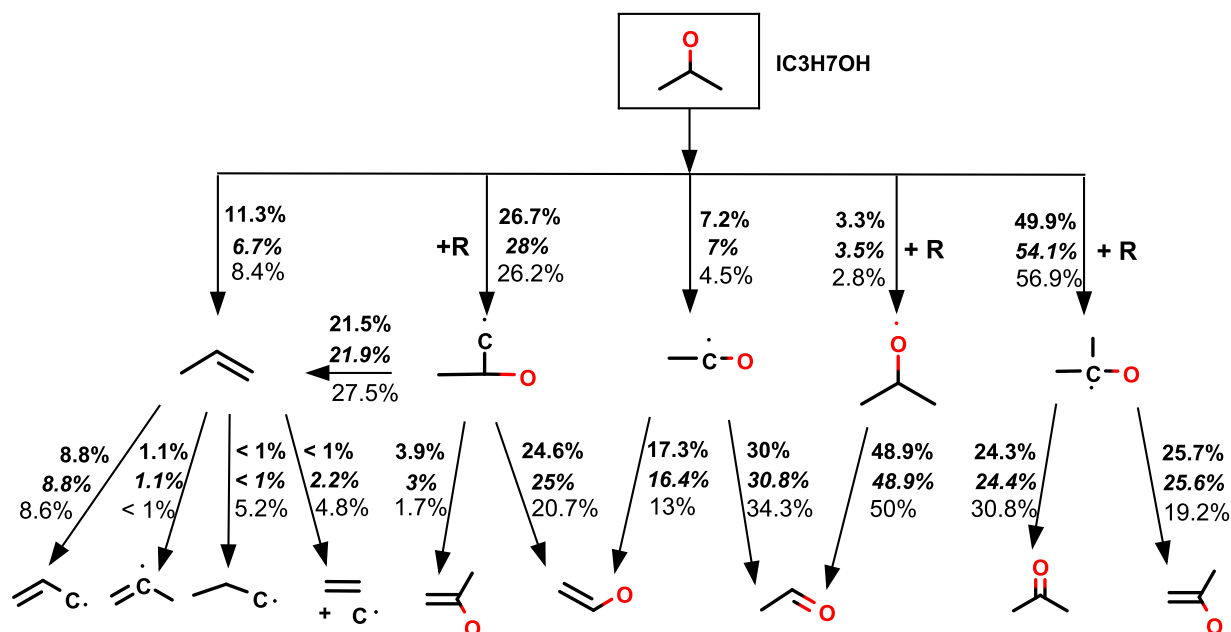


Figure 3.34: Reaction pathway for *iso*-propanol pyrolysis using model by Sarathy et al. [119] with three conditions. Condition 1 (in bold): 1% fuel, 1450 K, and 12 atm; Condition 2 (in bold italic): 1% fuel, 1450 K, and 12 atm; Condition 3 (in regular): 2% fuel, 1450 K, and 12 atm.

follows a channel not directly leading to CO.

The current experimental characterizations of ignition and pyrolysis times show the potential of accessing the complex chemical kinetics of combustion through global measures such as ignition and pyrolysis times. It has been shown that they can offer information about the effect of various control parameters of the reactive system. In conjunction with chemical kinetic model analysis, the global measures allow us to rationalize observed trends in terms of the underlying elementary chemical kinetic processes.

3.4 Global kinetic times of methyl tert butyl ether and 2-methyl tetrahydrofuran

Here, the ignition-resistant additive, MTBE, is characterized and contrasted with the kinetic of the cyclic ether with the hope of establishing kinetic differences or similarity for ignition resistance. Result of ignition delay times, followed by pyrolysis times and their contrast with ignition times are presented below. The experimental data are then compared with their respective model predictions. The models considered in these comparisons with experiments are the MTBE model by Curran et al. [67], the 2-MTHF models by Wang et al. [46] and Fenard et al. [49].

3.4.1 Ignition delay times

The uncertainties of the ignition delay time data are estimated to lie between 10% and 20% based on statistical propagations of uncertainties. The major contributions of these uncertainties are: temperature uncertainties (1.0 - 1.5%), pressure uncertainties (1.0-1.5%), line fits and ignition delay measurement (1%).

Ignition delay times for stoichiometric fuel/ O_2 /Ar mixtures are measured. The argon to oxygen ration, D , is 3.76; the fuel mole fraction is 3%. The temperature and pressure effect

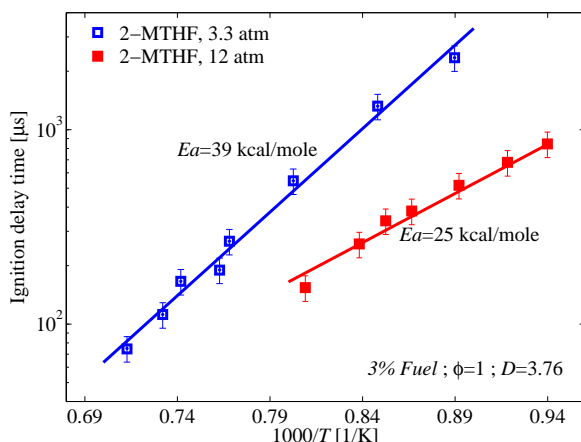


Figure 3.35: Pressure effect on 2-MTHF at 3.3 and 12 atm.

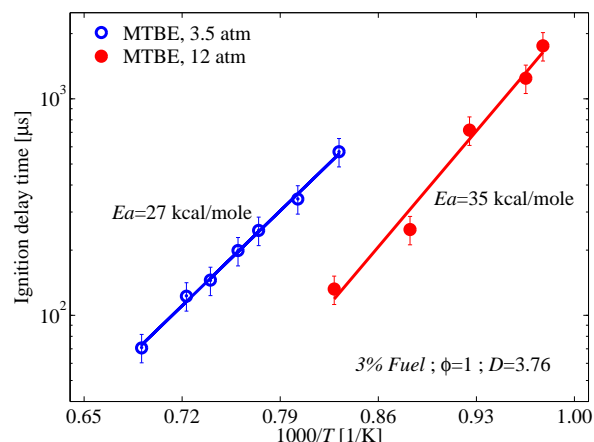


Figure 3.36: Pressure effect on MTBE at 3.5 and 12 atm.

are illustrated in Figures 3.35 and 3.36 for 2-MTHF and MTBE, respectively. Figure 3.35 shows that ignition delay times decrease with increasing temperature and pressure. A similar trend is observed for MTBE as shown in Figure 3.36.

Of interest is how these measured delay times compare with model predictions. The experimental data are therefore compared with the predictions obtained using two chemical kinetic

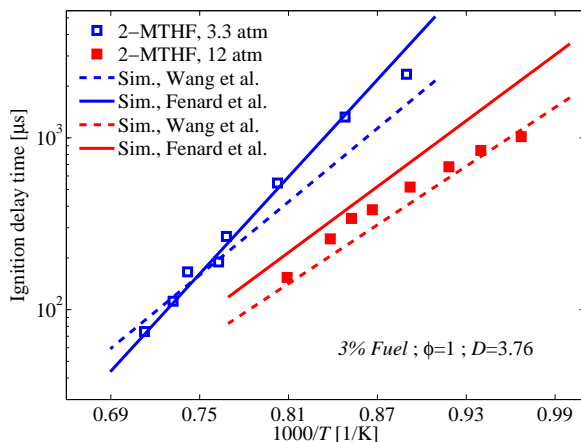


Figure 3.37: Comparison of measured 2-MTHF ignition delay times at 3.3 and 12 atm with model predictions [46, 49].

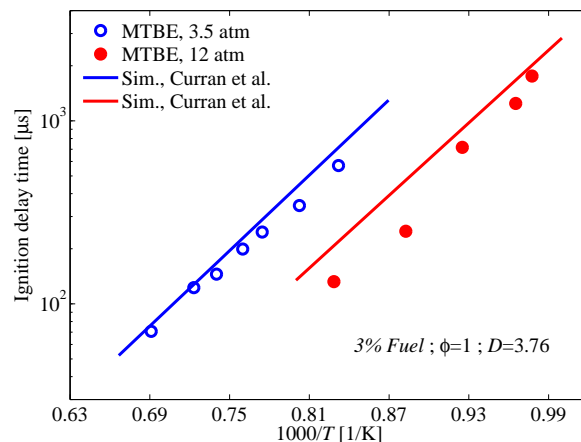


Figure 3.38: Comparison of measured MTBE ignition delay times at 3.5 and 12 atm with model predictions [67].

models [46, 49] for 2-MTHF and one chemical kinetic model [67] for MTBE . Figure 3.37 shows the comparison of model predictions with measured ignition delay times for stoichiometric mixtures of 3% 2-MTHF at 3.3 atm and 12 atm. Predictions of the model by Fenard et al. [49] are in close agreement with the experimental observations at the nominal pressure of 3.3 atm. In the case of MTBE, the experimental data of 3.5 atm are accurately predicted by the model of Curran et al. [67] as shown in Figure 3.38. The model over predicts delay times in the case of the higher pressure of 12 atm, especially at higher temperature.

The effect of equivalence ratio at a fixed fuel concentration is examined for the case of 2-MTHF. The results in Figure 3.39 show that with this constraint, ignition delay times increase with fuel concentration. This approach to establishing the effect of equivalence ratio is different for that of equivalence ratio effect for fuel air mixture, in which not the fuel, but the ratio of diluent to oxygen is kept constant. In this case of constant fuel concentration, the longer ignition delay is due to correspondingly lower oxygen concentration. Figure. 3.39 also shows that the model by Fenard et al. [49] properly capture the data.

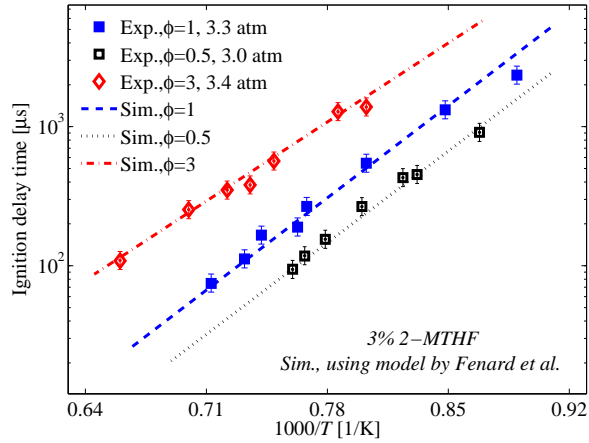


Figure 3.39: Comparison of measured 2-MTHF ignition delay times at three equivalence ratios with predictions of model by Fenard et al. [49].

To summarize, this subsection demonstrated that ignition delay times for both MTBE and 2-MTHF decrease with increasing temperature and pressure. In addition, results show that

ignition delay times increase with increasing equivalence ratio on account of the lower O_2 , since the fuel percentage is fixed.

3.4.2 Pyrolysis times

The global kinetics of the pyrolysis of these ethers can be assessed using the pyrolysis time previously described. Here, pyrolysis times are measured using a mixture of about 3% fuel in argon. The pyrolysis times are obtained from the time-to-maximum of the product of CO absorbance and its time-rate of change.

Several sources contribute to the uncertainty in the resulting pyrolysis time, including temperature (estimated at 1.0%), pressure (1.0%), fit parameters of the CO absorbance (10%). Assuming an Arrhenius dependence of the pyrolysis time on temperature, the combined uncertainty of the experimental pyrolysis time is estimated to be 22-25%.

The effect of temperature and pressure on pyrolysis times of 2-MTHF at average pressures of 3.3 atm and 11 atm are shown in Figure 3.40, where the pyrolysis times are observed to decrease with increasing temperature and pressure, similar to the effect of temperature and pressure on ignition delay times. As shown in Figure 3.40, the apparent activation energy of 2-MTHF pyrolysis is higher than that of 2-MTHF ignition. This points to a much stronger sensitivity to changes in the reactor temperature. In Figure 3.41, the pyrolysis times of 2-MTHF are compared with those of MTBE. Here, it is found that the pyrolysis of 2-MTHF is faster than that of MTBE, pointing to the greater resistance of the tert-butyl structure to thermal decomposition.

The observed pyrolysis times are also compared with model predictions. Figure 3.42 shows the comparison of model predictions by Fenard et al. [49] and Wang et al. [46] models with data for mixture of 3% 2-MTHF in argon at average pressures 3.3 atm and 11 atm. It is observed that the model by Fenard et al. [49] captures the pyrolysis times at the higher

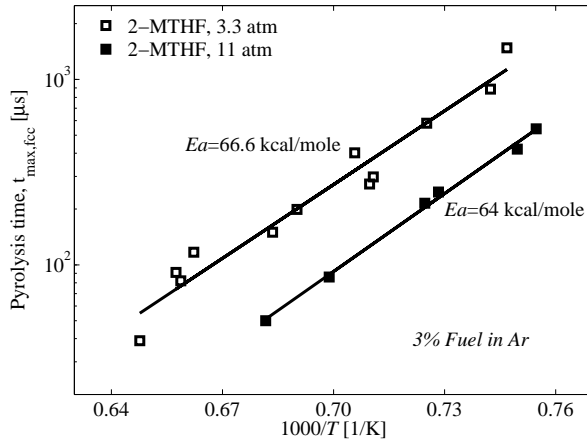


Figure 3.40: Pyrolysis time scales of 2-MTHF at 3.3 & 11 atm.

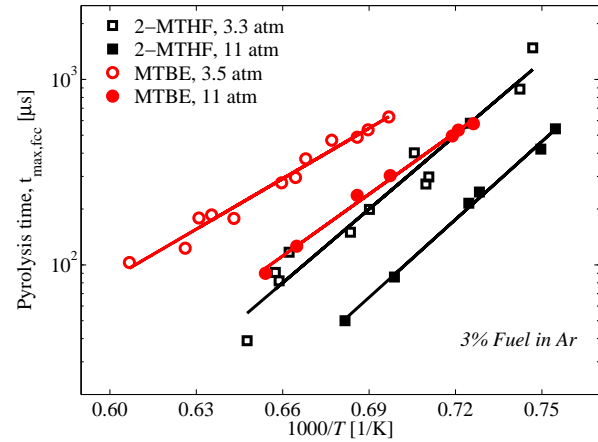


Figure 3.41: Pyrolysis time scales of 2-MTHF and MTBE at different pressures.

pressure while showing significant deviations at the lower pressure. The model by Wang et al. [46] predicts much shorter pyrolysis times than measured. The measured pyrolysis times of 3% MTBE in argon at average pressure 3.5 atm and 11 atm are also compared with predictions obtained using the model by Curran et al. [67]. Figure. 3.43 illustrates that the model predicts much shorter pyrolysis time. This must be understood together with the approach to the equilibrium concentration. Thus, the pyrolysis time and the time to

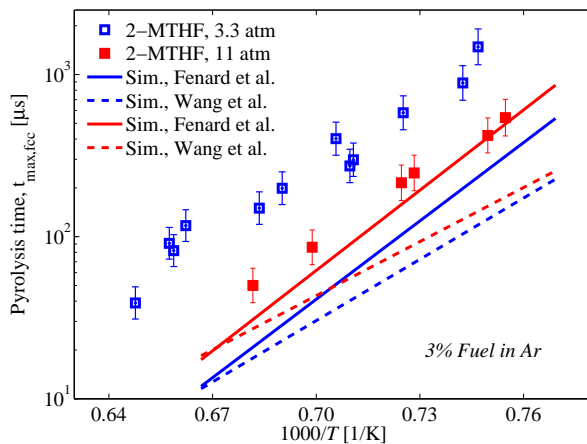


Figure 3.42: Comparison of pyrolysis time scales of 2-MTHF at 3.3 & 11 atm with simulations [46, 49].

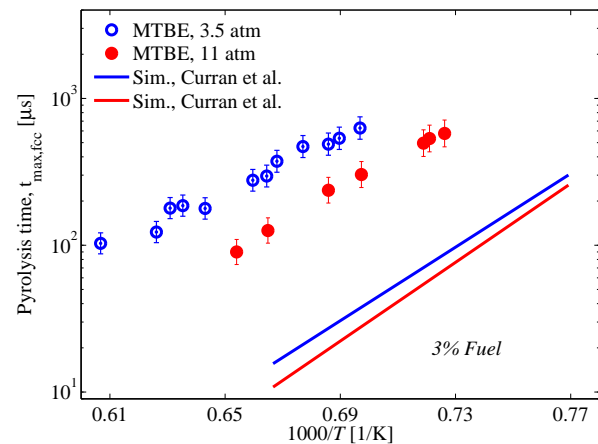


Figure 3.43: Comparison of pyrolysis time scales of MTBE at different pressures with simulation [67].

equilibrium will be further discussed.

The implication of the difference between the temperature sensitivity of pyrolysis and that of ignition is further explored by plotting these together as shown in Figures 3.44 and 3.45, for 2-MTHF and MTBE, respectively. In contrast to ignition process that generally has global activation energies in the range of about 20-40 kcal/mol [84, 229], the pyrolysis process has a higher global activation energy which might be as much as 1.5 times higher than the activation energy for ignition.

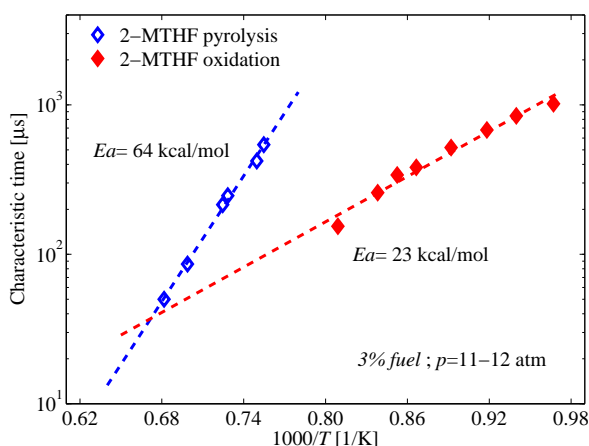


Figure 3.44: Comparison of ignition delay times ($\phi = 1$) with pyrolysis time scales for 3% of 2-MTHF at pressures of 11-12 atm.

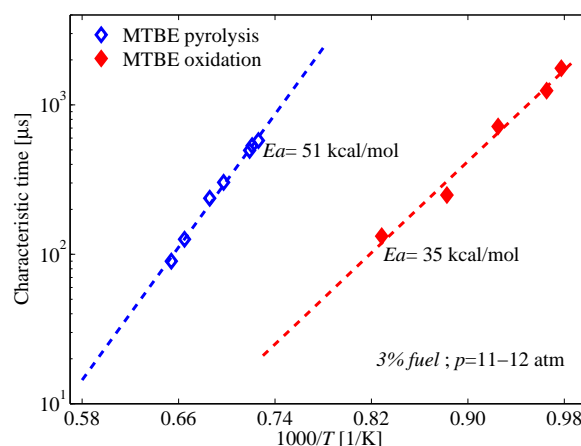


Figure 3.45: Comparison of ignition delay times ($\phi = 1$) with pyrolysis time scales for 3% MTBE at pressures of 11-12 atm.

This difference in temperature sensitivity leads to a competition between oxidative and pyrolytic processes (reactions only involving reactants from fuel decomposition) during ignition. Figure 3.44 shows the comparison between pyrolysis times of 3% 2-MTHF and ignition delay times of a stoichiometric mixture with 3% 2-MTHF at 12 atm. At low temperatures, pyrolysis times are longer than ignition delay times but the trend reverses at higher temperatures. This cross-over occurs at about 1490 K. At temperature below 1490 K, the ignition process is dominated by oxidative reactions. Above that temperature, pyrolytic reactions become dominant, such that direct C–C bond scission followed by subsequent production and reactions of H and CH₃ radicals dominate over fuel attack by molecular

oxygen and oxygenated radicals. The oxygenated reactions are more important at lower temperatures.

In case of MTBE, while the pyrolysis times are definitely longer and more temperature sensitive, no cross-over is observed in this experimental window. This means that for the combustion of MTBE, the chemistry is controlled by oxidative reactions up to a much higher temperature than for other fuels. Also the apparent activation energy of the pyrolysis process is less than in the case of 2-MTHF and propanols studied before [230].

The cross-over between pyrolysis and ignition times is interpreted in terms of competition between non-oxidative fuel reactions and oxidative reactions during ignition. Therefore, there is going to be a certain dependence between the cross-over temperature and different equivalence ratios for mixtures with a fixed fuel concentration.

The dependence of the cross-over is explored for 2-MTHF both experimentally and through kinetic simulations. Figure. 3.46 shows the comparison between pyrolysis times and ignition delay times at three different equivalence ratios for a fixed fuel concentration of 3% and nominal pressure of 3.3 atm. It is observed that subject to these constraints, the ignition delay times of rich mixtures are longer on account of the associated lower O_2 concentration while

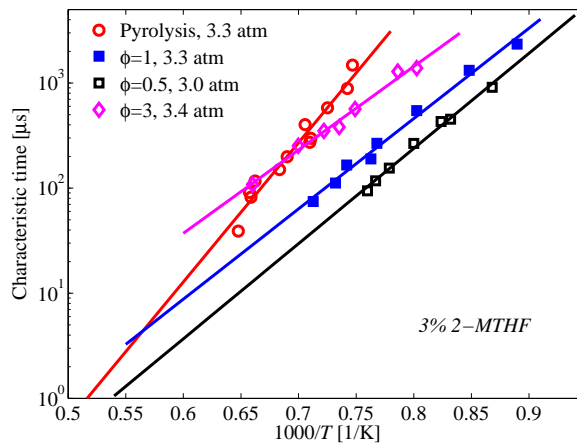


Figure 3.46: Comparison of 2-MTHF global kinetic times for mixtures with 3% fuel for the case of pyrolysis and ignition at equivalence ratios of $\phi = 1, 0.5$, and 3.

the temperature sensitivity does not change significantly. As a result of this, the lean mixture with a higher O_2 concentration at a fixed fuel concentration of 3%, shows that ignition delay times that are indicative of global oxidative kinetics predominate the combustion kinetics at much higher temperatures.

The experimental equivalence ratio cross-over trend can also be observed in simulation results. Figure 3.47 is based on simulations using the 2-MTHF model by Fenard et al. [49] and it illustrates that for each mixture, at high temperatures pyrolysis times are shorter than ignition delay times but the trend reverses at lower temperatures. The case of rich mixtures represents the kinetics of partial oxidation reactions. Therefore, for the rich mixture, the competition between pyrolysis and oxidative process is reached at lower temperatures than for stoichiometric and lean mixtures. Quantitatively, the predicted pyrolysis times are much shorter than the measured times. This point will be further discussed later. Although, the cross-over is not experimentally observed for MTBE, the effect of equivalence ratio can be explored using simulation. Figure 3.48 shows the simulated pyrolysis times and ignition delay times at three equivalence ratios using the model by Curran et al. [67]. It is similarly

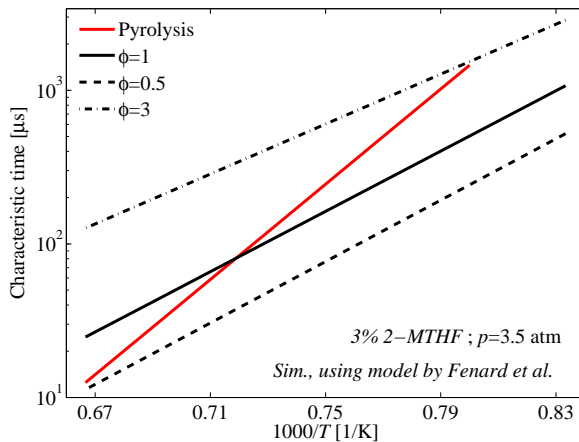


Figure 3.47: Comparison of ignition delay times at $\phi = 1, 0.5, 3$, with pyrolysis time scales of 3% 2-MTHF based on kinetic model simulations.

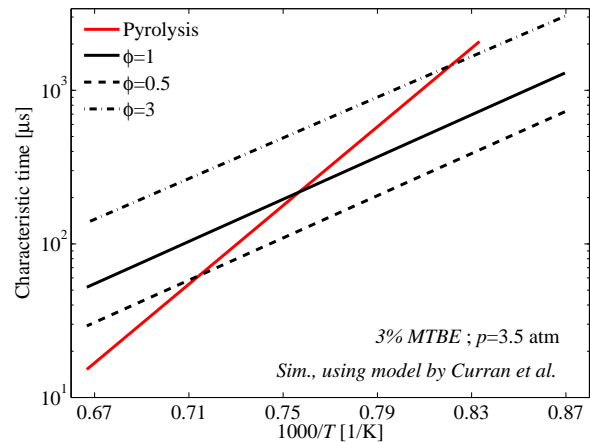


Figure 3.48: Comparison of ignition delay times at $\phi = 1, 0.5, 3$ with pyrolysis time scales of 3% MTBE based on kinetic model simulations.

observed that the higher oxygen in lean mixture shifts the competition between pyrolysis and ignition toward higher temperatures.

In essence, this subsection demonstrated that pyrolysis times of both MTBE and 2-MTHF decrease with increasing of temperature and pressure. Moreover, the results of pyrolysis times show that 2-MTHF is more reactive than MTBE. Comparing ignition and pyrolysis times of these fuels verifies the cross-over effect established in earlier studies. With respect to pyrolysis, the expected cross-over behavior in lean mixtures is shifted toward higher temperatures, so that oxidative processes dominate in leaner mixtures over a longer temperature range.

3.5 Global kinetic times of methyl propanoate and methane blends

Ignition delay times of MP, CH₄, and MP/CH₄ blend are measured to establish the enhancement of CH₄ ignition by the biodiesel surrogate, MP. Pyrolysis times of MP and its blend with CH₄ are also measured to find out if CH₄ significantly slows down MP decomposition.

3.5.1 Ignition delay times

Ignition delay times for mixtures of fuel/O₂/Ar are reported as plots of the delay times against inverse temperatures for given nominal pressures, equivalence ratios, and fuel concentrations. Uncertainties in measured delay times are estimated using statistical propagation of the errors of contributing factors. The major contributors to the uncertainty in measured ignition delay times include: temperature uncertainties (1.0 - 1.5%), pressure uncertainties (1.0-1.5%), fits and ignition delay measurement (1%). On account of the exponential dependence of ignition delay times on temperature, the propagated uncertainties in ignition delay times are dominated by the temperature uncertainties. Taking these into account, estimated ignition uncertainties are between 10% to 20%.

The differences in ignition propensity of 3% MP and 3% CH₄ are first established as shown

in Figure 3.49. The higher reactivity of MP is unmistakable since the ignition delay times of MP are shorter than those of CH_4 by close to two orders of magnitude. It can therefore be expected that adding MP to CH_4 can enhance the ignition of the blend. The effect of adding 20% and 50% MP to CH_4 is then investigated and the results are shown in Figure 3.50. One observes the disproportionate modification of CH_4 ignition by MP since ignition delay times of the blends are closer to those of MP, despite the high amount of CH_4 . For instance, the ignition delay times of CH_4 are as much as about 8 times longer than of those of the blend with 20% MP at 1377 K while they are about 18 times longer than those of the blend with 50% MP at 1360 K. The observed reactivity trends can be understood as resulting from the very strong C–H bonds in CH_4 which are resistant to chain reaction initiation and propagation of chain reactions that are ultimately responsible for ignition. Much higher temperatures are needed to induce the controlling chain reactions. The highly reactive nature of MP is connected to its weaker C–H bonds and the more readily generated reactive radicals that promote reactions once the fuel is attacked. With addition of a small amount of MP, many radicals are generated. Their subsequent reactions with CH_4 are marked by lower activation

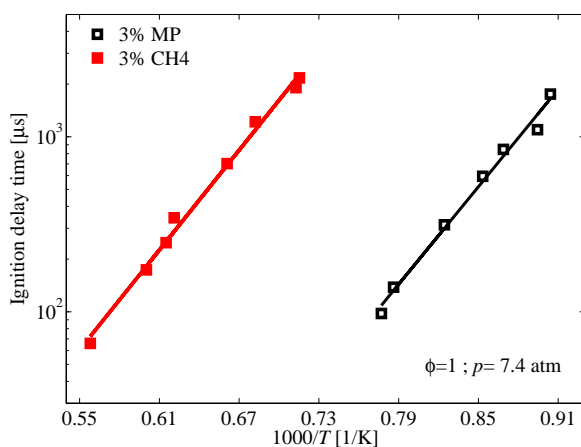


Figure 3.49: Ignition delay times of stoichiometric mixtures of fuel, oxygen, and argon for MP and CH_4 at scaled pressure of 7.4 atm. Solid lines represent Arrhenius fits

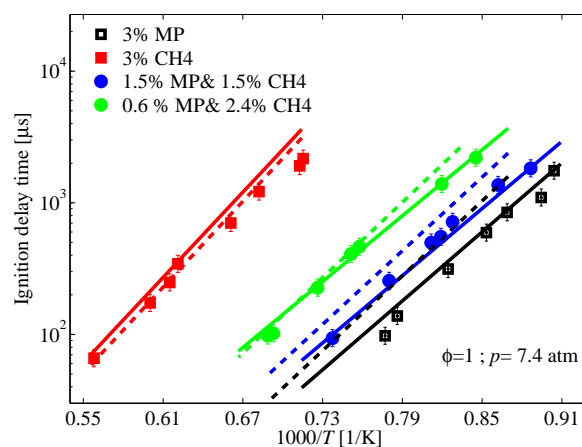


Figure 3.50: Experimental and model predictions of ignition delay times of MP, CH_4 and blend of both at scaled pressure of 7.4 atm. Solid lines: model by Zhang et al. [163] Dashed lines: model by Zhao et al. [164].

barriers compared to such high barrier reactions as decomposition of CH_4 to CH_3 and H by C–H bond breaking.

The observed ignition delay times are also compared with predictions of two chemical kinetic models by Zhang et al. [163] and Zhao et al. [164] as shown in Figure 3.50. We see that the model by Zhang et al. [163] more closely predicts the measured ignition delay times than the model by Zhao et al. [164]. Both models capture the significant reactivity differences, thus, reflecting a proper account of MP and CH_4 oxidation kinetics in the models.

Figure 3.51 shows ignition delay times of 3% MP, 3% CH_4 and blends of equal proportion of both fuels at a lower average pressure of 4 atm. Similar to the observations at 7.4 atm, adding MP to methane leads to significant reduction of the ignition delay times of methane, bringing them closer to those of MP. The model by Zhang et al. [163] consistently shows good agreement with the measurements of MP and the blend whereas the model by Zhao et al. [164] predicts longer ignition delay times than measured.

Differences in ignition behavior of the two fuels and their blend are further explored under lean conditions ($\phi = 0.5$) as shown in Figure 3.52. Similar to the case of the stoichiometric

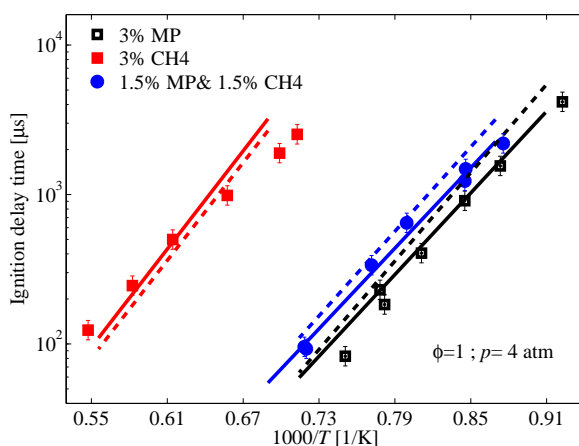


Figure 3.51: Experimental and model predictions of ignition delay times of MP, CH_4 and blend of both at scaled pressure of 4 atm. Solid lines: model by Zhang et al. [163] Dashed lines: model by Zhao et al. [164].

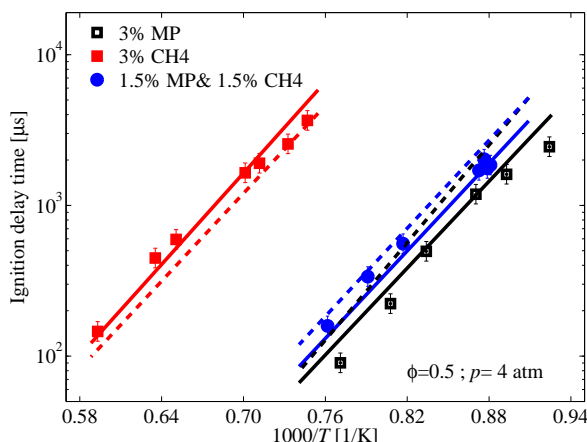


Figure 3.52: Experimental and model predictions of ignition delay times of MP, CH_4 and blend of both for mixtures with 3% fuel and $\phi = 0.5$ at a nominal pressure of 4 atm. Solid lines: model by Zhang et al. [163] Dashed lines: model by Zhao et al. [164].

mixtures, it is observed that while CH_4 has long ignition delay times, the ignition delay times of MP are over an order of magnitude shorter at comparable temperatures. As already established, the radicals generated by the more readily ignitable MP greatly enhance the ignition kinetics of the blend of MP and CH_4 of equal proportions, such that the ignition delay times of the blend are also closer to those of MP under these lean conditions. With respect to the performance of the two models considered, the model by Zhang et al. [163] more closely predicts the experimental data while the model by Zhao et al. [164] slightly underpredicts CH_4 delay times and over predicts those of MP and the blend.

Comparing lean and stoichiometric ignition delay times for these mixtures of fixed fuel percentage (3%), Figure 3.53 shows that lean mixtures of both fuels ignite more readily than the stoichiometric mixtures on account of the higher oxygen concentration that is conducive to rapid radical generation.

The reactivity trends above have been established by fixing the fuel concentration. Another approach is to fix the oxygen concentration, making the situation closer to the technical case where fuel reactivity trends are often judged based on fixed diluent to oxygen ratios as in air

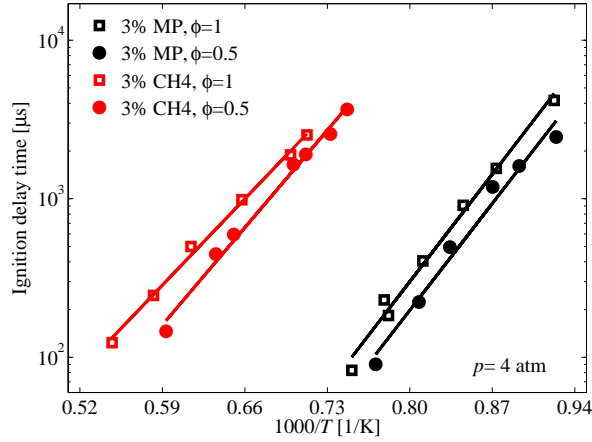


Figure 3.53: Experimental ignition delay times of stoichiometric and lean mixtures of MP and CH_4 with fuel maintained at 3% at an average pressure of 4 atm. Solid lines: model by Zhang et al. [163] Dashed lines: model by Zhao et al. [164].

and equivalence ratios. Figure 3.54 shows the ignition delay times for stoichiometric mixtures of CH_4 , MP, and a blend of the two fuels at an average pressure of 10 atm, whereby O_2 is maintained at 10%. Under these conditions, CH_4 delay times are also longer than those of MP by over an order of magnitude. The ignition delay times of the blend is similarly closer to those of MP. While both models accurately predict the CH_4 delay times, only the model

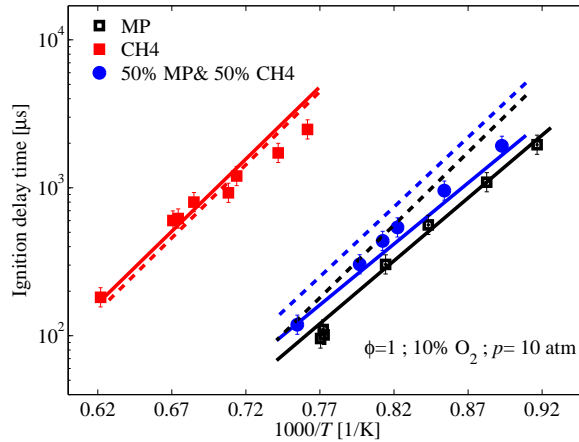


Figure 3.54: Experimental ignition delay times and model predictions of MP, CH_4 and blend of both fuels with O_2 maintained at 10% and at an average pressure of 10 atm. Solid lines: model by Zhang et al. [163] Dashed lines: model by Zhao et al. [164].

by Zhang et al. [163] properly captures the delay times of MP and the blend, whereas the model by Zhao et al. [164] over predicts the delay times of MP and the blend.

These comparisons establish the pronounced differences between the ignition delay times of CH_4 and MP, and further show the enhancement of CH_4 by MP toward the delay times of MP in blends of the two fuels. To understand the chemical influence of MP on the blend ignition, a reaction pathway analysis can be carried out.

Reaction pathway analysis: Reaction pathway analysis of representative oxidation processes are carried out using the model by Zhang et al. [163] on account of its better agreement with measurements.

Figure 3.55 shows the pathways during ignition of a stoichiometric mixture of 3% methane at temperature of 1500 K, pressure of 7.4 atm, at 600 μs when the ignition delay time is predicted to be 1250 μs . It is observed that the fuel is mostly attacked by radicals, which are generated from further reaction of products from chain initiation by strong C–H bond

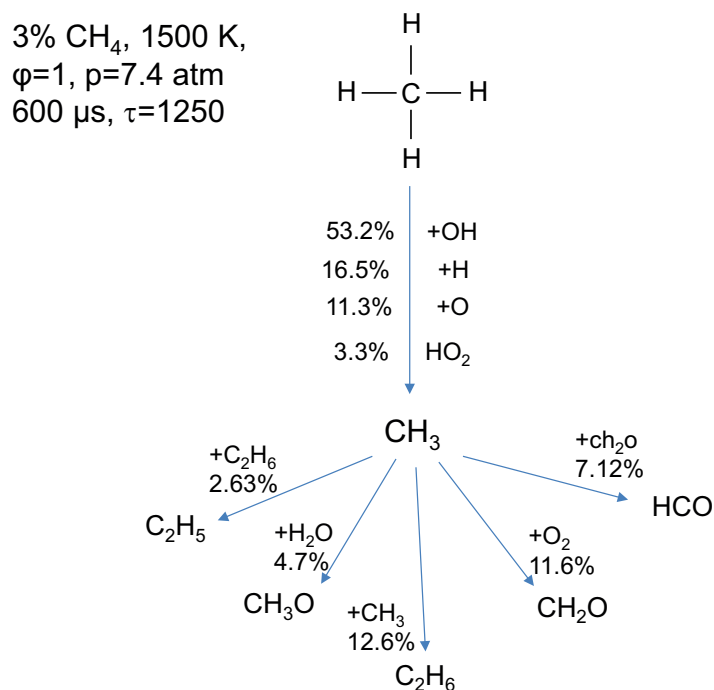


Figure 3.55: Reaction pathway for 3% CH_4 ($\phi=1$, $T=1500$ K, $p=7.4$ atm) using models by Zhang et al. [163].

3% MP, 1287 K,
 $\phi=1$, $p=7.4$ atm
 $50 \mu\text{s}$, $\tau=145$

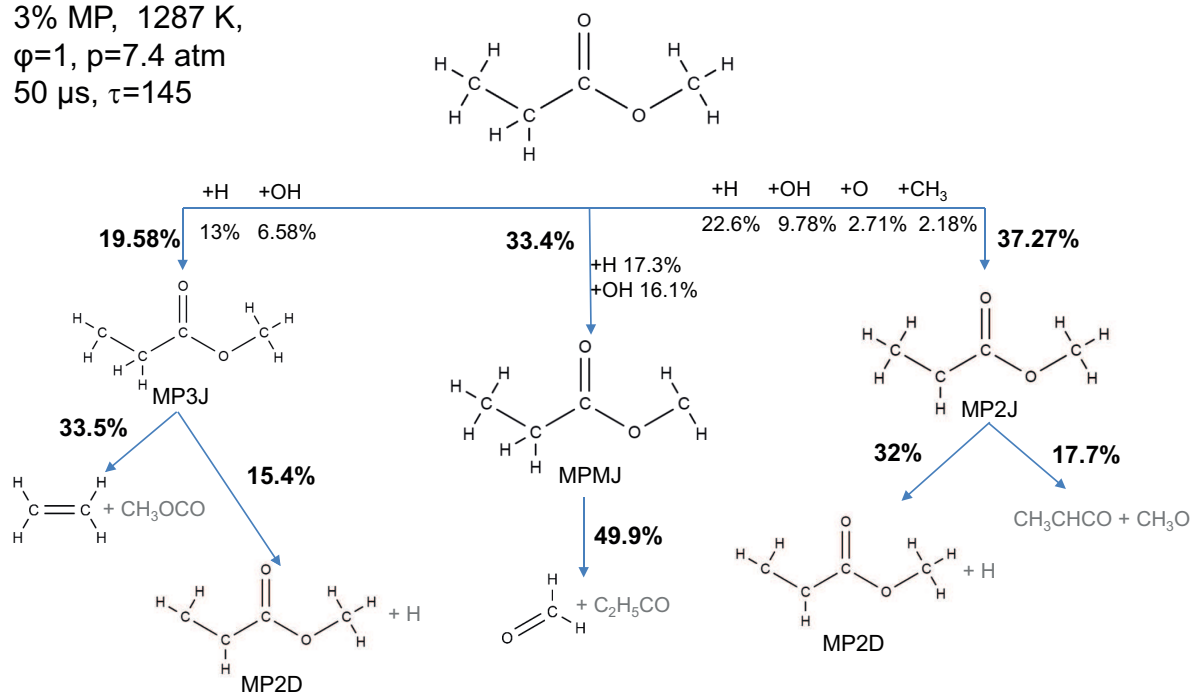


Figure 3.56: Reaction pathway for 3% MP ($\phi=1$, $T=1287$ K, $p=7.4$ atm) using models by Zhang et al. [163].

breaking. Then, the radical pool slowly builds up and leads to further reactions of methyl radical to products. It is noteworthy that high temperatures are needed to realize a methane ignition event within 2 ms.

For 3% MP system, a reaction pathway analysis is also conducted at a temperature of 1287 K, a pressure of 7.4 atm, and at $50 \mu\text{s}$ instance, for which the predicted ignition delay time is $145 \mu\text{s}$. As shown in Figure 3.56, MP is mainly consumed through H abstraction reactions by H, OH, O and CH₃. H-abstraction from the α -carbon is dominant and produces CH₃CHCOOCH₃ (MP2J). The other important path is H abstraction from the CH₃O group which leads to production of CH₃CH₂COOCH₂ (MPMJ). Finally, the less favored H abstraction site produces CH₂CH₂COOCH₃ (MP3J). These primary MP radicals further react by beta-scission to yield radicals and smaller stable oxygenated compounds or ethylene. The faster kinetics of MP is mainly related to the ease with which the primary MP radicals are formed and their subsequent beta-scission reactions.

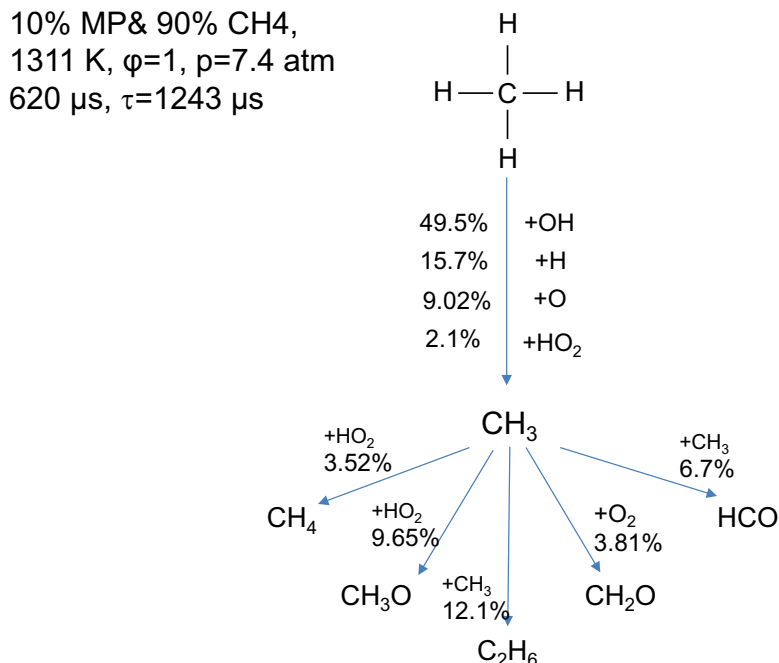


Figure 3.57: Reaction pathway for 90% CH₄ and 10% MP ($\phi=1$, $T=1311$ K, $p=7.4$ atm) using models by Zhang et al. [163].

To examine the sensitive kinetic effect of MP on methane ignition, further reaction pathway analysis is carried out for a mixture of 90% CH₄ and 10% MP at a temperature of 1311 K, a pressure of 7.4 atm, and at the 620 μ s instance, for which conditions the ignition delay time is predicted to be 1243 μ s. The results are shown in Figure 3.57. This blend ignition delay time is quite close to the delay time at the condition chosen to analyze the reaction pathway of methane but the blend mixture is at the lower temperature of 1311 K as compared to 1500 K in the case of pure CH₄. Influence of MP on CH₄ comes through the pool of radical, such as OH, H, HO₂, O that are generated from MP oxidation. The important chain branching reaction, $\text{H} + \text{O}_2 \rightleftharpoons \text{O} + \text{OH}$, is influenced by more the readily liberated H atoms from MP. Moreover, in the presence of MP, very low barrier reactions such as $\text{CH}_4 + \text{OH}$, are greatly enhanced, with OH coming from the enhanced chain branching reaction.

Thus, we see that the ease with which radicals are initially generated in MP and from the further decomposition of fuel radicals do yield a greater pool of radicals, which in turn promote the evolution of the MP reactor toward ignition. In the case of blends, radicals from

MP can also attack the CH_4 , with enhanced reaction rates for reactions with low activation barriers. The case of CH_4 with very long ignition times is mostly influenced by the strong C-H bonds that greatly lower the rate of initial radical generation.

In summary, this subsection demonstrated that the biodiesel surrogate, methyl propanoate (MP), is more reactive than methane. In addition, the evidence of chemical interactions during ignition of methane blends is observed through a reduction of methane ignition delay times as a result of MP addition. The influence is nonlinear, with the result that ignition delay times of blends of equal proportions of the two fuels are much closer to the ignition delay times of the more reactive MP. This is understood to result from the rapid generation of radicals during MP oxidation which further react with methane in low-activation energy elementary reactions, such as OH which reacts almost barrier-less.

3.5.2 Pyrolysis times

The pyrolysis of MP and its blend with CH_4 is investigated to establish the influence of CH_4 on the decomposition rate of MP and to be able to contrast the time scales of pyrolysis with those of ignition, indicating temperature ranges where one expects non-oxidative fuel decomposition processes to play a greater role during ignition. As previously discussed, the global kinetics of the pyrolysis of MP and CH_4 can be assessed using the pyrolysis time [230], where the absorbance of CO is used for the correlation on account of the oxygenated nature of MP.

The uncertainty in the resulting pyrolysis time comes from several sources including temperature (estimated at 1.0%), pressure (1.0%), fit parameters of the CO absorbance (10%). From these uncertainties and assuming an Arrhenius dependence of the pyrolysis time on temperature, the combined uncertainty of the experimental pyrolysis time is estimated to be 22-25%.

The effect of fuel concentration on pyrolysis times of MP and its blend with an equal proportion of CH_4 is shown in Figure 3.58a. The pyrolysis time is observed to be fairly insensitive to MP concentration or the presence of methane. The methane addition seems to lengthen the pyrolysis time at low temperatures but not significantly, compared to the case of 1.5% MP. It is possible that a very weak effect of fuel concentration also exists but it cannot be clearly discerned from the concentration doubling used here.

Figure 3.58a also shows the dependence of MP and CH_4 pyrolysis times on temperature. An Arrhenius-type dependence with a global activation energy between 50 to 60 kcal/mol is observed. This reflects the predominant role of C–C bond breaking and beta scission reactions during pyrolysis. This is in contrast with global activation energies of ignition process which are generally about 30-40 kcal/mol (about 40 kcal/mol in this study).

The observed pyrolysis times are also compared with model predictions in Figure 3.58b. Shown are results for mixtures of 3% MP and a mixture of MP and CH_4 in argon at average pressure 4 atm. It is observed that model by Zhao et al. [164] more closely captures the pyrolysis times at 3% MP while showing greater deviations for the blend mixture. The model

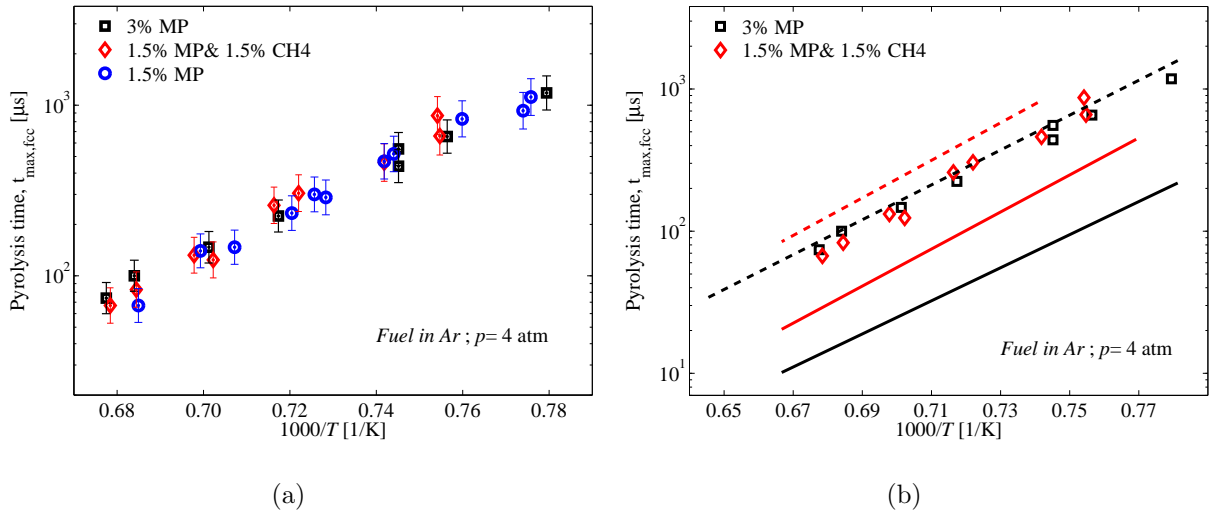


Figure 3.58: a) Pyrolysis time scales of MP and its equal blend with CH_4 . b) Comparison of pyrolysis time scales with simulations. Solid lines: model by Zhang et al. [163] Dashed lines: model by Zhao et al. [164]

by Zhang et al. [163] predicts much shorter pyrolysis times than measured. This is in contrast with the agreement observed for ignition, where the model by Zhang et al. [163] is consistently in closer agreement with the measured delay times for all mixtures considered.

Comparing the ignition and pyrolysis times, we can establish distinctive differences in global kinetics between oxidation and pyrolysis. Figure 3.59 is a plot of pyrolysis times of blend of 1.5% MP and 1.5% CH_4 and ignition delay times of a stoichiometric blend with 1.5% MP and 1.5% CH_4 at 4 atm over a range of temperatures. It is observed from the gradients that pyrolysis is more sensitive to temperature than ignition as previously mentioned. At lower temperatures, ignition delay times are shorter than pyrolysis time, but at higher temperatures, the trend reverses. For the mixture with 3% MP, the difference in the temperature sensitivity is weaker and the trend reversal is not observed in the measured temperature window as shown in Figure 3.60. The difference means that for ignition events, radical reactions involving oxygenated species, such as OH are crucial to the ignition process. As the temperature increases, more fuel-related radicals and direct C–C bond breaking reactions participate in the consumption of the fuel, with the ignition process resulting from the further oxidation of the fuel breakdown products.

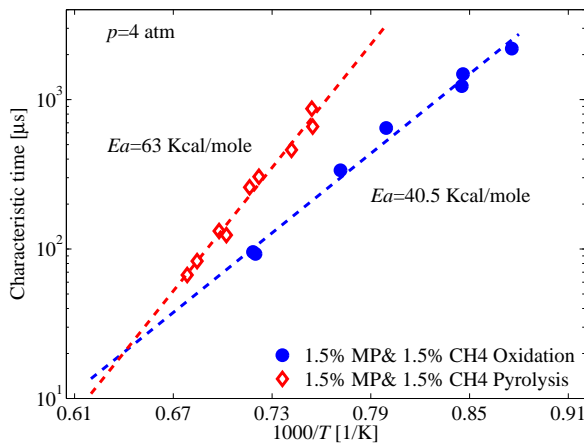


Figure 3.59: Comparison of ignition delay times ($\phi = 1$) with pyrolysis time scales of 1.5% MP with 1.5% CH_4 .

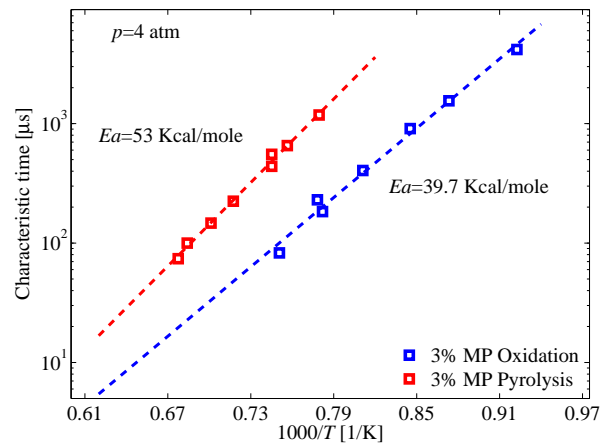


Figure 3.60: Comparison of ignition delay times ($\phi = 1$) with pyrolysis time scales of 3% MP.

These global time measurements establish the high degree of methane ignition enhancement. They also indicate the ineffectiveness of trying to increase MP stability by CH_4 addition.

In essence, it is shown in this subsection that the presence of methane is not observed to significantly influence the pyrolysis time of MP. This indicates limited radical withdrawal by methane during the pyrolysis of methyl propanoate.

In general, this chapter has presented global chemical time measurements. These times include the conventional ignition delay times and the newly developed concept of pyrolysis times. These times have been compared to reveal differences in the influence of pyrolysis. In addition, a number of chemical kinetic models have been validated.

Chapter 4. Fuel and CO time-history measurements

In this part of the work, the fuel and CO time-histories are presented for selected fuels. The measurements are carried out using direct laser absorption. They serve as more rigorous validation targets for chemical kinetic models. Fuel time-histories for 2-MTHF and 1,3-DMCH are first presented, followed by CO time-histories for propanol isomers, 2-MTHF, MTBE, and MP.

4.1 Fuel time-history measurement

The fuel time-histories are obtained using direct absorption of a HeNe laser beam at $3.39\text{ }\mu\text{m}$. The data for 2-MTHF are used to validate existing chemical kinetic model while those of DMCH are used to develop and improve a new chemical kinetic model.

4.1.1 2-Methyl tetrahydrofuran time-history measurements

The initial intention was to measure fuel time-histories for 2-MF and 2-MTHF but the feasibility depends on their absorption cross-section. The cross sections of 2-MF and 2-MTHF in stoichiometric mixtures are measured using the shock tube, whereby the known concentration from partial pressure mixture preparation allows for three cross-sections to be determined: before the incident shock, after the incident shock arrival and behind the reflected shock wave. The concentration based on prevailing pressure, temperature, and mixture fraction are used in the Beer-Lambert Law to calculate the corresponding absorption cross-section. Although these three cross-sections can be measured from one experimental realization, only the one determined at conditions behind the reflected shock wave is used

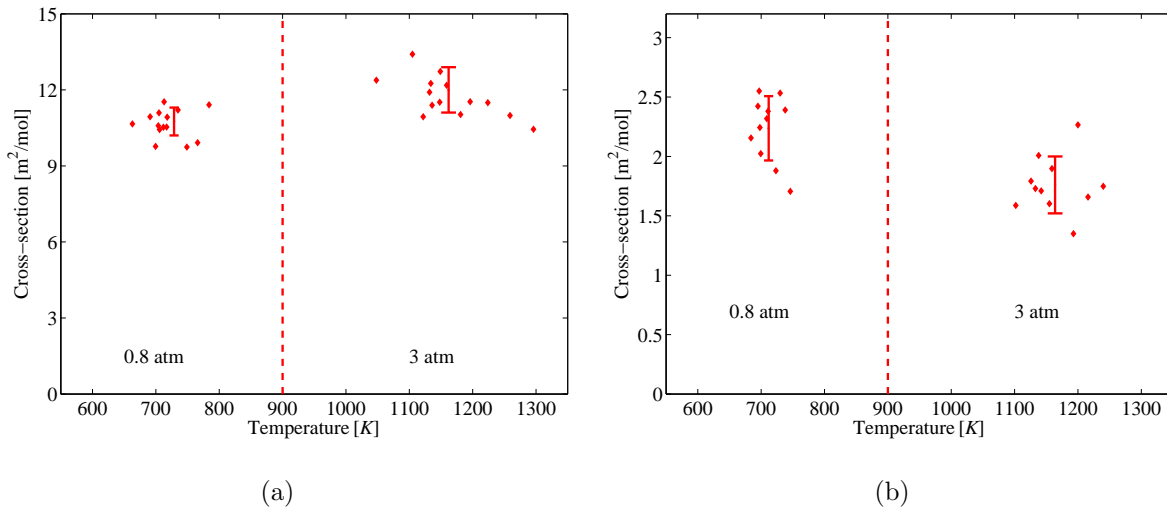


Figure 4.1: a) Shock tube measurements of 2-MTHF absorption cross sections, $\phi=1$ and $D = 3.76$, before the incident shock and behind the reflected shock. b) Shock tube measurements of 2-MF absorption cross sections, $\phi=1$ and $D = 3.76$, before the incident shock and behind the reflected shock.

for fuel mole fraction calculation during evolution of the reactor. In all calculations of fuel concentrations for the measured absorbance, the effects of pressure and temperature variations during reactor evolution on the absorption cross-section are assumed to be negligible, based on observed variations of cross-sections at different post-reflected shock conditions. The results of cross-section measurements are shown in Figure 4.1 where it can be seen that the combined effects of pressure and temperature are such that under the post-reflected shock conditions, the cross-section of 2-MTHF is $12 \text{ m}^2/\text{mol}$, on average, compared to the small cross-section of less than $2 \text{ m}^2/\text{mol}$ for 2-MF. This makes it difficult to measure 2-MF concentrations distinct from associated intermediate species, some of which may have higher cross-sections. The cross-section of 2-MTHF is sufficiently high to enable concentration measurements with appropriate corrections. The measurement of 2-MTHF time-histories is therefore further pursued.

4.1.1.1 Time-history profiles of 2-MTHF during ignition

Temporal evolution of laser absorbance is measured during the ignition of stoichiometric mixtures of 2-MTHF at 3 atm and lean ($\phi=0.5$) mixtures at 12 atm for a number of post-reflected shock temperatures. For each experiment the cross-section is determined from the post-reflected shock absorbance, prior to initiation of chemical reactions. The absorption at $3.39\ \mu\text{m}$ is necessarily non-specific to a given fuel since most hydrocarbons absorb at this wavelength. Here the model by Moshhammer et al. [219] is used to predict the mole fractions of intermediate hydrocarbons during ignition and pyrolysis, so that these can be used to correct the measurements. From the knowledge of species abundance and cross-sections, the most influential species are identified. In this case, interference by the following chemical species are found to be significant: CH_4 , C_2H_4 , C_3H_6 , C_4H_6 , $\text{C}_4\text{H}_8 - 1$, and CH_3CHO . The temporal evolution of the absorbance of predominant interfering species and their sum are shown in Figure 4.2a. The mole fractions have been converted to absorbance using their respective

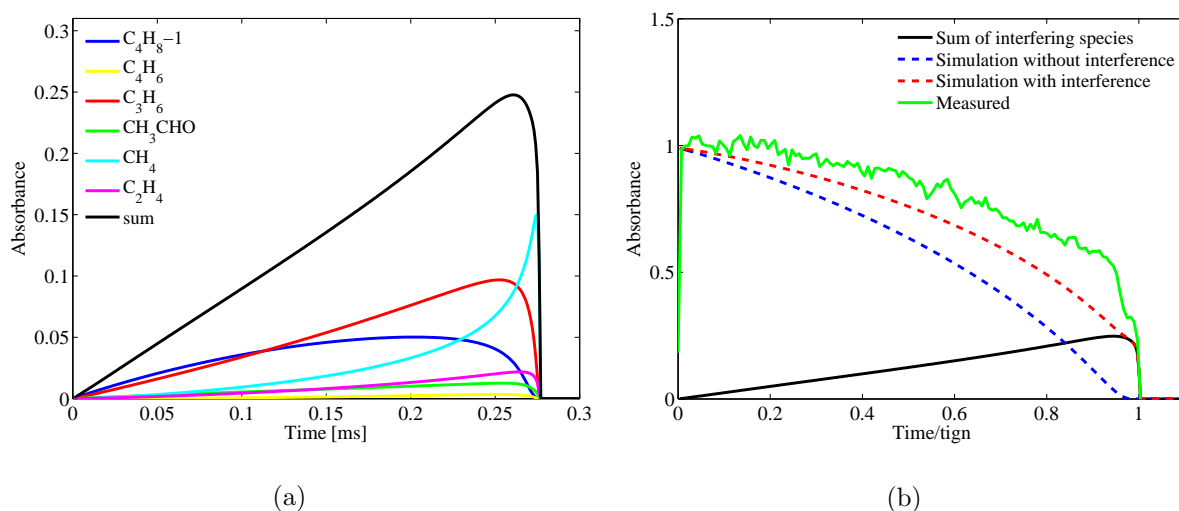


Figure 4.2: Summary of the interference correction method for a shock at 1257 K, 3 atm and stoichiometric mixture a) Absorbance time-histories due to six interfering species and their sum. b) Uncorrected experimental absorbance plotted against normalized time and absorbances obtained from simulations using model [219]. The simulations are with and without accounting for interference absorption.

high-temperature absorption cross-sections at the prevailing thermodynamic conditions. These cross sections are chosen from the literature [193, 231–233] and from the HITRAN database, resulting in the values of $5 \text{ m}^2/\text{mol}$ for CH_4 , $0.9 \text{ m}^2/\text{mol}$ for C_2H_4 , $4.5 \text{ m}^2/\text{mol}$ for C_3H_6 , $0.6 \text{ m}^2/\text{mol}$ for C_4H_6 , $9.25 \text{ m}^2/\text{mol}$ for $\text{C}_4\text{H}_8 - 1$, and $1 \text{ m}^2/\text{mol}$ for CH_3CHO .

To use the chemical kinetic model predictions of interfering species for correction, we assume that the main difference is that the model predicts shorter ignition delay times. So, if one normalizes the time by the respective ignition delay time, the chemical structure of the model reactor and the experiment are comparable. One can then infer the necessary correction to the measured absorbance from the difference between the absorbance obtained from summing absorbances of all relevant species and the absorbance due to the simulated fuel concentration. This is exemplified in Figure 4.2b where absorbances of the major interfering species, simulated fuel concentration with and without interference, and the measured absorbance are plotted against non-dimensional time. A correction polynomial is then applied to the measured absorbance before calculating the fuel mole fraction using the Beer-Lambert law in conjunction with the ideal gas law, $X = \frac{RT}{P} \frac{A}{\sigma L}$.

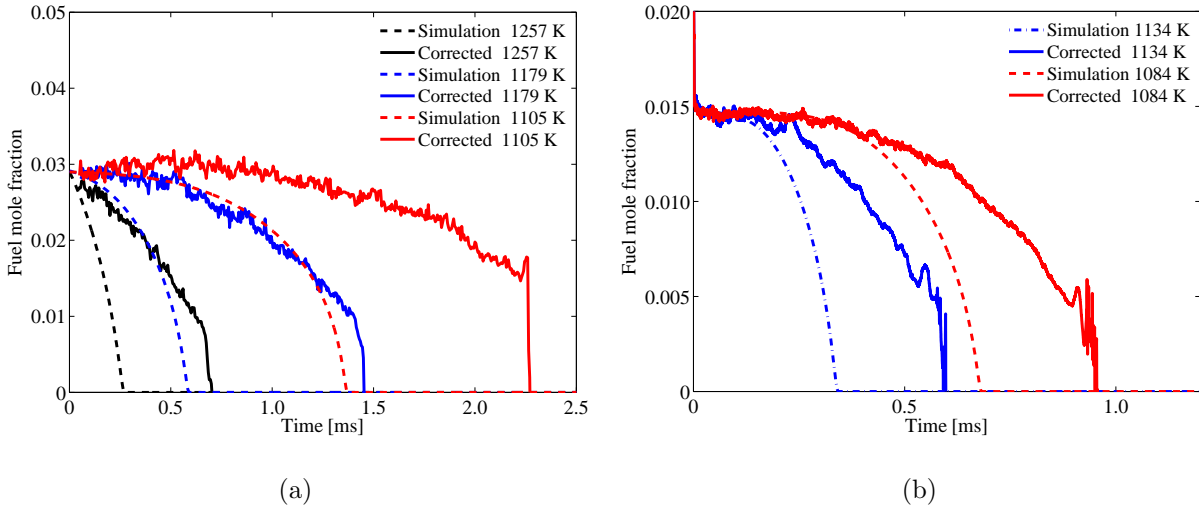


Figure 4.3: a) Comparison of corrected 2-MTHF mole fraction against model simulations at three temperatures, pressure of 3 atm, and $\phi=1$. b) Comparison of corrected 2-MTHF mole fraction against model simulations at two temperatures, pressure of 12 atm, and $\phi=0.5$.

The corrected fuel mole fractions are shown in Figures 4.3a and 4.3b for the stoichiometric case at 3 atm and the lean case at 12 atm, respectively. This correction preserves the observed fact that the model under-predicts the ignition delay time that corresponds with the time of complete fuel consumption. It is also observed that at lean conditions, the model captures the fuel profiles within the first half of the ignition time, suggesting that model deficiencies are more closely aligned with pyrolytic reactions at conditions of fuel rich combustion. Further, Figures 4.3a and 4.3b confirm that fuel oxidation is faster at higher temperature.

4.1.1.2 Time-history profiles of 2-MTHF during pyrolysis

Interferences in fuel absorption measurements are expected to be greater during pyrolysis since resulting hydrocarbon products are not oxidized as in the case of ignition. It is determined from simulations, using the same model above, that the major interfering species are C_2H_4 , C_3H_6 , C_2H_6 , CH_4 , $C_4H_8 - 1$, CH_3CHO , and CH_3COCH_3 . The high-temperature cross-sections of these species are also chosen from the literature [193, 231–233] and from the HITRAN database. Figure 4.4a is a plot of the temporal evolution of the absorbance of interfering species and their sum. The C4 species, $C_4H_8 - 1$, is formed within the first hundred micro seconds but is then slowly consumed. The rest of the pyrolysis products are C1-C3 alkenes and alkanes. A further challenge to the previous correction approach is the absence of a reference time in pyrolysis by means of which correction factors can be determined, assuming a self-similar chemical structure of the reactor. One way to overcome this is illustrated in Figure 4.4b. It consists in stretching the time scale of simulated absorbances, such that the absorbance of simulated fuel with interference aligns with the uncorrected experimental absorbance. The time-dependent correction factor for simulated profiles is then determined and used to correct the measured absorbance before calculating the fuel mole fraction.

The effect of this correction is shown in Figure 4.5 where the model prediction of fuel mole fraction is compared with mole fractions obtained from corrected and uncorrected mole

fractions. In this case, as in ignition, the correction method preserves the main observation that the model predicts much faster ignition and pyrolysis kinetics than observed in experiments. The correction shows that the interference of the other chemical species is minimal at the beginning but increase with progress of the pyrolysis. In Figure 4.6, two pyrolysis conditions are shown, and the discrepancy persists between model predictions and corrected experimental

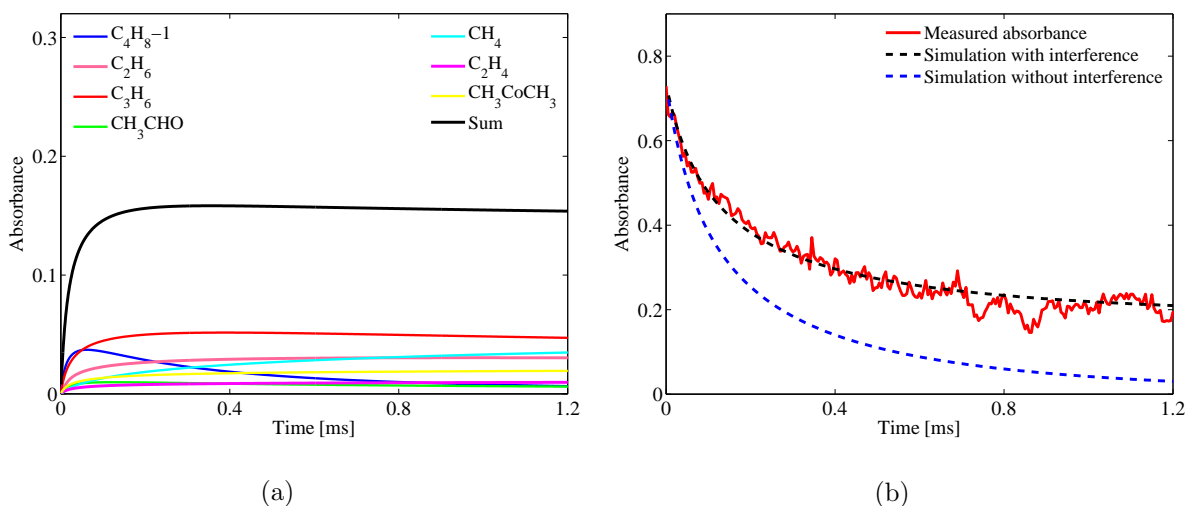


Figure 4.4: Summary of the interference correction method for a shock at temperature of 1442 K, pressure of 3 atm and 3% fuel. a) Absorbance time-histories due to six interfering species and their sum. b) Absorbance profiles of 2-MTHF pyrolysis. Simulations are based on model by Moshhammer et al. [219] and the simulation time has been multiplied by a factor of 6.

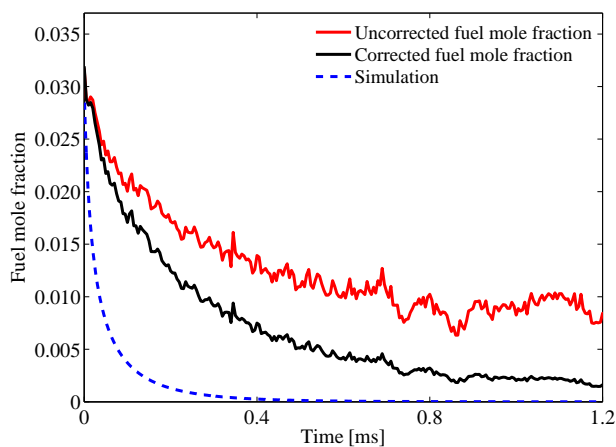


Figure 4.5: Concentration profiles of 2-MTHF pyrolysis at 1442 K, pressure 3 atm and 3% fuel. Simulations based on model by Moshhammer et al. [219].

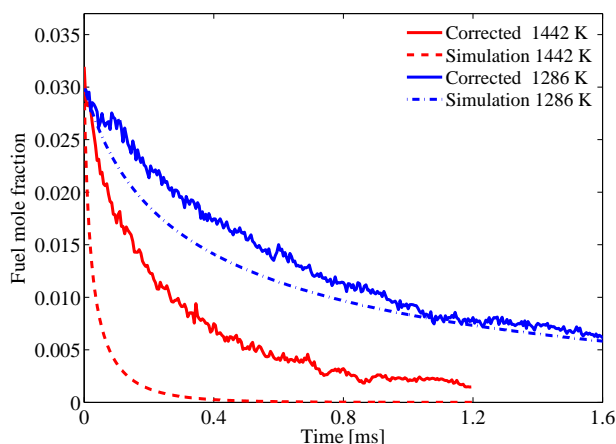


Figure 4.6: Concentration profiles of 2-MTHF pyrolysis at two temperatures, pressure of 3 atm and 3% fuel. Simulations based on model by Moshhammer et al. [219].

profiles. It is observed that fuel decomposition is faster at higher temperatures. The previously discussed prediction of faster kinetics is observed to be higher at the higher temperature.

One approach to improving the model could be to review the kinetic parameters assigned to fuel and fuel radical decomposition reactions. The uncorrected absorbance at $3.39\ \mu\text{m}$ is provided as supplementary material and can be used to obtain corrected fuel concentrations using other 2-MTHF chemical kinetic models. Another approach to using the uncorrected absorbance is to calculate the absorbance of all species with substantial absorption activity at $3.39\ \mu\text{m}$ and use the measured absorbance data directly for validation. In this case, the focus is not on a specific fuel, but rather on the fuel and intermediate hydrocarbon species. The challenge in this approach is finding the necessary absorption cross-sections at the thermodynamic conditions of interest. Mevel et al. [234] have proposed approximate additivity rules for estimating absorption cross-sections of combustion-relevant species at $3.39\ \mu\text{m}$. However, these data are only obtained for a few temperatures and limited range of hydrocarbons.

In summary, this subsection reports on measured absorption cross-sections and 2-MTHF time-histories during ignition and pyrolysis. Where measured time-histories are compared

with model predictions, models are observed to predict faster kinetics than experiments.

4.1.2 1,3-Dimethylcyclohexane time-histories during ignition and pyrolysis

The experimental results of this fuel, 1,3-DMCH, are used to validate a new model developed with the help of ignition times. Fuel concentration time-histories are measured during ignition of a stoichiometric mixture of 1,3-DMCH with Ar/O₂ of 3.76 and 10.0 and pyrolysis of 1.54% 13DMCH/Ar. The new 1,3-DMCH model is used to compare predictions with experimental data. To correct for absorption by interfering hydrocarbon species, their contributions are estimated using the model and literature data on their respective cross-sections, similar to previous work on fuel measurement [210, 235]. By multiplying species abundance and respective cross-sections, the most influential species are identified. In the present study, interference by the following species are found to be significant: CH₄, C₂H₄, C₃H₆, C₄H₆, C₄H₈-1, and CH₃CHO. The high-temperature absorption cross sections of these species are obtained from the literature [235–238] and from the HITRAN database.

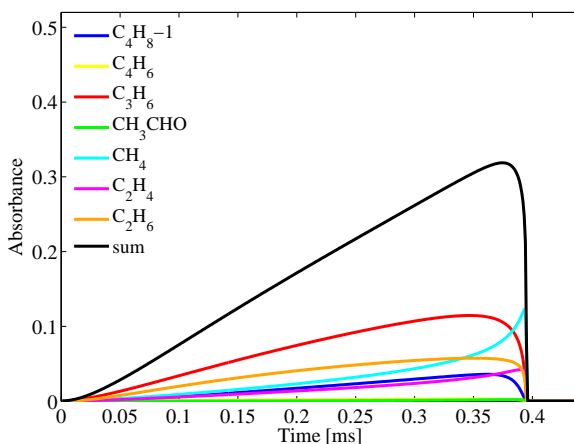


Figure 4.7: Absorbance of interfering species obtained from the ignition simulation of a stoichiometric mixture of 1,3-DMCH/O₂/Ar at 1249 K. The sum is used to correct the measured absorbance.

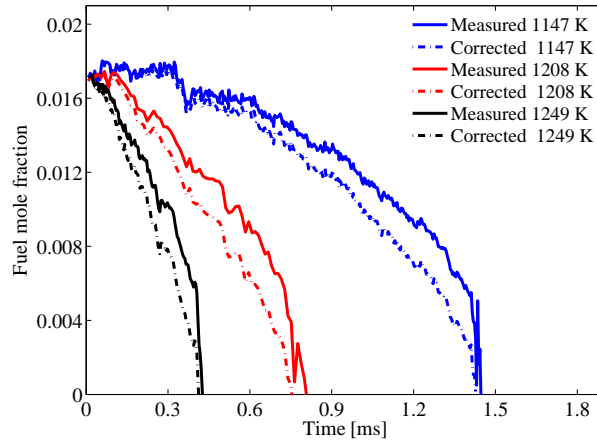


Figure 4.8: Fuel mole fractions based on uncorrected and corrected absorbance for three ignition experiments.

Figure 4.7 is a plot of the absorbance of major interfering species during an ignition event and their sum. For ignition correction, the time-dependent absorbance correction factor is obtained by using simulated mole fractions to calculate the absorbance of the fuel and the combined absorbance of the fuel and the key interfering species. Differences in absorbance are cast in a polynomial form, whereby the time variable is normalized by the respective ignition delay time. Figure 4.8 is a comparison of fuel mole fractions calculated directly from the measured (uncorrected) absorbance at $3.39 \mu\text{m}$ with the mole fractions obtained from the corrected absorbance.

Uncertainties in the calculated mole fractions arise from uncertainties in the total absorbance and absorbance of interfering species; thermodynamics conditions; the fuel absorption cross-section; and the absorption path length. The uncertainty in absorbance of the interfering species have been mainly attributed to uncertainties in their cross-sections, here estimated at 15-22%. The temperature and pressure uncertainties are determined to be in the range of 1.0-1.5% while the uncertainty in the absorption path length is estimated at 0.2%. These uncertainties are propagated at selected conditions and found to range from 16-27%. They are indicated at selected times in the corrected fuel mole fraction plots shown later.

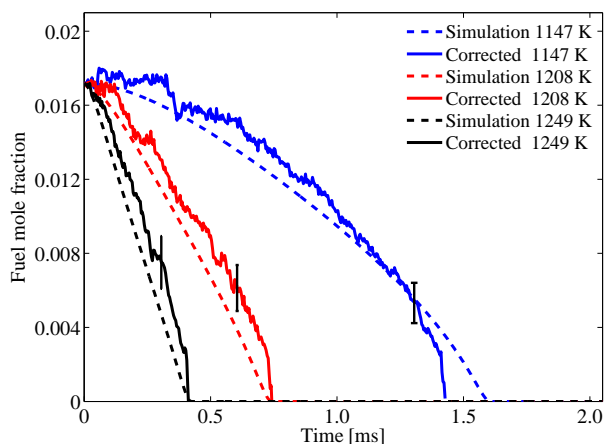


Figure 4.9: Comparison of corrected 1,3-DMCH concentration profiles with predictions of the 1,3-DMCH model at $\phi = 1.0$ and Ar/O₂ ratio of 3.76 at average pressure of 4.2 atm.

In Figures 4.9 and 4.10, the corrected fuel concentration profiles are compared to the predictions of the 1,3-DMCH model for stoichiometric 1,3-DMCH at pressures of 4.1–4.7 atm, temperatures of 1147–1258 K, and Ar/O₂ ratios of 3.76 and 10.0, respectively. It is observed that at high temperatures, predicted fuel time-histories are in close agreement with measured profiles. At lower temperatures, deviations are observed, in line with the observation that the model predicts longer delay times at low temperatures. Another key difference is the change in the curvature of concentration profiles in Figures 4.9 and 4.10, whereby the profiles of the more dilute mixture at high temperatures suggest the increased importance of first-order pyrolysis kinetics in the overall fuel consumption through the curvature of the profiles.

During pyrolysis of this fuel, interferences in fuel absorption measurements are also expected to be greater since the small hydrocarbon products being formed are not oxidized as in the case of ignition. It is determined from simulations using the 1,3-DMCH model, that the major interfering species during pyrolysis are C₂H₄, C₃H₆, C₂H₆, CH₄, C₄H₈, CH₃CHO, and CH₃COCH₃.

Using simulated mole fractions and high-temperature literature cross-sections, the combined absorbance can be directly compared with measured absorbance. For the pyrolysis conditions

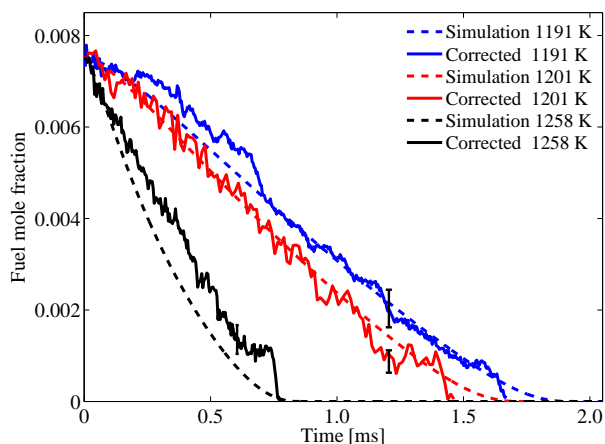


Figure 4.10: Comparison of corrected 13DMCH concentration profiles with predictions of the 13DMCH model at $\phi = 1.0$ and Ar/O_2 ratio of 10.0 at average pressure of 4.7 atm.

considered, it was observed that the absorbance obtained from simulated mole fractions of the fuel, interfering species, and respective cross-sections, closely match the raw experimental absorbances. The results are not shown here.

Figure 4.11 shows the evolution of the absorbance of interfering species as well as their time-dependent sum. Time-dependent correction factors are determined from the simulation results and used to obtain the corrected fuel absorbance, and subsequently, the fuel mole

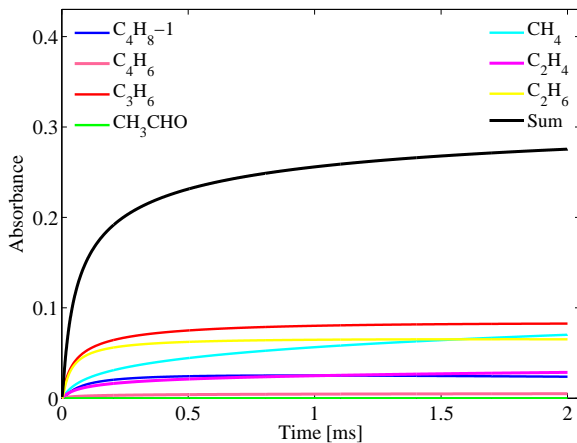


Figure 4.11: Absorbance of interfering species obtained from the simulation of 1.54 % fuel pyrolysis at 1406 K. The sum is used to correct the measured absorbance during pyrolysis at simulated conditions.

fractions. Examples of the experimental fuel mole fractions based on uncorrected and corrected absorbance during fuel pyrolysis are shown in Figure 4.12.

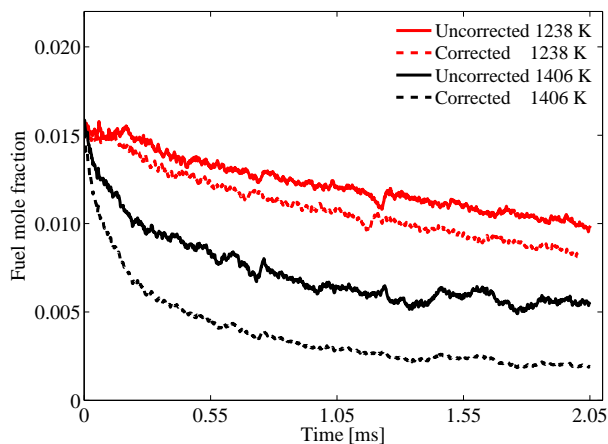


Figure 4.12: Fuel mole fractions based on uncorrected and corrected absorbance for two pyrolysis experiments.

Figure 4.13 shows the concentration profiles of 1,3-DMCH during the pyrolysis of 1.54% fuel in argon, at temperatures of 1238, 1320, and 1406 K. Good agreement is observed between model predictions and corrected experimental profiles at all three temperatures. This performance suggests that the proposed model captures very well the pyrolysis kinetics of 1,3-DMCH and does a reasonably good job predicting ignition delay times and fuel time-histories. It

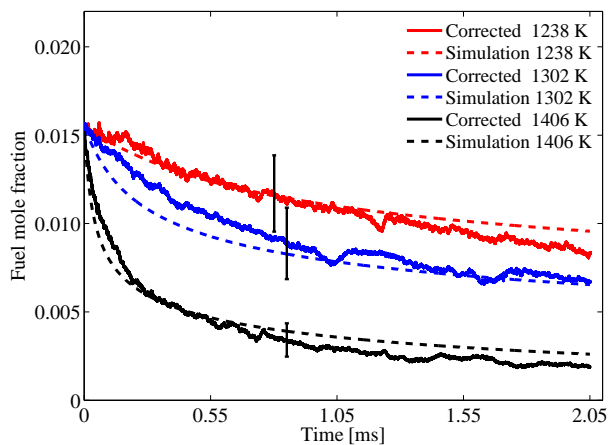


Figure 4.13: Comparison of corrected 1,3-DMCH concentration profiles during pyrolysis with predictions of the 1,3-DMCH model for pyrolysis 1.54% fuel in argon at 4 atm.

should be noted that a subset of the ignition data was used iteratively in the development and refinement of the model.

To summarize, in this subsection, time-histories of 1,3-DMCH during ignition and pyrolysis are presented. It is observed that fuel oxidation is faster at higher temperatures. Model predictions of the fuel time-histories during ignition and pyrolysis are found to accord with measured time-histories.

4.2 CO time-history measurements

CO measurement via direct laser absorption is used for pyrolysis time measurement and for time-histories that can be used to validate models. The time-histories are discussed here for the pyrolysis of propanol isomers, 2-MTHF, MTBE, MP and MP blend with methane.

4.2.1 CO time-histories during pyrolysis of propanol isomers

Selected experiments from the pyrolysis time studies are processed to obtain *CO* mole fraction profiles for comparison with model predictions. For the required absorption cross-sections, the line strengths at the laser wavelength are obtained from the HITRAN corresponding to the R9 CO absorption band (2179.8 cm^{-1}) and the line shape is determined using the Voigt fit, that accounts for collisional and Doppler broadening. As previously mentioned, both temperature and pressure of a constant volume reactor drop during pyrolysis (up to 8%). This has been taken into account by assessing the effect of this drop on absorption cross-section. At the instances shown in the results below, the main contributions to uncertainties in the CO concentration time-histories are: initial reactor temperature (1.0%), initial reactor pressure (1.0%), absorption cross-section (8%, including effects of varying reactor conditions), absorbance (1%), and absorption path length (2%). Propagating these uncertainties leads to overall CO mole fraction uncertainties of 13-14%.

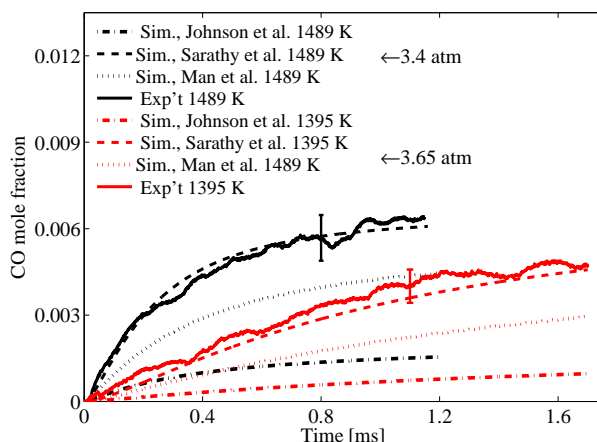


Figure 4.14: Comparison of CO concentration with simulations using the Johnson et al. [110], Sarathy et al. [119] and Man et al. [112] mechanisms during pyrolysis of 1% iso-propanol in argon at two different temperatures.

For the pyrolysis of 1% *iso*-propanol in argon two concentration profiles are obtained at 1489 K and 3.4 atm as well as at 1395 K and 3.65 atm as illustrated in Figure 4.14. The measured profiles are compared with predictions of three models by Johnson et al. [110], Sarathy et al. [119], and Man et al. [112]. It is found that the model by Sarathy et al. [119] generally predicts a CO time-histories that are in closer agreement with the measured histories, while the other two models under predict the rate of CO formation and the approaching to equilibrium CO concentration.

The CO predictions of the model by Johnson et al. [110] are significantly lower than measured. This contrasts with the closer agreement in prediction of the pyrolysis time shown in Figure 3.27. To understand the reason for this, we consider the various correlation functions in Figure 4.15 for the pyrolysis of 1% *iso*-propanol at 1489 K and 3.5 atm. As previously discussed, the actual correlation of fuel and CO concentration features an earlier maximum and decreases to near zero on account of the diminishing fuel concentration. The experimental function features a maximum at a later time as discussed, and it also decreases gradually to low values on account of the CO profile approaching equilibrium concentration. This is not the case for the model prediction of the correlation between CO and rate of CO formation. It

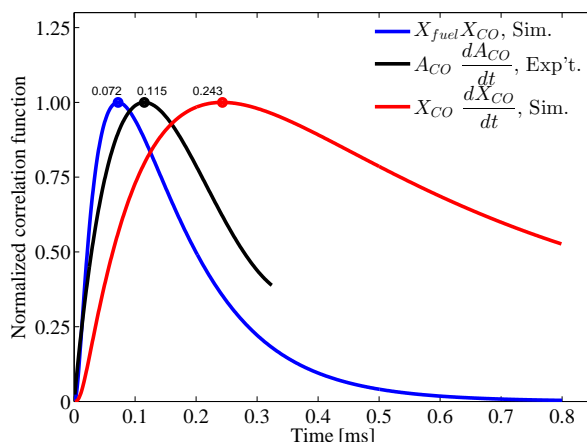


Figure 4.15: Correlation functions (normalized by respective maxima) for pyrolysis of 1% iso-propanol in argon at 3.5 atm and 1489 K, showing times to maximum and decay rates.

shows that it takes a much longer time for this last profile to attain near zero values even though its time to maximum is only about twice that of the experimental correlation function. This discrepancy between the time to maximum of the correlation function and how fast it approaches equilibrium concentration suggests that while the fuel decay rate might be rightly captured at early times, according to the model, the resulting intermediates react at a much slower rate to form the stable product, CO.

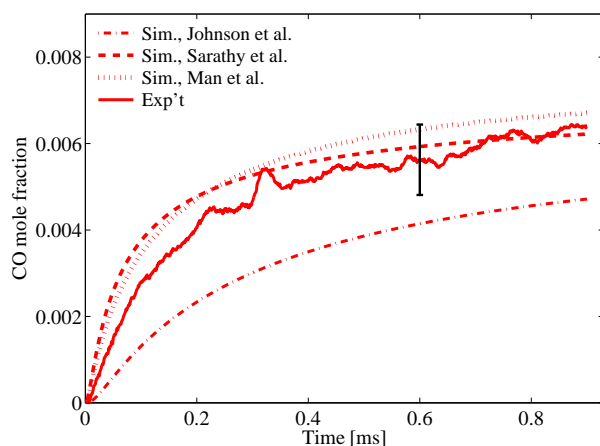


Figure 4.16: CO time-history during 1% n-propanol pyrolysis ($T=1476$ K, $p=3.3$ atm) with comparison of three models.

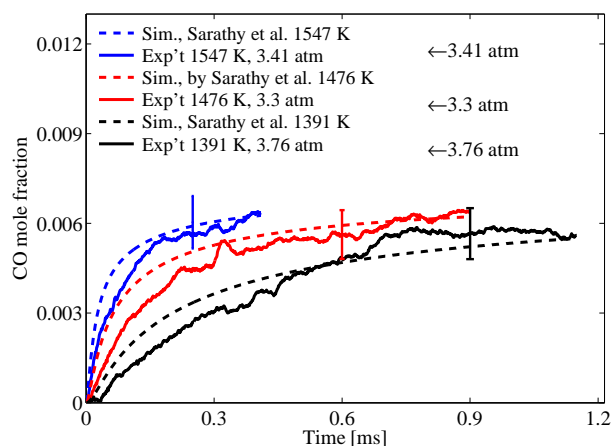


Figure 4.17: CO time-history of 1% n-propanol at three different temperatures with the Sarathy et al. [119] mechanism.

Selected CO concentration time-histories during pyrolysis of 1% *n*-propanol in argon have also been determined. Figure 4.16 shows the comparison of three model predictions with an experimental realization at 1476 K and 3.3 atm. It is observed that the models by Sarathy et al. [119] and Man et al. [112] predict faster initial rates of CO formation, while the model by Johnson et al. [110] also under predicts the rate and final CO profile in this case. Two other experimental conditions are added and compared with the Sarathy et al. [119] model prediction in Figure 4.17. The model consistently predicts a faster initial rate of CO formation while the CO profile is well captured at later times.

This fairly good prediction of the concentration profiles contrasts with the under prediction of the pyrolysis times noted in Figure 3.28. This can be understood by looking at the correlation functions for one of the experimental conditions as shown in Figure 4.18. It is observed that the correlation of simulated CO and its rate of formation features an earlier maximum than experimentally observed, coinciding with the correlation of fuel and CO. At later times, however, both simulated and experimentally determined correlation functions tend to zero, indicating near equilibrium CO attainment. These correlations suggest that reactions responsible for CO formation in the model are faster than required to capture the

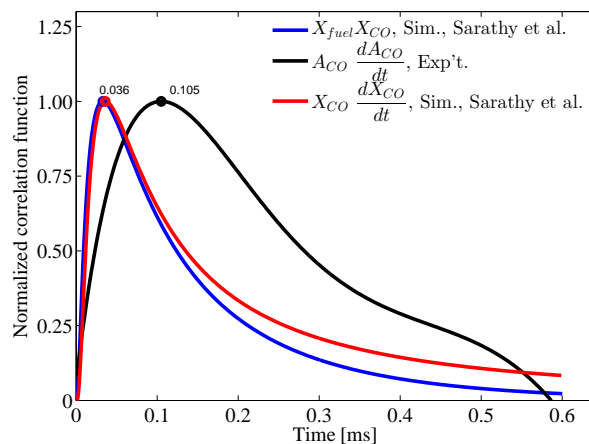


Figure 4.18: Correlations functions (normalized by respective maxima) for pyrolysis of 1% *n*-propanol in argon at 1476 K and 3.5 atm, showing different times to maximum

experimentally observed initial rate of CO production in Figure 4.17.

By choosing experimental realizations with comparable temperatures, the higher reactivity of *n*-propanol relative to *iso*-propanol is represented in Figure 4.19. The rate of CO formation and approach to equilibrium CO concentration is faster in *n*-propanol, in agreement with the reactivity trend established on the basis of ignition delay and pyrolysis times.

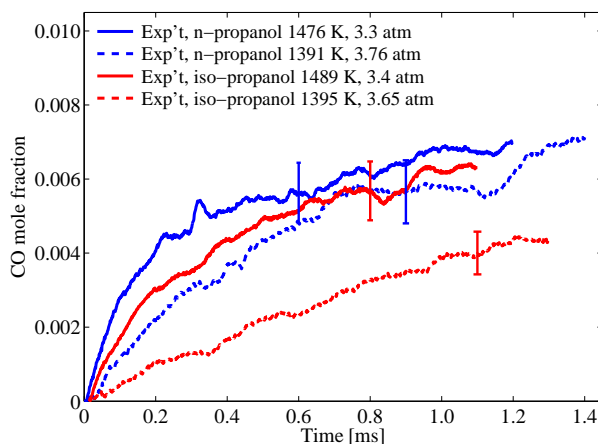


Figure 4.19: Comparison of CO concentration during pyrolysis of 1% *n*-propanol and *iso*-propanol in argon at different temperatures.

In essence, this subsection established that the rate of CO formation during *n*-propanol pyrolysis is faster than in *iso*-propanol. In addition, selected CO time-histories obtained during pyrolysis are compared with predictions of current chemical kinetic models, revealing varying degrees of agreement and discrepancies among the models.

4.2.2 CO time-histories during pyrolysis of 2-methyl tetrahydrofuran and methyl tert butyl ether

A similar approach to that described for CO measurement during propanol pyrolysis is used to study CO formation during 2-MTHF and MTBE pyrolysis. Shown in Figure 4.20 are CO time-histories during pyrolysis of 3% 2-MTHF in argon at two different temperatures of 1379

K and 1449 K both at 3.5 atm. The measured profiles are also compared with predictions of the two 2-MTHF models by Fenard et al. [49] and Wang et al. [46]. It is observed that CO formation is faster at the higher temperature as expected. In addition, it is found that both models by Fenard et al. [49] and Wang et al. [46] capture the initial rate of CO formation but under-predict the time to attain equilibrium CO concentration.

This problem can be better understood by considering the anticipated equilibrium CO concentration ($x_{CO,eq}$), the pyrolysis time, and a later time such as the time required to attain 90% of the equilibrium concentration ($t_{90\%,eq}$). Since the equilibrium concentration is approached almost asymptotically with time, one might then examine the ratio of the pyrolysis time to the time needed to attain 90% of $x_{CO,eq}$. The value of $x_{CO,eq}$ depends on the type of model reactor considered but remains fairly close for both adiabatic constant pressure (hp) and adiabatic constant volume (uv) reactors. It is observed from the experimental and simulated CO profiles which accord with experiments that $\frac{t_p}{t_{90\%,eq}} \approx \frac{1}{10}$. In the case of the two models used in this work, however, $\frac{t_p}{t_{90\%,eq}} \approx \frac{1}{100}$. This is indicative of very slow intermediate reactions which should lead to the formation of CO at later times, passing through stable

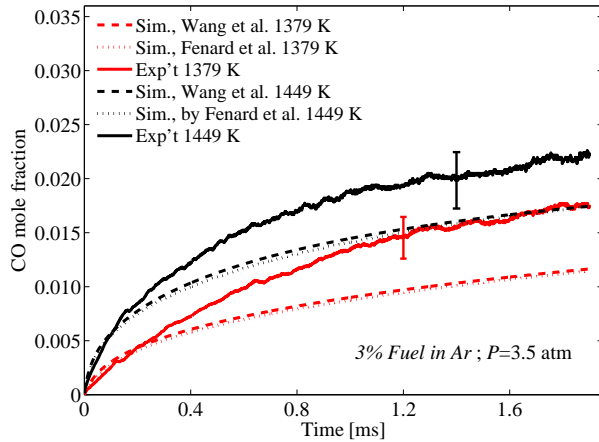


Figure 4.20: CO time-histories during 2-MTHF pyrolysis at two different temperatures compared to predictions by two different models [46, 49].

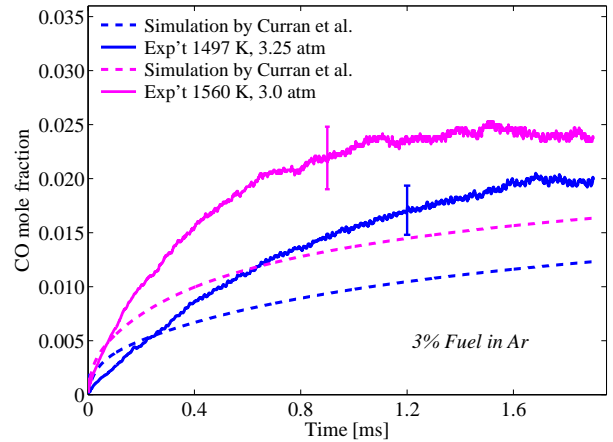


Figure 4.21: CO time-histories during MTBE pyrolysis at two different temperatures including predicted time-histories using the model by the Curran et al. [67] model.

species such as CH_2O and CH_2CO .

For the case of MTBE pyrolysis using 3% MTBE in argon, CO concentration time-histories at two different temperatures of 1497 K at 3.25 atm and 1560 K at 3.0 atm are shown in Figure 4.21. It is found that CO formation is faster at the higher temperature as expected. The model by Curran et al. [67] under-predicts the CO formation. The problem is similar to the simulated 2-MTHF profiles. The ratio of the pyrolysis times to the time to 90% of $x_{\text{CO},eq}$ approaches zero. This is also indicative of very slow CO formation kinetics after the initial reaction pathways are activated.

The higher reactivity of 2-MTHF relative to MTBE is illustrated in Figure 4.22 by comparing their CO concentration time-histories at temperatures that are close. The rate of CO formation and time to attain equilibrium CO concentration is faster in 2-MTHF, in agreement with the reactivity trend obtained based on pyrolysis times.

Figure 4.23 shows CO time-history up to the time when 90% of $x_{\text{CO},eq}$ is attained for 2-MTHF at 1449 K and 3.5 atm, compared with simulation results using Fenard et al. [49] model for the cases of adiabatic constant pressure (*hp*) and volume (*uv*) reactors. It is observed that the model predicts that the equilibrium CO concentration would be attained at very long times

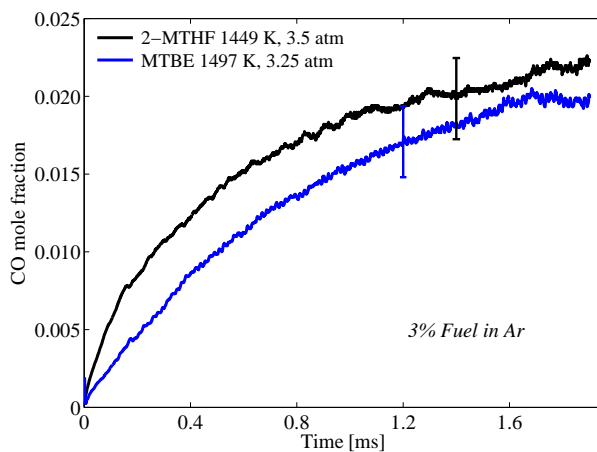


Figure 4.22: Comparison of CO concentration during pyrolysis of 3% 2-MTHF and MTBE in argon.

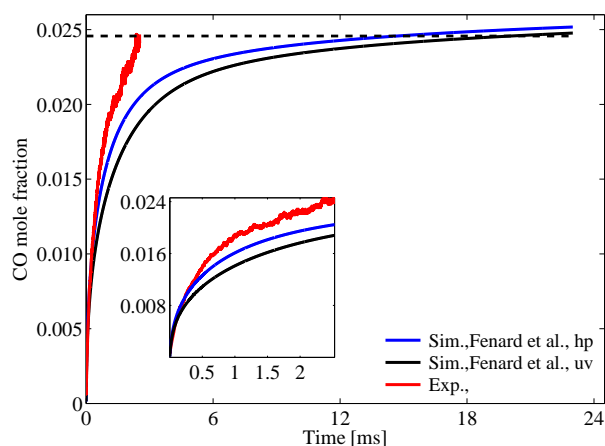


Figure 4.23: Comparison of CO time-history with simulation using Fenard et al. [49] model at both constant pressure (hp) and constant volume (uv) reactors for time to 90% of $x_{CO,eq}$.

of over 20 ms. The slow growth of CO from the simulations is indicative of slow intermediate reactions that convert the CO precursors to CO. This kinetic behavior is rarely the focus of model developers but might be central to any effort seeking to use kinetic model to predict CO emissions.

In order to provide a better understanding of how CO emerges from the pyrolysis of 2-MTHF, the main reaction pathways are obtained from the simulation results in Figure 4.24. The model used is that by Fenard et al. [49] and the simulation is carried out for 3% 2-MTHF at 1450K and 3.5 atm, with pathways analyzed at 40 μ s from reactor onset. It is observed that

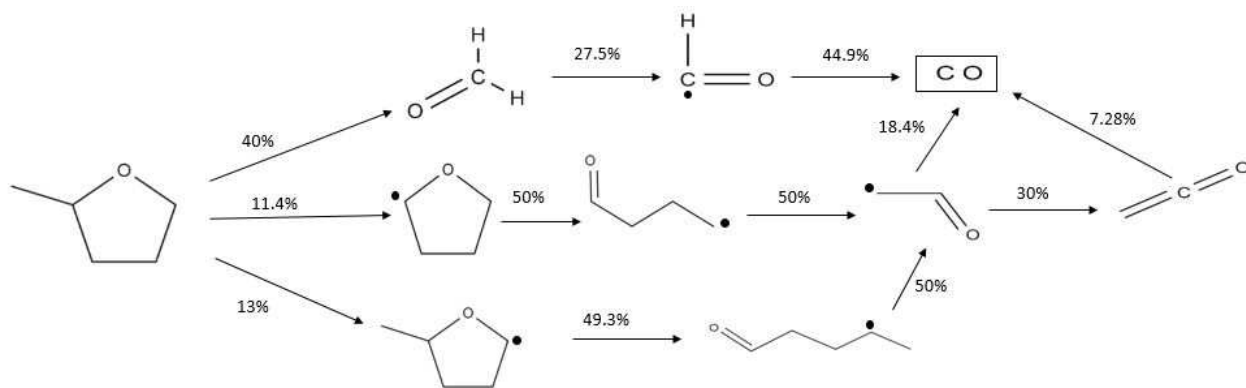


Figure 4.24: Reaction pathway for CO production during 2-MTHF pyrolysis (3% fuel, 3.5 atm and 1450 K) from model by Fenard et al. [49] at 40 μ s.

the model offers three main channels for CO production from the initial fuel molecule. The most influential decomposition reaction is the elimination of stable molecules from the fuel leading to the formation of butene and formaldehyde. The other two main channels include H abstraction by H atoms and C-C bond scission. The latter two channels from the fuel lead to the formation of ketene from which CO later emerges. Formaldehyde and ketene are implicated in CO formation.

The predicted slow formation of CO can be understood by examining the time- histories of these stable intermediates. In Figure 4.25, using the model by Fenard et al. [49], it is established that these intermediates are formed rapidly but are slowly consumed, thereby also leading to slow later formation of CO.

In the case of MTBE, based on the simulated pyrolysis of 3% MTBE at 1497 K and 3.25 atm and analysis at 40 μ s using the model by Curran et al. [67], Figure 4.26 shows that there are two main channels for CO formation. These include fuel decomposition via unimolecular decomposition and H abstraction by H atoms, leading to CO production. The stable molecules, methanol and formaldehyde, are key to understanding the observed slow approach to equilibrium CO.

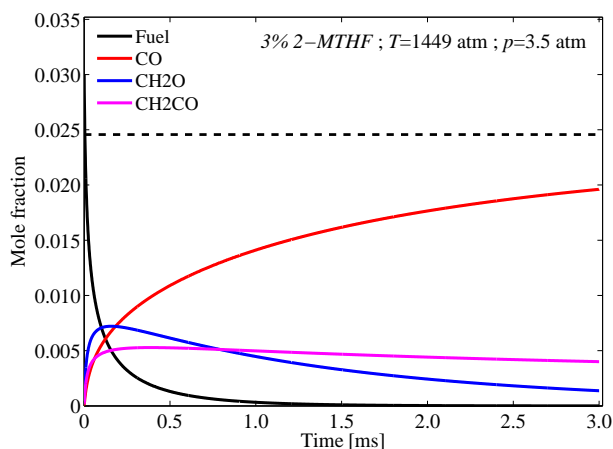


Figure 4.25: Time histories of fuel, CO and key intermediates for CO production during pyrolysis of 2-MTHF, namely, CH_2O and CH_2CO using the model by Fenard et al. [49].

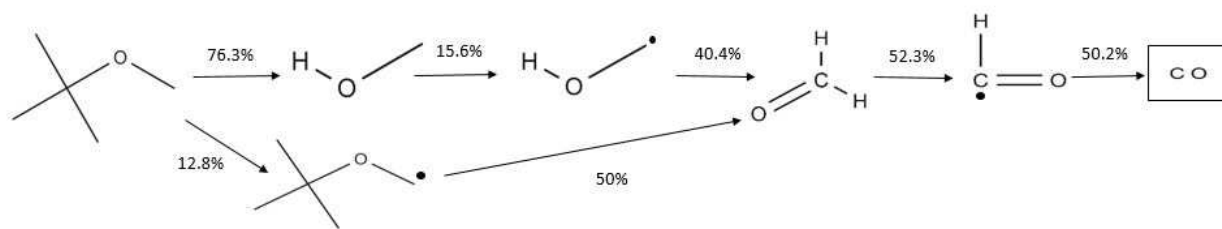


Figure 4.26: Reaction pathway for CO production during MTBE pyrolysis (3% fuel, 3.25 atm and 1497 K) from model by Curran et al. [67] at 40 μ s.

These considerations establish that while the pyrolysis time captures the global kinetics, it might not capture the temporal approach to equilibrium of the product used. The apparent general feature that the pyrolysis time is about a third of the time used to attain 90% of the equilibrium concentration might be useful in further interpreting the observed pyrolysis times and the product time-histories.

To summarize, direct laser absorption has been successfully used here to measure CO time-histories for the C5 ethers, 2-MTHF and MTBE. Comparison of these with model predictions have revealed some deficiencies in the intermediate kinetics leading to CO formation.

4.2.3 CO time-histories during pyrolysis of methyl propanoate and its blend with methane

CO absorbance has been used to determine pyrolysis time but the absorbance time-history can also be converted into CO time-histories for a given experimental realization. Here, selected CO profiles are compared with model predictions to provide a broader kinetic perspective. We expect the CO profiles for the 1.5% MP mixture and the blend of 1.5% MP and 1.5 % CH_4 to temporally evolve in a similar manner.

Regarding the accuracy of the CO time-histories thus obtained, there are several sources of uncertainties, including: the initial reactor temperature (1.0%), initial reactor pressure (1.0%),

absorption cross-section (8%), absorption path length (0.2%), and absorbance measurement (1%). The combined uncertainty of the experimental CO mole fraction is estimated to be 13-14% determined by propagating the contributory uncertainties.

Three different experimental realizations under comparable thermodynamic conditions are shown in Figure 4.27. CO production is faster for 3% MP and this is followed by the 1.5% MP mixture before the blend of 1.5% MP with 1.5% CH₄. Looking at the profiles, it is observed that CO formation is initially very rapid, but after a short while the CO production becomes very slow as it slowly approaches equilibrium. The equilibrium concentration for 1.5% MP and the blend of 1.5% MP with 1.5% CH₄ is about the same, unaffected by methane addition.

The measured profiles are also compared with model predictions in Figure 4.28. It is found that the model by Zhang et al. [163] captures the initial formation of CO but over-predict the time to attain equilibrium CO concentration. The model by Zhao et al. [164] under-predict the initial production and over-predict the equilibrium CO production.

In essence, this subsection demonstrated the CO formation for pyrolysis of pure or blended

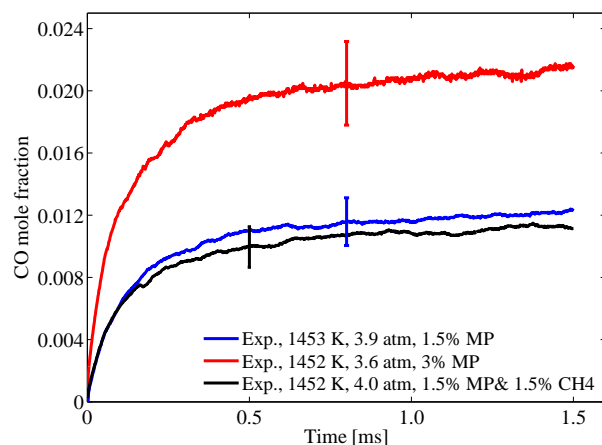


Figure 4.27: CO time-history during pyrolysis of two different MP concentration and its equal blend with CH₄.

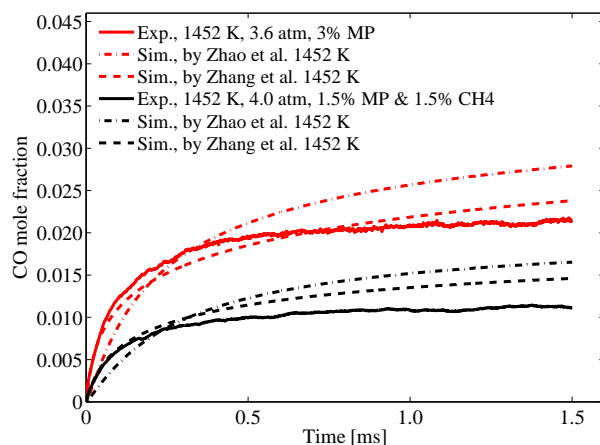


Figure 4.28: Comparison of CO histories with simulations using the Zhao et al. [164], Zhang et al. [163] mechanisms during pyrolysis of 3% MP and its equal blend with CH₄.

MP. There was a rapid initial rise and gradual approach to equilibrium in CO profiles. Comparison of experimental results with model predictions showed significant discrepancies in predicting CO time-histories.

In general, this part of the thesis successfully use direct laser absorption near $4.6\ \mu\text{m}$ to measure CO time-histories during pyrolysis of selected oxygenated fuels. These results have been used to further validate chemical kinetic models.

Chapter 5. Conclusion and outlook

The objective of this thesis was to advance the characterization and modeling of combustion properties by providing experimental data that include ignition delay times, pyrolysis times, and time-histories of species, such as the fuel and CO. The measured data were also used to investigate kinetic differences and to validate kinetic models. The key findings can be summarized under global chemical times and the measured species time histories.

Global chemical times

Ignition delay times of 2-methyl furan, 2-methyl tetrahydrofuran, and 1,3-dimethylcyclohexane were measured. In addition, global kinetic times of propanol isomers, methyl tert butyl ether, methyl propanoate and methane were measured. A novel approach has been developed to determine a global chemical kinetic time for pyrolysis. By means of this pyrolysis time, the effects of reactor temperature, pressure, and fuel concentration on pyrolysis were established. Contrast was further made between the global kinetics of pyrolysis and purely oxidative kinetics during ignition. The following findings regarding chemical times were made.

- It is observed that under stoichiometric conditions, 2-MTHF has longer ignition delay times than 2-MF, with differences of about a factor of 2 at 3 atm. The differences are less pronounced for lean mixtures at 12 atm, and a complex behavior is observed for rich mixtures where 2-MTHF can be more reactive at lower temperatures. For 2-MTHF, it is observed that ignition delay times generally decrease with increasing equivalence ratios.
- A detailed chemical kinetic model for 1,3-DMCH combustion is developed based on partial data obtained from ignition delay times along with other kinetic data. The

proposed chemical kinetic model predicts reasonably well the effects of equivalence ratio and pressure, with overall good agreement between predicted and all measured ignition delay times, except at low dilution levels and high pressures.

- Comparison of ignition delay times and pyrolysis results confirm the higher reactivity of *n*-propanol compared to *iso*-propanol. This thesis brings out the stronger temperature sensitivity of fuel pyrolysis (activation energies are greater than 60 kcal/mol) compared to the weaker temperature sensitivity of ignition processes, which are generally in the range 20-40 kcal/mol. The implication of this difference is that during ignition processes, the role of pyrolytic reactions increases with increasing temperatures. Comparison of experimental results with predictions using literature models show that current models predict ignition delay and pyrolysis times fairly reasonably, with noted differences among the three models examined.
- With respect to the C5 ethers, MTBE and 2-MTHF, the results indicate that ignition delay and pyrolysis times of both fuels decrease with increasing of temperature and pressure. Results further show that ignition delay times increase with increasing equivalence ratio on account of the lower O₂, since the fuel percentage is fixed. Comparing ignition and pyrolysis times of these fuels suggest a cross-over effect. With respect to pyrolysis, the expected cross-over behavior in lean mixtures is shifted toward higher temperatures, so that oxidative processes dominate in leaner mixtures over a longer temperature range. The pyrolysis data indicate that 2-MTHF is characterized by higher reactivity than MTBE.
- Ignition and pyrolysis of methane as a natural gas surrogate and MP as a biodiesel surrogate and their mixtures have been explored. It is observed that MP has shorter ignition delay times than methane (almost two order of magnitude differences at given conditions of pressure, temperature and fuel percentage). The thesis establishes the disproportionate enhancement of methane ignition through MP addition, such that a

blend of equal proportions yields ignition delay times that are much closer to those of MP. With regards to MP pyrolysis, the presence of methane is observed not to significantly influence the pyrolysis time.

Fuel and CO time-histories

Fuel and CO time-history measurements have been developed and applied to the study of selected fuel systems. This provides further constraints to chemical kinetic models. Fuel time-histories of 2-methyl tetrahydrofuran and 1,3-dimethylcyclohexane were measured. Moreover, the CO measurement was carried out using a mid-infrared QCL to access the R(9) transition of the CO fundamental ro-vibrational band near $4.56\text{ }\mu\text{m}$. The CO time-histories were obtained during pyrolysis of propanol isomers, methyl tert butyl ether, 2-methyl tetrahydrofuran, methyl propanoate and its blend with methane. The main findings are as follows:

- Based on the fuel time-histories measurements during ignition and pyrolysis of 2-MTHF, it is observed that the chosen chemical kinetic model underpredicts ignition delay times and this consequently leads to much faster fuel depletion rates than observed in experiments during pyrolysis. This fuel depletion is especially faster at higher temperatures.
- It is shown that, the new 1,3-DMCH model predictions agree reasonably well with the experimental 1,3-DMCH time-histories during ignition and pyrolysis, with better performance against pyrolysis measurements.
- Regarding CO formation during propanol pyrolysis, it is faster at higher temperatures for both isomers, as expected. Also, the rate of CO formation and the approach to equilibrium CO concentration is faster in *n*-propanol. Selected CO time-histories obtained during pyrolysis are also compared with predictions of current chemical kinetic models, revealing varying degrees of agreement and discrepancies among the models.
- For the C5 ethers, 2-MTHF and MTBE, it is found that, the models underpredict the

formation of CO for both fuels.

- In assessing the impact of methane on MP decomposition, it was found that methane does not significantly slow down MP pyrolysis. The evolution of CO for pyrolysis of pure or blended MP showed a rapid initial rise and gradual approach to equilibrium. Comparison of experimental results with model predictions showed significant discrepancies in predicting CO time-histories, contrasting with the better performance of models against ignition times.

Outlook

Further work in this area of research could build on the current results.

- In this thesis, it was demonstrated that pyrolysis time can be obtained based on laser absorption measurements of a single product of pyrolysis. This was shown for oxygenated fuels and CO was used. This can be expanded for non-oxygenated fuels and develop direct laser absorption for C_2H_2 or C_2H_4 .
- Enhancement of methane ignition through methyl propanoate addition was shown in this thesis. Other biodiesel surrogates could be explored for methane ignition enhancement in order to generalize the results.
- Although the main focus of Thermodynamics and Combustion Lab (TCL) at Syracuse University is characterization of combustion properties, further improvement of models could be attempted.
- Assumption about temperature of reactor could be further validated using spectroscopic temperature measurements.

Bibliography

- [1] B. Metz, O. Davidson, P. Bosch, R. Dave, and L. Meyer, “Climate change 2007”, *eds. Kahn RS, Kobayashi S, Beuthe M, Gasca J, Greene D, Lee DS, Muromachi Y, Newton PJ, Plotkin S, Sperling D, Wit R, and Zhou PJ, Cambridge University, Cambridge*, pp. 323–385, 2007.
- [2] R. N. DOE/EIA-0484(2017), “U.s. energy information administration,international energy outlook 2017”, *Department of Energy*,, 2017.
- [3] I Glassman, *Combustion. 3rd*, 1996.
- [4] M. G. Allen, “Diode laser absorption sensors for gas-dynamic and combustion flows”, *Measurement Science and Technology*, vol. 9, no. 4, p. 545, 1998.
- [5] F. Geilen, T. vom Stein, B. Engendahl, S. Winterle, M. A. Liauw, J. Klankermayer, and W. Leitner, “Highly selective decarbonylation of 5-(hydroxymethyl) furfural in the presence of compressed carbon dioxide”, *Angewandte Chemie International Edition*, vol. 50, no. 30, pp. 6831–6834, 2011.
- [6] Y. Román-Leshkov, C. J. Barrett, Z. Y. Liu, and J. A. Dumesic, “Production of dimethylfuran for liquid fuels from biomass-derived carbohydrates”, *Nature*, vol. 447, no. 7147, pp. 982–985, 2007.
- [7] W. Yang and A. Sen, “One-step catalytic transformation of carbohydrates and cellulosic biomass to 2, 5-dimethyltetrahydrofuran for liquid fuels”, *ChemSusChem*, vol. 3, no. 5, pp. 597–603, 2010.
- [8] J. M. Simmie, “Kinetics and thermochemistry of 2, 5-dimethyltetrahydrofuran and related oxolanes: Next next-generation biofuels”, *The Journal of Physical Chemistry A*, vol. 116, no. 18, pp. 4528–4538, 2012.

- [9] T. W. Kirchstetter, B. C. Singer, R. A. Harley, G. R. Kendall, and W. Chan, “Impact of oxygenated gasoline use on california light-duty vehicle emissions”, *Environmental Science & Technology*, vol. 30, no. 2, pp. 661–670, 1996.
- [10] L. Wei and P. Geng, “A review on natural gas/diesel dual fuel combustion, emissions and performance”, *Fuel Processing Technology*, vol. 142, pp. 264–278, 2016.
- [11] H. M. Cho and B.-Q. He, “Spark ignition natural gas enginesa review”, *Energy conversion and management*, vol. 48, no. 2, pp. 608–618, 2007.
- [12] J. Hill, E. Nelson, D. Tilman, S. Polasky, and D. Tiffany, “Environmental, economic, and energetic costs and benefits of biodiesel and ethanol biofuels”, *Proceedings of the National Academy of sciences*, vol. 103, no. 30, pp. 11 206–11 210, 2006.
- [13] A. Demirbas, “Progress and recent trends in biofuels”, *Progress in energy and combustion science*, vol. 33, no. 1, pp. 1–18, 2007.
- [14] N. Leplat, P. Dagaut, C. Togbé, and J. Vandooren, “Numerical and experimental study of ethanol combustion and oxidation in laminar premixed flames and in jet-stirred reactor”, *Combustion and Flame*, vol. 158, no. 4, pp. 705–725, 2011.
- [15] T. Norton and F. Dryer, “An experimental and modeling study of ethanol oxidation kinetics in an atmospheric pressure flow reactor”, *International Journal of Chemical Kinetics*, vol. 24, no. 4, pp. 319–344, 1992.
- [16] D. Tomes, P. Lakshmanan, and D. Songstad, *Biofuels: Global impact on renewable energy, production agriculture, and technological advancements*. Springer Science & Business Media, 2010.
- [17] B. Sirjean, R. Fournet, P.-A. Glaude, F. Battin-Leclerc, W. Wang, and M. A. Oehlschlaeger, “Shock tube and chemical kinetic modeling study of the oxidation of 2, 5-dimethylfuran”, *The Journal of Physical Chemistry A*, vol. 117, no. 7, pp. 1371–1392, 2013.
- [18] K. P. Somers, J. M. Simmie, F. Gillespie, C. Conroy, G. Black, W. K. Metcalfe, F. Battin-Leclerc, P. Dirrenberger, O. Herbinet, P.-A. Glaude, *et al.*, “A comprehensive

- experimental and detailed chemical kinetic modelling study of 2, 5-dimethylfuran pyrolysis and oxidation”, *Combustion and flame*, vol. 160, no. 11, pp. 2291–2318, 2013.
- [19] K. P. Somers, J. M. Simmie, W. K. Metcalfe, and H. J. Curran, “The pyrolysis of 2-methylfuran: A quantum chemical, statistical rate theory and kinetic modelling study”, *Physical Chemistry Chemical Physics*, vol. 16, no. 11, pp. 5349–5367, 2014.
- [20] X. Wu, Z. Huang, T. Yuan, K. Zhang, and L. Wei, “Identification of combustion intermediates in a low-pressure premixed laminar 2, 5-dimethylfuran/oxygen/argon flame with tunable synchrotron photoionization”, *Combustion and Flame*, vol. 156, no. 7, pp. 1365–1376, 2009.
- [21] S. Zhong, R. Daniel, H. Xu, J. Zhang, D. Turner, M. L. Wyszynski, and P. Richards, “Combustion and emissions of 2, 5-dimethylfuran in a direct-injection spark-ignition engine”, *Energy & Fuels*, vol. 24, no. 5, pp. 2891–2899, 2010.
- [22] R. Daniel, G. Tian, H. Xu, M. L. Wyszynski, X. Wu, and Z. Huang, “Effect of spark timing and load on a DISI engine fuelled with 2, 5-dimethylfuran”, *Fuel*, vol. 90, no. 2, pp. 449–458, 2011.
- [23] R. Daniel, H. Xu, C. Wang, D. Richardson, and S. Shuai, “Combustion performance of 2, 5-dimethylfuran blends using dual-injection compared to direct-injection in a SI engine”, *Applied Energy*, vol. 98, pp. 59–68, 2012.
- [24] C. Wang, H. Xu, R. Daniel, A. Ghafourian, J. M. Herreros, S. Shuai, and X. Ma, “Combustion characteristics and emissions of 2-methylfuran compared to 2, 5-dimethylfuran, gasoline and ethanol in a DISI engine”, *Fuel*, vol. 103, pp. 200–211, 2013.
- [25] N. Xu, J. Gong, and Z. Huang, “Review on the production methods and fundamental combustion characteristics of furan derivatives”, *Renewable and Sustainable Energy Reviews*, vol. 54, pp. 1189–1211, 2016.
- [26] Y. Qian, L. Zhu, Y. Wang, and X. Lu, “Recent progress in the development of biofuel 2, 5-dimethylfuran”, *Renewable and Sustainable Energy Reviews*, vol. 41, pp. 633–646, 2015.

- [27] M. A. Eldeeb and B. Akih-Kumgeh, “Recent trends in the production, combustion and modeling of furan-based fuels”, *Energies*, vol. 11, no. 3, p. 512, 2018.
- [28] M. Thewes, M. Muether, S. Pischinger, M. Budde, A. Brunn, A. Sehr, P. Adomeit, and J. Klankermayer, “Analysis of the impact of 2-methylfuran on mixture formation and combustion in a direct-injection spark-ignition engine”, *Energy & Fuels*, vol. 25, no. 12, pp. 5549–5561, 2011.
- [29] M. A. Eldeeb and B. Akih-Kumgeh, “Reactivity trends in furan and alkyl furan combustion”, *Energy & Fuels*, vol. 28, no. 10, pp. 6618–6626, 2014.
- [30] L. Wei, C. Tang, X. Man, and Z. Huang, “Shock-tube experiments and kinetic modeling of 2-methylfuran ignition at elevated pressure”, *Energy & Fuels*, vol. 27, no. 12, pp. 7809–7816, 2013.
- [31] L.-S. Tran, C. Togbé, D. Liu, D. Felsmann, P. Oßwald, P.-A. Glaude, R. Fournet, B. Sirjean, F. Battin-Leclerc, and K. Kohse-Höinghaus, “Combustion chemistry and flame structure of furan group biofuels using molecular-beam mass spectrometry and gas chromatography—part ii: 2-methylfuran”, *Combustion and flame*, vol. 161, no. 3, pp. 766–779, 2014.
- [32] Y. Uygun, S. Ishihara, and H. Olivier, “A high pressure ignition delay time study of 2-methylfuran and tetrahydrofuran in shock tubes”, *Combustion and Flame*, vol. 161, no. 10, pp. 2519–2530, 2014.
- [33] K. P. Somers, J. M. Simmie, F. Gillespie, U. Burke, J. Connolly, W. K. Metcalfe, F. Battin-Leclerc, P. Dirrenberger, O. Herbinet, P.-A. Glaude, *et al.*, “A high temperature and atmospheric pressure experimental and detailed chemical kinetic modelling study of 2-methyl furan oxidation”, *Proceedings of the Combustion Institute*, vol. 34, no. 1, pp. 225–232, 2013.
- [34] D. J. Hayes, S. Fitzpatrick, M. H. Hayes, and J. R. Ross, “The biofine process—production of levulinic acid, furfural, and formic acid from lignocellulosic feedstocks”, *Biorefineries—Industrial Processes and Product*, vol. 1, pp. 139–164, 2006.

- [35] W. Yang and A. Sen, “One-step catalytic transformation of carbohydrates and cellulosic biomass to 2, 5-dimethyltetrahydrofuran for liquid fuels”, *ChemSusChem*, vol. 3, no. 5, pp. 597–603, 2010.
- [36] T. J. Wallington, W. O. Siegl, R. Liu, Z. Zhang, R. E. Huie, and M. J. Kurylo, “The atmospheric reactivity of. alpha.-methyltetrahydrofuran”, *Environmental Science & Technology*, vol. 24, no. 10, pp. 1596–1599, 1990.
- [37] D. J. Hayes and M. H. Hayes, “The role that lignocellulosic feedstocks and various biorefining technologies can play in meeting ireland’s biofuel targets”, *Biofuels, Bioproducts and Biorefining*, vol. 3, no. 5, pp. 500–520, 2009.
- [38] L. S. Tran, B. Sirjean, P.-A. Glaude, R. Fournet, and F. Battin-Leclerc, “Progress in detailed kinetic modeling of the combustion of oxygenated components of biofuels”, *Energy*, vol. 43, no. 1, pp. 4–18, 2012.
- [39] A. Sudholt, L. Cai, J. Heyne, F. M. Haas, H. Pitsch, and F. L. Dryer, “Ignition characteristics of a bio-derived class of saturated and unsaturated furans for engine applications”, *Proc. Combust. Inst.*, vol. 35, no. 3, pp. 2957–2965, 2015.
- [40] T. Rudolph and J. Thomas, “Nox, nmhc and co emissions from biomass derived gasoline extenders”, *Biomass*, vol. 16, no. 1, pp. 33–49, 1988.
- [41] Y. Kar and H. Deveci, “Importance of p-series fuels for flexible-fuel vehicles (ffvs) and alternative fuels”, *Energy Sources, Part A*, vol. 28, no. 10, pp. 909–921, 2006.
- [42] A. J. Janssen, F. W. Kremer, J. H. Baron, M. Muether, S. Pischinger, and J. Klankermayer, “Tailor-made fuels from biomass for homogeneous low-temperature diesel combustion”, *Energy & Fuels*, vol. 25, no. 10, pp. 4734–4744, 2011.
- [43] J. M. Simmie, “Kinetics and thermochemistry of 2,5-dimethyltetrahydrofuran and related oxolanes: Next next-generation biofuels”, *J. Phys. Chem. A*, vol. 116, no. 18, pp. 4528–4538, 2012.

- [44] H. K. Chakravarty and R. X. Fernandes, “Reaction kinetics of hydrogen abstraction reactions by hydroperoxyl radical from 2-methyltetrahydrofuran and 2,5-dimethyltetrahydrofuran”, *J. Phys. Chem. A*, vol. 117, no. 24, pp. 5028–5041, 2013.
- [45] K. Moshhammer, S. Vranckx, H. K. Chakravarty, P. Parab, R. X. Fernandes, and K. Kohse-Höinghaus, “An experimental and kinetic modeling study of 2-methyltetrahydrofuran flames”, *Combust. Flame*, vol. 160, no. 12, pp. 2729–2743, 2013.
- [46] J. Wang, X. Wang, X. Fan, K. Yang, and Y. Zhang, “An ignition delay time and kinetic study of 2-methyltetrahydrofuran at high temperatures”, *Fuel*, vol. 186, pp. 758–769, 2016.
- [47] L.-S. Tran, M. Verdicchio, F. Monge, R. C. Martin, R. Bounaceur, B. Sirjean, P.-A. Glaude, M. U. Alzueta, and F. Battin-Leclerc, “An experimental and modeling study of the combustion of tetrahydrofuran”, *Combustion and Flame*, vol. 162, no. 5, pp. 1899–1918, 2015.
- [48] R. De Bruycker, L.-S. Tran, H.-H. Carstensen, P.-A. Glaude, F. Monge, M. U. Alzueta, F. Battin-Leclerc, and K. M. Van Geem, “Experimental and modeling study of the pyrolysis and combustion of 2-methyl-tetrahydrofuran”, *Combustion and Flame*, vol. 176, pp. 409–428, 2017.
- [49] Y. Fenard, M. Boumehdi, and G. Vanhove, “Experimental and kinetic modeling study of 2-methyltetrahydrofuran oxidation under engine-relevant conditions”, *Combustion and Flame*, vol. 178, pp. 168–181, 2017.
- [50] R. Hanson and D. Davidson, “Recent advances in laser absorption and shock tube methods for studies of combustion chemistry”, *Progress in Energy and Combustion Science*, vol. 44, pp. 103–114, 2014.
- [51] J. Brocard, F. Baronnet, and H. O’Neal, “Chemical kinetics of the oxidation of methyl tert-butyl ether (MTBE)”, *Combustion and Flame*, vol. 52, pp. 25–35, 1983.

- [52] T. Norton, F. Dryer, and K. Brezinsky, "Some preliminary observations on the high-temperature oxidation of tert-butyl alcohol and methyl tert-butyl ether.", in *Combustion Inst*, 1985.
- [53] T. S. Norton and F. L. Dryer, "The flow reactor oxidation of C1–C4 alcohols and MTBE", in *Symposium (International) on Combustion*, Elsevier, vol. 23, 1991, pp. 179–185.
- [54] A. Goldaniga, T. Faravelli, E. Ranzi, P. Dagaut, and M. Cathonnet, "Oxidation of oxygenated octane improvers: MTBE, ETBE, DIPE, and TAME", in *Symposium (International) on Combustion*, Elsevier, vol. 27, 1998, pp. 353–360.
- [55] A. Ciajolo, "Low-temperature oxidation of MTBE in a high-pressure jet-stirred flow reactor", *Combustion science and technology*, vol. 123, no. 1-6, pp. 49–61, 1997.
- [56] P. Glaude, F. Battin-Leclerc, B. Judenherc, V. Warth, R. Fournet, G. Côme, G. Scacchi, P. Dagaut, and M. Cathonnet, "Experimental and modeling study of the gas-phase oxidation of methyl and ethyl tertiary butyl ethers", *Combustion and flame*, vol. 121, no. 1, pp. 345–355, 2000.
- [57] D. Lee, S. Hochgreb, and J. C. Keck, *Autoignition of alcohols and ethers in a rapid compression machine*. Society of Automotive Engineers, 1993.
- [58] S. K. Hoekman, "Speciated measurements and calculated reactivities of vehicle exhaust emissions from conventional and reformulated gasolines", *Environmental science & technology*, vol. 26, no. 6, pp. 1206–1216, 1992.
- [59] M. M. Osman, M. S. Matar, and S. Koreish, "Effect of methyl tertiary butyl ether (MTBE) as a gasoline additive on engine performance and exhaust emissions", *Fuel science & technology international*, vol. 11, no. 10, pp. 1331–1343, 1993.
- [60] C. S. McEnally and L. D. Pfefferle, "Experimental study of fuel decomposition and hydrocarbon growth processes for practical fuel components in nonpremixed flames: MTBE and related alkyl ethers", *International journal of chemical kinetics*, vol. 36, no. 6, pp. 345–358, 2004.

- [61] A. Van Der Loos, J. Vandooren, and P. Van Tiggelen, “Kinetic study of methyl tert-butyl ether (MTBE) oxidation in flames”, in *Symposium (International) on Combustion*, Elsevier, vol. 27, 1998, pp. 477–484.
- [62] M. P. Dunphy and J. M. Simmie, “Combustion of methyl tert-butyl ether. part i: Ignition in shock waves”, *Combustion and Flame*, vol. 85, no. 3-4, pp. 489–498, 1991.
- [63] K. Fieweger, R. Blumenthal, and G. Adomeit, “Shock-tube investigations on the self-ignition of hydrocarbon-air mixtures at high pressures”, in *Symposium (International) on Combustion*, Elsevier, vol. 25, 1994, pp. 1579–1585.
- [64] K. Fieweger, R. Blumenthal, and G. Adomeit, “Self-ignition of SI engine model fuels: A shock tube investigation at high pressure”, *Combust. Flame*, vol. 109, no. 4, pp. 599–619, 1997.
- [65] J. A. Gray and C. K. Westbrook, “High-temperature ignition of propane with MTBE as an additive: Shock tube experiments and modeling”, *International journal of chemical kinetics*, vol. 26, no. 7, pp. 757–770, 1994.
- [66] J. Brocard and F. Baronnet, “Pyrolysis of methyl tert-butyl ether”, *Oxid. Commun.*, vol. 1, 1980.
- [67] H. J. Curran, M. P. Dunphy, J. M. Simmie, C. K. Westbrook, and W. J. Pitz, “Shock tube ignition of ethanol, isobutene and MTBE: Experiments and modeling”, in *Symposium (International) on Combustion*, Elsevier, vol. 24, 1992, pp. 769–776.
- [68] K. Yasunaga, J. Simmie, H. Curran, T. Koike, O. Takahashi, Y. Kuraguchi, and Y. Hidaka, “Detailed chemical kinetic mechanisms of ethyl methyl, methyl tert-butyl and ethyl tert-butyl ethers: The importance of uni-molecular elimination reactions”, *Combustion and Flame*, vol. 158, no. 6, pp. 1032–1036, 2011.
- [69] H. R. Zhang, E. G. Eddings, and A. F. Sarofim, “Pollutant emissions from gasoline combustion. 1. dependence on fuel structural functionalities”, *Environ. Sci. Technol.*, vol. 42, no. 15, pp. 5615–5621, 2008.

- [70] T. Zhang, J. Wang, T. Yuan, X. Hong, L. Zhang, and F. Qi, "Pyrolysis of methyl tert-butyl ether (MTBE). 1. experimental study with molecular-beam mass spectrometry and tunable synchrotron vuv photoionization", *The Journal of Physical Chemistry A*, vol. 112, no. 42, pp. 10 487–10 494, 2008.
- [71] J. E. Reuter, B. C. Allen, R. C. Richards, J. F. Pankow, C. R. Goldman, R. L. Scholl, and J. S. Seyfried, "Concentrations, sources, and fate of the gasoline oxygenate methyl tert-butyl ether (MTBE) in a multiple-use lake", *Environmental science & technology*, vol. 32, no. 23, pp. 3666–3672, 1998.
- [72] C. D. Church, L. M. Isabelle, J. F. Pankow, D. L. Rose, and P. G. Tratnyek, "Method for determination of methyl tert-butyl ether and its degradation products in water", *Environmental Science & Technology*, vol. 31, no. 12, pp. 3723–3726, 1997.
- [73] D. Lince, L. Wilson, and G. Carlson, "Methyl tert-butyl ether (MTBE) contamination in private wells near gasoline stations in upstate new york", *Bulletin of environmental contamination and toxicology*, vol. 61, no. 4, pp. 484–488, 1998.
- [74] R. A. Deeb, K. M. Scow, and L. Alvarez-Cohen, "Aerobic MTBE biodegradation: An examination of past studies, current challenges and future research directions", *Biodegradation*, vol. 11, no. 2-3, pp. 171–185, 2000.
- [75] M. M. Haggblom, L. K. Youngster, P. Somsamak, and H. H. Richnow, "Anaerobic biodegradation of methyl tert-butyl ether (MTBE) and related fuel oxygenates", *Advances in applied microbiology*, vol. 62, no. 62, pp. 1–20, 2007.
- [76] M. Thewes, M. Muether, S. Pischinger, M. Budde, A. Brunn, A. Sehr, P. Adomeit, and J. Klankermayer, "Analysis of the impact of 2-methylfuran on mixture formation and combustion in a direct-injection spark-ignition engine", *Energy Fuels*, vol. 25, no. 12, pp. 5549–5561, 2011.
- [77] A. Demirbas, "Biofuels sources, biofuel policy, biofuel economy and global biofuel projections", *Energy conversion and management*, vol. 49, no. 8, pp. 2106–2116, 2008.

- [78] J. M. Bergthorson and M. J. Thomson, “A review of the combustion and emissions properties of advanced transportation biofuels and their impact on existing and future engines”, *Renew. Sust. Energ. Rev.*, vol. 42, no. 0, pp. 1393–1417, 2015.
- [79] A. Demirbas, “Competitive liquid biofuels from biomass”, *Applied Energy*, vol. 88, no. 1, pp. 17–28, 2011.
- [80] P. Lamers, C. Hamelinck, M. Junginger, and A. Faaij, “International bioenergy tradea review of past developments in the liquid biofuel market”, *Renewable and Sustainable Energy Reviews*, vol. 15, no. 6, pp. 2655–2676, 2011.
- [81] R. Arvidsson, K. Fransson, M. Fröling, M. Svanström, and S. Molander, “Energy use indicators in energy and life cycle assessments of biofuels: Review and recommendations”, *Journal of Cleaner Production*, vol. 31, pp. 54–61, 2012.
- [82] V. H. Rapp, J. H. Mack, P. Tschann, W. Hable, R. J. Cattolica, and R. W. Dibble, “Research octane numbers of primary and mixed alcohols from biomass-based syngas”, *Energy & Fuels*, vol. 28, no. 5, pp. 3185–3191, 2014.
- [83] A. Frassoldati, A. Cuoci, T. Faravelli, U. Niemann, E. Ranzi, R. Seiser, and K. Seshadri, “An experimental and kinetic modeling study of n-propanol and iso-propanol combustion”, *Combustion and Flame*, vol. 157, no. 1, pp. 2–16, 2010.
- [84] K. Noorani, B. Akih-Kumgeh, and J. Bergthorson, “Comparative High Temperature Shock Tube Ignition of C1–C4 Primary Alcohols”, *Energy Fuels*, vol. 24, pp. 5834–5843, 2010.
- [85] F. Zhang, Z. Wang, Z. Wang, L. Zhang, Y. Li, and F. Qi, “Kinetics of decomposition and isomerization of methylcyclohexane: Starting point for studying monoalkylated cyclohexanes combustion”, *Energy Fuels*, vol. 27, no. 3, pp. 1679–1687, 2013.
- [86] L. Cai, Y. Uygün, C. Togbé, H. Pitsch, H. Olivier, P. Dagaut, and S. M. Sarathy, “An experimental and modeling study of n-octanol combustion”, *Proc. Combust. Inst.*, vol. 35, no. 1, pp. 419–427, 2015.

- [87] C. Tang, L. Wei, X. Man, J. Zhang, Z. Huang, and C. Law, “High temperature ignition delay times of C5 primary alcohols”, *Combustion and Flame*, vol. 160, no. 3, pp. 520–529, 2013.
- [88] K. A. Heufer, S. M. Sarathy, H. J. Curran, A. C. Davis, C. K. Westbrook, and W. J. Pitz, “Detailed kinetic modeling study of n-pentanol oxidation”, *Energy & Fuels*, vol. 26, no. 11, pp. 6678–6685, 2012.
- [89] X. Gu, Z. Huang, S. Wu, and Q. Li, “Laminar burning velocities and flame instabilities of butanol isomers–air mixtures”, *Combustion and Flame*, vol. 157, no. 12, pp. 2318–2325, 2010.
- [90] Q. Li, E. Hu, X. Zhang, Y. Cheng, and Z. Huang, “Laminar flame speeds and flame instabilities of pentanol isomer–air mixtures at elevated temperatures and pressures”, *Energy & Fuels*, vol. 27, no. 2, pp. 1141–1150, 2013.
- [91] Q. Li, C. Tang, Y. Cheng, L. Guan, and Z. Huang, “Laminar flame speeds and kinetic modeling of n-pentanol and its isomers”, *Energy & Fuels*, vol. 29, no. 8, pp. 5334–5348, 2015.
- [92] H.-P. S. Shen, J. Vanderover, and M. A. Oehlschlaeger, “A shock tube study of iso-octane ignition at elevated pressures: The influence of diluent gases”, *Combust. Flame*, vol. 155, no. 4, pp. 739–755, 2008.
- [93] S. Atsumi and J. C. Liao, “Metabolic engineering for advanced biofuels production from escherichia coli”, *Current opinion in biotechnology*, vol. 19, no. 5, pp. 414–419, 2008.
- [94] T. Wallner, A. Ickes, and K. Lawyer, “Analytical assessment of C2–C8 alcohols as spark-ignition engine fuels”, in *Proceedings of the FISITA 2012 World Automotive Congress*, Springer, 2013, pp. 15–26.
- [95] M. Eyidogan, A. Ozsezen, M. Canakci, and A. Turkcan, “Impact of alcoholgasoline fuel blends on the performance and combustion characteristics of an SI engine”, *Fuel*, vol. 89, no. 10, pp. 2713–2720, 2010.

- [96] A. Keskin and M. Gürü, “The effects of ethanol and propanol additions into unleaded gasoline on exhaust and noise emissions of a spark ignition engine”, *Energy Sources, Part A: Recovery, Utilization, and Environmental Effects*, vol. 33, no. 23, pp. 2194–2205, 2011.
- [97] B. Masum, H. Masjuki, M. A. Kalam, S. Palash, and M. Habibullah, “Effect of alcohol–gasoline blends optimization on fuel properties, performance and emissions of a SI engine”, *Journal of Cleaner Production*, vol. 86, pp. 230–237, 2015.
- [98] S. Smith and A. Gordon, “Studies of diffusion flames. ii. diffusion flames of some simple alcohols.”, *The Journal of Physical Chemistry*, vol. 60, no. 8, pp. 1059–1062, 1956.
- [99] K. Kohse-Höinghaus, P. Oßwald, T. A. Cool, T. Kasper, N. Hansen, F. Qi, C. K. Westbrook, and P. R. Westmoreland, “Biofuel combustion chemistry: From ethanol to biodiesel”, *Angew. Chem. Int. Ed.*, vol. 49, no. 21, pp. 3572–3597, 2010.
- [100] L. Xingcai, H. Yuchun, J. Libin, Z. Linlin, and H. Zhen, “Heat release analysis on combustion and parametric study on emissions of hcci engines fueled with 2-propanol/n-heptane blend fuels”, *Energy & fuels*, vol. 20, no. 5, pp. 1870–1878, 2006.
- [101] T. Balamurugan and R. Nalini, “Experimental investigation on performance, combustion and emission characteristics of four stroke diesel engine using diesel blended with alcohol as fuel”, *Energy*, vol. 78, pp. 356–363, 2014.
- [102] A. Atmanli, “Comparative analyses of diesel–waste oil biodiesel and propanol, n-butanol or 1-pentanol blends in a diesel engine”, *Fuel*, vol. 176, pp. 209–215, 2016.
- [103] Y. Li, L. Wei, Z. Tian, B. Yang, J. Wang, T. Zhang, and F. Qi, “A comprehensive experimental study of low-pressure premixed c 3-oxygenated hydrocarbon flames with tunable synchrotron photoionization”, *Combustion and Flame*, vol. 152, no. 3, pp. 336–359, 2008.
- [104] T. Kasper, P. Oßwald, U. Struckmeier, K. Kohse-Höinghaus, C. A. Taatjes, J. Wang, T. Cool, M. Law, A. Morel, and P. R. Westmoreland, “Combustion chemistry of

- the propanol isomers investigated by electron ionization and VUV-photoionization molecular-beam mass spectrometry”, *Combustion and Flame*, vol. 156, no. 6, pp. 1181–1201, 2009.
- [105] C. Togbe, P. Dagaut, F. Halter, and F. Foucher, “2-propanol oxidation in a pressurized jet-stirred reactor (JSR) and combustion bomb: Experimental and detailed kinetic modeling study”, *Energy & fuels*, vol. 25, no. 2, pp. 676–683, 2011.
- [106] B. Galmiche, C. Togbe, P. Dagaut, F. Halter, and F. Foucher, “Experimental and detailed kinetic modeling study of the oxidation of 1-propanol in a pressurized jet-stirred reactor (jsr) and a combustion bomb”, *Energy & fuels*, vol. 25, no. 5, pp. 2013–2021, 2011.
- [107] P. S. Veloo and F. N. Egolfopoulos, “Studies of n-propanol, iso-propanol, and propane flames”, *Combustion and Flame*, vol. 158, no. 3, pp. 501–510, 2011.
- [108] J. Beeckmann, L. Cai, and H. Pitsch, “Experimental investigation of the laminar burning velocities of methanol, ethanol, n-propanol, and n-butanol at high pressure”, *Fuel*, vol. 117, pp. 340–350, 2014.
- [109] J. Gong, S. Zhang, Y. Cheng, Z. Huang, C. Tang, and J. Zhang, “A comparative study of n-propanol, propanal, acetone, and propane combustion in laminar flames”, *Proceedings of the Combustion Institute*, vol. 35, no. 1, pp. 795–801, 2015.
- [110] M. V. Johnson, S. S. Goldsborough, Z. Serinyel, P. OToole, E. Larkin, G. OMalley, and H. J. Curran, “A shock tube study of n-and iso-propanol ignition”, *Energy & Fuels*, vol. 23, no. 12, pp. 5886–5898, 2009.
- [111] B. Akih-Kumgeh and J. M. Bergthorson, “Ignition of C3 oxygenated hydrocarbons and chemical kinetic modeling of propanal oxidation”, *Combustion and Flame*, vol. 158, no. 10, pp. 1877–1889, 2011.
- [112] X. Man, C. Tang, J. Zhang, Y. Zhang, L. Pan, Z. Huang, and C. K. Law, “An experimental and kinetic modeling study of n-propanol and i-propanol ignition at high temperatures”, *Combustion and Flame*, vol. 161, no. 3, pp. 644–656, 2014.

- [113] K. Yang, C. Zhan, X. Man, L. Guan, Z. Huang, and C. Tang, “Shock tube study on propanal ignition and the comparison to propane, n-propanol and i-propanol”, *Energy & Fuels*, 2015.
- [114] J. Barnard and H. Hughes, “The pyrolysis of n-propanol”, *Transactions of the Faraday Society*, vol. 56, pp. 64–71, 1960.
- [115] J. Barnard, “The pyrolysis of isopropanol”, *Transactions of the Faraday Society*, vol. 56, pp. 72–79, 1960.
- [116] B. Bui, R. Zhu, M. Lin, *et al.*, “Thermal decomposition of iso-propanol: First-principles prediction of total and product-branching rate constants”, *Journal of Chemical Physics*, vol. 117, no. 24, pp. 11 188–11 195, 2002.
- [117] C. Esarte, M. Abián, Á. Millera, R. Bilbao, and M. U. Alzueta, “Gas and soot products formed in the pyrolysis of acetylene mixed with methanol, ethanol, isopropanol or n-butanol”, *Energy*, vol. 43, no. 1, pp. 37–46, 2012.
- [118] J. S. Heyne, S. Dooley, Z. Serinyel, F. L. Dryer, and H. Curran, “Decomposition studies of isopropanol in a variable pressure flow reactor”, *Zeitschrift für Physikalische Chemie*, vol. 229, no. 6, pp. 881–907, 2015.
- [119] S. M. Sarathy, P. Oswald, N. Hansen, and K. Kohse-Hoinghaus, “Alcohol combustion chemistry”, *Progress in Energy and Combustion Science*, vol. 44, pp. 40–102, 2014.
- [120] J. Guthrie, P. Fowler, and R. Sabourin, “Gasoline and diesel fuel survey”, *Driveability Index (DI) and Oxygenates in Gasoline*, 2003.
- [121] N. Grumman, “Diesel fuel oils, 2003”, *Report NGMS-232 PPS*, 2004.
- [122] F. Wu, A. P. Kelley, and C. K. Law, “Laminar flame speeds of cyclohexane and mono-alkylated cyclohexanes at elevated pressures”, *Combustion and Flame*, vol. 159, no. 4, pp. 1417–1425, 2012.
- [123] Y. Yang, A. L. Boehman, and J. M. Simmie, “Effects of molecular structure on oxidation reactivity of cyclic hydrocarbons: Experimental observations and conformational analysis”, *Combustion and Flame*, vol. 157, no. 12, pp. 2369–2379, 2010.

- [124] C. Ji, E. Dames, B. Sirjean, H. Wang, and F. N. Egolfopoulos, “An experimental and modeling study of the propagation of cyclohexane and mono-alkylated cyclohexane flames”, *Proceedings of the Combustion Institute*, vol. 33, no. 1, pp. 971–978, 2011.
- [125] C. M. Rosado-Reyes and W. Tsang, “Isomerization of cis-1,2-dimethylcyclohexane in single-pulse shock tube experiments”, *The Journal of Physical Chemistry A*, vol. 118, no. 36, pp. 7707–7714, 2014.
- [126] D. Kang, G. Lilik, V. Dillstrom, J. Agudelo, M. Lapuerta, K. Al-Qurashi, and A. L. Boehman, “Impact of branched structures on cycloalkane ignition in a motored engine: Detailed product and conformational analyses”, *Combust. Flame*, vol. 162, no. 4, pp. 877–892, 2015.
- [127] C. S. McEnally and L. D. Pfefferle, “Fuel decomposition and hydrocarbon growth processes for substituted cyclohexanes and for alkenes in nonpremixed flames”, *Proc. Combust. Inst.*, vol. 30, no. 1, pp. 1425–1432, 2005.
- [128] D. Sun, Y. Du, C. Li, J. Zhang, J. Lu, Z. Wang, J. Li, and J. Lü, “Theoretic heat sink simulation and experimental investigation of the pyrolysis of substituted cyclohexanes”, *J. Energy Chem.*, vol. 24, no. 1, pp. 119–125, 2015.
- [129] S. L. González-Cortés, S. Dorkjampa, P. T. Do, Z. Li, J. M. Ramallo-López, and F. G. Requejo, “Tuning the ring-opening reaction of 1,3-dimethylcyclohexane with the addition of potassium over ir-containing catalysts”, *Chem. Eng. J.*, vol. 139, no. 1, pp. 147–156, 2008.
- [130] S. Dokjampa, T. Rirksomboon, D. T. Phuong, and D. E. Resasco, “Ring opening of 1, 3-dimethylcyclohexane on ir catalysts: Modification of product distribution by addition of ni and k to improve fuel properties”, *J. Mol. Catal. A: Chem.*, vol. 274, no. 1, pp. 231–240, 2007.
- [131] P. T. Do, W. E. Alvarez, and D. E. Resasco, “Ring opening of 1,2-and 1,3-dimethylcyclohexane on iridium catalysts”, *J. Catal.*, vol. 238, no. 2, pp. 477–488, 2006.

- [132] M. I. Sway, “Kinetics of abstraction reactions of tert-butoxyl radicals with cyclohexane and methyl-substituted cyclohexanes in the gas phase”, *J. Chem. Soc., Faraday Trans.*, vol. 87, no. 14, pp. 2157–2159, 1991.
- [133] T. Korakianitis, A. Namasivayam, and R. Crookes, “Natural-gas fueled spark-ignition (SI) and compression-ignition (CI) engine performance and emissions”, *Progress in energy and combustion science*, vol. 37, no. 1, pp. 89–112, 2011.
- [134] A. Burcat, K. Scheller, and A. Lifshitz, “Shock-tube investigation of comparative ignition delay times for C1–C5 alkanes”, vol. 16, pp. 29–33, 1971.
- [135] F. Ma and M. Hanna, “Biodiesel production: A review”, *Bioresource Technology*, vol. 70, pp. 1–15, 1999.
- [136] J. Hill, E. Nelson, D. Tilman, S. Polasky, and D. Tiffany, “Environmental, economic, and energetic costs and benefits of biodiesel and ethanol biofuels”, *Proc. Natl. Acad. Sci. U.S.A.*, vol. 103, pp. 11 206–11 210, 2006.
- [137] R. Papagiannakis and D. Hountalas, “Experimental investigation concerning the effect of natural gas percentage on performance and emissions of a dual fuel diesel engine”, *Applied Thermal Engineering*, vol. 23, no. 3, pp. 353–365, 2003.
- [138] J. Kusaka, T. Okamoto, Y. Daisho, R. Kihara, and T. Saito, “Combustion and exhaust gas emission characteristics of a diesel engine dual-fueled with natural gas”, *JSAE review*, vol. 21, no. 4, pp. 489–496, 2000.
- [139] R. Papagiannakis and D. Hountalas, “Combustion and exhaust emission characteristics of a dual fuel compression ignition engine operated with pilot diesel fuel and natural gas”, *Energy conversion and management*, vol. 45, no. 18-19, pp. 2971–2987, 2004.
- [140] A. Namasivayam, T. Korakianitis, R. Crookes, K. Bob-Manuel, and J. Olsen, “Biodiesel, emulsified biodiesel and dimethyl ether as pilot fuels for natural gas fuelled engines”, *Applied Energy*, pp. 769–778, 2010.

- [141] K. Ryu, “Effects of pilot injection timing on the combustion and emissions characteristics in a diesel engine using biodiesel–cng dual fuel”, *Applied Energy*, vol. 111, pp. 721–730, 2013.
- [142] R. Mohsin, Z. Majid, A. Shihnan, N. Nasri, and Z. Sharer, “Effect of biodiesel blends on engine performance and exhaust emission for diesel dual fuel engine”, *Energy Conversion and Management*, vol. 88, pp. 821–828, 2014.
- [143] S. Hiremath, S. Khandal, N. Banapurmath, V. Math, and V. Gaitonde, “Comparative analysis of performance of dual fuel and homogeneous charge compression ignition engines fuelled with honne oil methyl ester and compress natural gas”, *Fuel*, vol. 196, pp. 134–143, 2017.
- [144] E. M. Fisher, W. J. Pitz, H. J. Curran, and C. K. Westbrook, “Detailed chemical kinetic mechanisms for combustion of oxygenated fuels”, *Proceedings of the combustion institute*, vol. 28, no. 2, pp. 1579–1586, 2000.
- [145] B. Akih-Kumgeh and J. M. Bergthorson, “Structure-reactivity trends of C1–C4 alkanoic acid methyl esters”, *Combustion and Flame*, vol. 158, no. 6, pp. 1037–1048, 2011.
- [146] A.-H. Kakaee, A. Paykani, and M. Ghajar, “The influence of fuel composition on the combustion and emission characteristics of natural gas fueled engines”, *Renewable and Sustainable Energy Reviews*, vol. 38, pp. 64–78, 2014.
- [147] J. Huang, P. Hill, W. Bushe, and S. Munshi, “Shock-tube study of methane ignition under engine-relevant conditions: Experiments and modeling”, *Combustion and flame*, vol. 136, no. 1-2, pp. 25–42, 2004.
- [148] M. Frenklach, “Systematic optimization of a detailed kinetic model using a methane ignition example”, *Combustion and flame*, vol. 58, no. 1, pp. 69–72, 1984.
- [149] E. Petersen, J. Hall, S. Smith, J. de Vries, A. Amadio, and M. Crofton, “Ignition of lean methane-based fuel blends at gas turbine pressures”, *Journal of Engineering for Gas Turbines and Power*, vol. 129, no. 4, pp. 937–944, 2007.

- [150] H. El Merhubi, A. Kéromnès, G. Catalano, B. Lefort, and L. Le Moyne, “A high pressure experimental and numerical study of methane ignition”, *Fuel*, vol. 177, pp. 164–172, 2016.
- [151] Y. Hidaka, K. Sato, Y. Henmi, H. Tanaka, and K. Inami, “Shock-tube and modeling study of methane pyrolysis and oxidation”, *Combustion and Flame*, vol. 118, pp. 340–358, 1999.
- [152] D. Davidson and R. Hanson, “Fundamental kinetics database utilizing shock tube measurements”, *Mechanical Engineering Department, Stanford University, Stanford CA*, 2005.
- [153] H. E. Merhubi, A. Kéromnès, G. Catalano, B. Lefort, and L. Moyne, “High-pressure oxidation of methane”, *Combustion and Flame*, vol. 172, pp. 349–364, 2016.
- [154] H. Hashemi, J. Christensen, S. Gersen, H. Levinsky, S. Klippenstein, and P. Glarborg, “High-pressure oxidation of methane”, *Combustion and Flame*, vol. 172, pp. 349–364, 2016.
- [155] V. Leschevich, V. Martynenko, O. Penyazkov, L. Sevrouk, and S. Shabunya, “Auto-ignitions of a methane/air mixture at high and intermediate temperatures”, *Shock Waves*, vol. 26, pp. 657–672, 2016.
- [156] J. Naber, D. Siebers, S. D. Julio, and C. Westbrook, “Effects of natural gas composition on ignition delay under diesel conditions”, *Combustion and Flame*, vol. 99, pp. 192–200, 1994.
- [157] E. Petersen, D. Kalitan, S. Simmons, G. Bourque, H. Curran, and J. Simmie, “Methane/propane oxidation at high pressures: Experimental and detailed chemical kinetic modeling”, *Proc. Comb. Inst.*, vol. 31, pp. 447–454, 2007.
- [158] J. de Vries and E. Petersen, “Autoignition of methane-based fuel blends under gas turbine conditions”, *Proc. Comb. Inst.*, vol. 31, pp. 3163–3171, 2007.
- [159] D. Healy, H. Curran, J. Simmie, D. Kalitan, C. Zinner, A. Barrett, E. Petersen, and G. Bourque, “Methane/propane mixture oxidation at high pressures and at high,

- intermediate and low temperatures”, *Combustion and Flame*, vol. 155, pp. 441–448, 2008.
- [160] D. Healy, H. Curran, S. Dooley, J. Simmie, D. Kalitan, E. Petersen, and G. Bourque, “Methane/ethane/propane mixture oxidation at high pressures and at high, intermediate and low temperatures”, *Combustion and Flame*, vol. 155, pp. 451–461, 2008.
- [161] D. Healy, M. Kopp, N. Polley, E. Petersen, G. Bourque, and H. Curran, “Methane/n-butane ignition delay measurements at high pressure and detailed chemical kinetic simulations”, *Energy & fuels*, vol. 24, no. 3, pp. 1617–1627, 2010.
- [162] D. Healy, D. Kalitan, C. Aul, E. Petersen, G. Bourque, and H. Curran, “Oxidation of C1–C5 alkane quaternary natural gas mixtures at high pressures”, *Energy & Fuels*, vol. 24, no. 3, pp. 1521–1528, 2010.
- [163] Z. Zhang, E. Hu, L. Pan, Y. Chen, J. Gong, and Z. Huang, “Shock-tube measurements and kinetic modeling study of methyl propanoate ignition”, *Energy & Fuels*, vol. 28, no. 11, pp. 7194–7202, 2014.
- [164] L. Zhao, M. Xie, L. Ye, Z. Cheng, J. Cai, Y. Li, F. Qi, and L. Zhang, “An experimental and modeling study of methyl proanoate pyrolysis at low pressure”, *Combustion and Flame*, vol. 160, pp. 1958–1966, 2013.
- [165] K. Kumar, C. Sung, B. Weber, and J. Bunnell, “Autoignition of methyl propanoate and its comparison with methyl ethanoate and methyl butanoate”, *Combustion and Flame*, vol. 188, pp. 116–128, 2018.
- [166] A. Farooq, D. Davidson, R. Hanson, and C. Westbrook, “A comparative study of the chemical kinetics of methyl and ethyl propanoate”, *Fuel*, vol. 134, pp. 26–38, 2014.
- [167] H. Ning, J. Wu, L. Ma, W. Ren, D. Davidson, and R. Hanson, “Chemical kinetic modeling and shock tube study of methyl propanoate decomposition”, *Combustion and Flame*, vol. 184, pp. 30–40, 2017.
- [168] D. Felsmann, H. Zhao, Q. Wang, I. Graf, T. Tan, X. Yang, E. A. Carter, Y. Ju, and K. Kohse-Höinghaus, “Contributions to improving small ester combustion chemistry:

- Theory, model and experiments”, *Proceedings of the Combustion Institute*, vol. 36, no. 1, pp. 543–551, 2017.
- [169] D. J. Seery and C. T. Bowman, “An experimental and analytical study of methane oxidation behind shock waves”, *Combustion and Flame*, vol. 14, no. 1, pp. 37–47, 1970.
 - [170] L. D. Smoot, W. C. Hecker, and G. A. Williams, “Prediction of propagating methane-air flames”, *Combustion and flame*, vol. 26, pp. 323–342, 1976.
 - [171] C. T. Bowman, “A shock-tube investigation of the high-temperature oxidation of methanol”, *Combustion and Flame*, vol. 25, pp. 343–354, 1975.
 - [172] C. K. Westbrook, F. L. Dryer, and K. Schug, “A comprehensive mechanism for the pyrolysis and oxidation of ethylene”, in *Symposium (International) on Combustion*, Elsevier, vol. 19, 1982, pp. 153–166.
 - [173] D. Nötzold and J. Algermissen, “Chemical kinetics of the ethane-oxygen reaction part i: High temperature oxidation at ignition temperatures between 1400 k and 1800 k”, *Combustion and Flame*, vol. 40, pp. 293–313, 1981.
 - [174] C. K. Westbrook and W. J. Pitz, “A comprehensive chemical kinetic reaction mechanism for oxidation and pyrolysis of propane and propene”, *Combustion Science and Technology*, vol. 37, no. 3-4, pp. 117–152, 1984.
 - [175] W. J. Pitz, C. K. Westbrook, W. M. Proscia, and F. L. Dryer, “A comprehensive chemical kinetic reaction mechanism for the oxidation of n-butane”, in *Symposium (International) on Combustion*, Elsevier, vol. 20, 1985, pp. 831–843.
 - [176] C. Westbrook, W. Pitz, J. Boercker, H. Curran, J. Griffiths, C Mohamed, and M Ribaucour, “Detailed chemical kinetic reaction mechanisms for autoignition of isomers of heptane under rapid compression”, *Proceedings of the combustion institute*, vol. 29, no. 1, pp. 1311–1318, 2002.
 - [177] S. Dooley, S. H. Won, J. Heyne, T. I. Farouk, Y. Ju, F. L. Dryer, K. Kumar, X. Hui, C.-J. Sung, H. Wang, *et al.*, “The experimental evaluation of a methodology

- for surrogate fuel formulation to emulate gas phase combustion kinetic phenomena”, *Combustion and Flame*, vol. 159, no. 4, pp. 1444–1466, 2012.
- [178] H. Wang, “On potential energy landscape and combustion chemistry modeling”, *Combustion and Flame*, vol. 1, no. 160, pp. 222–223, 2013.
- [179] H. Wang, *AFOSR Contractors Meeting Washington, DC, June 3*, 2014.
- [180] E. Ranzi, M. Dente, A. Goldaniga, G. Bozzano, and T. Faravelli, “Lumping procedures in detailed kinetic modeling of gasification, pyrolysis, partial oxidation and combustion of hydrocarbon mixtures”, *Progress in Energy and Combustion Science*, vol. 27, no. 1, pp. 99–139, 2001.
- [181] Y. Gao, R. Shan, S. Lyra, C. Li, H. Wang, J. Chen, and T. Lu, “On lumped-reduced reaction model for combustion of liquid fuels”, *Combustion and Flame*, vol. 163, pp. 437–446, 2016.
- [182] K. Kohse-Höinghaus, R. S. Barlow, M. Aldén, and J. Wolfrum, “Combustion at the focus: Laser diagnostics and control”, *Proceedings of the Combustion Institute*, vol. 30, no. 1, pp. 89–123, 2005.
- [183] M. G. Allen, “Diode laser absorption sensors for gas-dynamic and combustion flows”, *Measurement Science and Technology*, vol. 9, no. 4, p. 545, 1998.
- [184] D. F. Davidson and R. Hanson, “Recent advances in shock tube/laser diagnostic methods for improved chemical kinetics measurements”, *Shock Waves*, vol. 19, no. 4, pp. 271–283, 2009.
- [185] R. K. Hanson, “Applications of quantitative laser sensors to kinetics, propulsion and practical energy systems”, *Proceedings of the Combustion Institute*, vol. 33, no. 1, pp. 1–40, 2011.
- [186] E. Tomita, N. Kawahara, S. Yoshiyama, A. Kakuho, T. Itoh, and Y. Hamamoto, “In situ fuel concentration measurement near spark plug in spark-ignition engines by 3.39 μm infrared laser absorption method”, *Proceedings of the Combustion Institute*, vol. 29, no. 1, pp. 735–741, 2002.

- [187] E. Tomita, N. Kawahara, A. Nishiyama, and M. Shigenaga, “In situ measurement of hydrocarbon fuel concentration near a spark plug in an engine cylinder using the 3.392 μm infrared laser absorption method: Application to an actual engine”, *Measurement Science and Technology*, vol. 14, no. 8, p. 1357, 2003.
- [188] A. Klingbeil, J. Jeffries, and R. Hanson, “Temperature-and pressure-dependent absorption cross sections of gaseous hydrocarbons at 3.39 μm ”, *Measurement Science and Technology*, vol. 17, no. 7, p. 1950, 2006.
- [189] D. Haylett, R. Cook, D. Davidson, and R. Hanson, “OH and C₂H₄ species time-histories during hexadecane and diesel ignition behind reflected shock waves”, *Proceedings of the Combustion Institute*, vol. 33, no. 1, pp. 167–173, 2011.
- [190] D. Davidson, Z Hong, G. Pilla, A Farooq, R. Cook, and R. Hanson, “Multi-species time-history measurements during n-dodecane oxidation behind reflected shock waves”, *Proceedings of the Combustion Institute*, vol. 33, no. 1, pp. 151–157, 2011.
- [191] D. Davidson, Z Hong, G. Pilla, A Farooq, R. Cook, and R. Hanson, “Multi-species time-history measurements during n-heptane oxidation behind reflected shock waves”, *Combustion and flame*, vol. 157, no. 10, pp. 1899–1905, 2010.
- [192] S. H. Pyun, J. Cho, D. F. Davidson, and R. K. Hanson, “Interference-free mid-ir laser absorption detection of methane”, *Measurement Science and Technology*, vol. 22, no. 2, p. 025 303, 2011.
- [193] M. E. MacDonald, “Decomposition kinetics of the rocket propellant rp-1 and its chemical kinetic surrogates”, PhD thesis, Stanford University, 2012.
- [194] S. H. Pyun, W. Ren, K.-Y. Lam, D. F. Davidson, and R. K. Hanson, “Shock tube measurements of methane, ethylene and carbon monoxide time-histories in dme pyrolysis”, *Combustion and Flame*, vol. 160, no. 4, pp. 747–754, 2013.
- [195] W. Ren, A. Farooq, D. Davidson, and R. Hanson, “Co concentration and temperature sensor for combustion gases using quantum-cascade laser absorption near 4.7 μm ”, *Applied Physics B*, vol. 107, no. 3, pp. 849–860, 2012.

- [196] W. Ren, K.-Y. Lam, S. Pyun, A. Farooq, D. F. Davidson, and R. K. Hanson, “Shock tube/laser absorption studies of the decomposition of methyl formate”, *Proceedings of the Combustion Institute*, vol. 34, no. 1, pp. 453–461, 2013.
- [197] A. Camou, J. Vivanco, D. Cusano, and E. Petersen, “Laser absorption measurements of co at elevated pressures behind reflected shock waves”, in *29th International Symposium on Shock Waves 1*, Springer, 2015, pp. 221–226.
- [198] I. Stranic, D. P. Chase, J. T. Harmon, S. Yang, D. F. Davidson, and R. K. Hanson, “Shock tube measurements of ignition delay times for the butanol isomers”, *Combustion and Flame*, vol. 159, no. 2, pp. 516–527, 2012.
- [199] I. Stranic, S. Pyun, D. Davidson, and R. Hanson, “Multi-species measurements in 2-butanol and i-butanol pyrolysis behind reflected shock waves”, *Combustion and Flame*, vol. 160, no. 6, pp. 1012–1019, 2013.
- [200] A. G. Gaydon and I. R. Hurle, *The shock tube in high-temperature chemical physics*. Chapman and Hall, 1963.
- [201] D. Davidson, “Rgfrosh: A real gas frozen shock equation solver”, *Mechanical Engineering Department, Stanford University, Stanford (Ca, 94305), Tech. Rep*, pp. 001–1, 1995.
- [202] S. Browne, J. Ziegler, and J. Shepherd, “Numerical solution methods for shock and detonation jump conditions”, *Energy Conservation*, vol. 1, no. w2, w2, 2004.
- [203] D. Goodwin, “An open-source, extensible software suite for cvd process simulation”, *Chemical Vapor Deposition XVI and EUROCVCD*, vol. 14, no. 40, pp. 2003–08, 2003.
- [204] D. C. Horning, “A study of the high-temperature autoignition and thermal decomposition of hydrocarbons”, PhD thesis, Stanford University Stanford, 2001.
- [205] E. L. Petersen, M. J. Rickard, M. W. Crofton, E. D. Abbey, M. J. Traum, and D. M. Kalitan, “A facility for gas-and condensed-phase measurements behind shock waves”, *Measurement Science and Technology*, vol. 16, no. 9, p. 1716, 2005.

- [206] J. P. Holman and W. J. Gajda, *Experimental methods for engineers*. McGraw-Hill New York, 2001, vol. 7.
- [207] A. Klingbeil, J. Jeffries, and R. Hanson, “Temperature-and pressure-dependent absorption cross sections of gaseous hydrocarbons at $3.39\text{ }\mu\text{m}$ ”, *Meas. Sci. Technol.*, vol. 17, no. 7, p. 1950, 2006.
- [208] E. Tomita, N. Kawahara, A. Nishiyama, and M. Shigenaga, “In situ measurement of hydrocarbon fuel concentration near a spark plug in an engine cylinder using the $3.392\text{ }\mu\text{m}$ infrared laser absorption method: Application to an actual engine”, *Meas. Sci. Technol.*, vol. 14, no. 8, p. 1357, 2003.
- [209] A. E. Klingbeil, J. B. Jeffries, and R. K. Hanson, “Temperature-dependent mid-ir absorption spectra of gaseous hydrocarbons”, *J. Quant. Spectrosc. Radiat. Transfer*, vol. 107, no. 3, pp. 407–420, 2007.
- [210] S. Li, S. M. Sarathy, D. F. Davidson, R. K. Hanson, and C. K. Westbrook, “Shock tube and modeling study of 2, 7-dimethyloctane pyrolysis and oxidation”, *Combustion and Flame*, vol. 162, no. 5, pp. 2296–2306, 2015.
- [211] J. Vanderover and M. A. Oehlschlaeger, “A mid-infrared scanned-wavelength laser absorption sensor for carbon monoxide and temperature measurements from 900 to 4000 k”, *Applied Physics B*, vol. 99, no. 1-2, pp. 353–362, 2010.
- [212] W. Ren, A. Farooq, D. F. Davidson, and R. K. Hanson, “Co concentration and temperature sensor for combustion gases using quantum-cascade laser absorption near $4.7\text{ }\mu\text{m}$ ”, *Applied Physics B*, vol. 107, no. 3, pp. 849–860, 2012.
- [213] L. Rothman, S. Tashkun, S. Mikhailenko, I. Gordon, and Y. Babikov, “Hitran on the web”, *Harvard-Smithsonian Center for Astrophysics (CFA), Cambridge, MA, USA*, 2014.
- [214] F. Thibault, R. Martinez, J. Domenech, D. Bermejo, and J.-P. Bouanich, “Raman and infrared linewidths of co in ar”, *The Journal of chemical physics*, vol. 117, no. 6, pp. 2523–2531, 2002.

- [215] M. MacDonald, W. Ren, Y. Zhu, D. Davidson, and R. Hanson, “Fuel and ethylene measurements during n-dodecane, methylcyclohexane, and iso-cetane pyrolysis in shock tubes”, *Fuel*, vol. 103, pp. 1060–1068, 2013.
- [216] S. Jouzdani, M. Eldeeb, L. Zhang, and B. Akih-Kumgeh, “High-temperature study of 2-methyl furan and 2-methyl tetrahydrofuran combustion”, *International Journal of Chemical Kinetics*, 2016.
- [217] M. Eldeeb, S. Jouzdani, Z. Wang, S. Sarathy, and B. Akih-Kumgeh, “An experimental and chemical kinetic modeling study of dimethylcyclohexane oxidation and pyrolysis”, *Energy & Fuels*, 2016.
- [218] J. M. Simmie and H. J. Curran, “Formation Enthalpies and Bond Dissociation Energies of Alkylfurans. The Strongest C-X Bonds Known?”, *The Journal of Physical Chemistry A*, vol. 113, no. 17, pp. 5128–5137, 2009.
- [219] K. Moshhammer, S. Vranckx, H. K. Chakravarty, P. Parab, R. X. Fernandes, and K. Kohse-Höinghaus, “An experimental and kinetic modeling study of 2-methyltetrahydrofuran flames”, *Combustion and Flame*, vol. 160, no. 12, pp. 2729–2743, 2013.
- [220] M. J. Frisch, G. W. Trucks, H. B. Schlegel, G. E. Scuseria, M. A. Robb, J. R. Cheeseman, G. Scalmani, V. Barone, B. Mennucci, G. A. Petersson, H. Nakatsuji, M. Caricato, X. Li, H. P. Hratchian, A. F. Izmaylov, J. Bloino, G. Zheng, J. L. Sonnenberg, M. Hada, M. Ehara, K. Toyota, R. Fukuda, J. Hasegawa, M. Ishida, T. Nakajima, Y. Honda, O. Kitao, H. Nakai, T. Vreven, J. A. Montgomery Jr., J. E. Peralta, F. Ogliaro, M. Bearpark, J. J. Heyd, E. Brothers, K. N. Kudin, V. N. Staroverov, R. Kobayashi, J. Normand, K. Raghavachari, A. Rendell, J. C. Burant, S. S. Iyengar, J. Tomasi, M. Cossi, N. Rega, J. M. Millam, M. Klene, J. E. Knox, J. B. Cross, V. Bakken, C. Adamo, J. Jaramillo, R. Gomperts, R. E. Stratmann, O. Yazyev, A. J. Austin, R. Cammi, C. Pomelli, J. W. Ochterski, R. L. Martin, K. Morokuma, V. G. Zakrzewski, G. A. Voth, P. Salvador, J. J. Dannenberg, S. Dapprich, A. D. Daniels, Farkas, J. B. Foresman,

- J. V. Ortiz, J. Cioslowski, and D. J. Fox, *Gaussian 09 Revision A.1*, Gaussian Inc. Wallingford CT 2009.
- [221] A. C. Davis and S. M. Sarathy, “Computational study of the combustion and atmospheric decomposition of 2-methylfuran”, *The Journal of Physical Chemistry A*, vol. 117, no. 33, pp. 7670–7685, 2013.
- [222] H. K. Chakravarty and R. X. Fernandes, “Reaction kinetics of hydrogen abstraction reactions by hydroperoxyl radical from 2-methyltetrahydrofuran and 2, 5-dimethyltetrahydrofuran”, *The Journal of Physical Chemistry A*, vol. 117, no. 24, pp. 5028–5041, 2013.
- [223] B. Akih-Kumgeh and J. Bergthorson, “Skeletal chemical kinetic mechanisms for syngas, methyl butanoate, n-heptane and n-decane”, vol. 27, pp. 2316–2326, 2013.
- [224] Z. Wang, Z. Cheng, W. Yuan, J. Cai, L. Zhang, F. Zhang, F. Qi, and J. Wang, “An experimental and kinetic modeling study of cyclohexane pyrolysis at low pressure”, *Combust. Flame*, vol. 159, no. 7, pp. 2243–2253, 2012.
- [225] Z. Wang, L. Ye, W. Yuan, L. Zhang, Y. Wang, Z. Cheng, F. Zhang, and F. Qi, “Experimental and kinetic modeling study on methylcyclohexane pyrolysis and combustion”, *Combust. Flame*, vol. 161, no. 1, pp. 84–100, 2014.
- [226] Z. Wang, L. Zhao, Y. Wang, H. Bian, L. Zhang, F. Zhang, Y. Li, S. M. Sarathy, and F. Qi, “Kinetics of ethylcyclohexane pyrolysis and oxidation: An experimental and detailed kinetic modeling study”, *Combust. Flame*, vol. 162, no. 7, pp. 2873–2892, 2015.
- [227] E. R. Ritter, “Therm: A computer code for estimating thermodynamic properties for species important to combustion and reaction modeling”, *J. Chem. Inform. Comput. Sci.*, vol. 31, no. 3, pp. 400–408, 1991.
- [228] S. Burke, J. Simmie, and H. Curran, “Critical evaluation of thermochemical properties of C1–C4 species: Updated group-contributions to estimate thermochemical properties”, *J. Phys. Chem. Ref. Data*, vol. 44, no. 1, p. 013101, 2015.

- [229] D. Horning, D. Davidson, and R. Hanson, “Study of the high-temperature autoignition of n-alkane/o/ar mixtures”, *J. Propul. Power*, vol. 18, no. 2, pp. 363–371, 2002.
- [230] S. Jouzdani, A. Zhou, and B. Akih-Kumgeh, “Propanol isomers: Investigation of ignition and pyrolysis time scales”, *Combustion and Flame*, vol. 176, pp. 229–244, 2017.
- [231] M. A. Alrefae, “Mid-ir absorption cross-section measurements of hydrocarbons”, PhD thesis, 2013.
- [232] W. Mallard and W. Gardiner, “Absorption of the 3.39 μm he-ne laser line by methane from 300 to 2400 k”, *Journal of Quantitative Spectroscopy and Radiative Transfer*, vol. 20, no. 2, pp. 135–149, 1978.
- [233] S. W. Sharpe, T. J. Johnson, R. L. Sams, P. M. Chu, G. C. Rhoderick, and P. A. Johnson, “Gas-phase databases for quantitative infrared spectroscopy”, *Applied spectroscopy*, vol. 58, no. 12, pp. 1452–1461, 2004.
- [234] R. Mével, P. Boettcher, and J. Shepherd, “Absorption cross section at 3.39 μm of alkanes, aromatics and substituted hydrocarbons”, *Chemical Physics Letters*, vol. 531, pp. 22–27, 2012.
- [235] M. E. MacDonald, D. F. Davidson, R. K. Hanson, W. J. Pitz, M. Mehl, and C. K. Westbrook, “Formulation of an RP-1 pyrolysis surrogate from shock tube measurements of fuel and ethylene time histories”, DTIC Document, Tech. Rep., 2012.
- [236] M. A. Alrefae, “Mid-ir absorption cross-section measurements of hydrocarbons”, PhD thesis, 2013.
- [237] W. Mallard and W. Gardiner, “Absorption of the 3.39 μm he-ne laser line by methane from 300 to 2400 k”, *J. Quant. Spectrosc. Radiat. Transfer*, vol. 20, no. 2, pp. 135–149, 1978.
- [238] S. W. Sharpe, T. J. Johnson, R. L. Sams, P. M. Chu, G. C. Rhoderick, and P. A. Johnson, “Gas-phase databases for quantitative infrared spectroscopy”, *App. Spectrosc.*, vol. 58, no. 12, pp. 1452–1461, 2004.

Vita

Author's Name: Shirin Jouzdani

Place of Birth: Isfahan, Iran

Degrees Awarded:

Master of Science, University of Dayton, 2013

Bachelor of Science, Azad University, Iran, 2002

Professional Experience:

Research and teaching Assistant, Syracuse University Department of MAE, 2013-2018

Teaching Assistant, Syracuse University Department of Physics, 2017

Technical Sales Manager, Zobavaran Safahan Company, Iran, 2009-2011

Purchasing Department Assistant, Kahrobagostar Company, Iran, 2004-2009